Small scale processing of nanoscopic formulations for preclinical development of poorly soluble compounds

Dissertation zur Erlangung des Grades

„Doktor der Naturwissenschaften“

im Promotionsfach Pharmazie

am Fachbereich Chemie, Pharmazie und Geowissenschaften
der Johannes Gutenberg-Universität
in Mainz

Simon Geißler
geb. in Würzburg

Mainz, den 13.04.2014

1. Berichterstatter:

2. Berichterstatter:

Tag der mündlichen Prüfung: 03.07.2014

Acknowledgements

"Die Tiere, die Pflanzen, die Götter und das Denken - sie sind alle keine Freunde des Menschen. Zum Schauen kommen auf der Höhe des Unterrichts. Uns, die das Wissen überstieg, genügte ein einziges über den Berg schauendes Wort."

Botho Strauss

Contents

Nomenclature

API Active Pharmaceutical Ingredient

AUC Area Under the Curve

BCS Biopharmaceutical Classification System

CD Cyclodextrin

CMC Critical Micelle Concentration

cryoTEM cryogenic Transmission Electron Microscopy

DDS Drug Delivery System

DLS Dynamic Light Scattering

DMEM Dulbecco's Modified Eagle Medium

DMSO Dimethylsulfoxide

DOSS Docusate Sodium

DSC Differential Scanning Calorimetry

FaSSIF Fasted State Simulated Intestinal Fluid

FeSSIF Fed State Simulated Intestinal Fluid

FF Fenofibrate

FFA Fenofibric acid

GF Griseofulvin

GIT Gastrointestinal Tract

HBSS Hank's Buffered Saline Solution

HEC Hydroxyethyl cellulose

HEPES 2-[4-(2-hydroxyethyl)piperazin-1-yl]ethanesulfonic acid

HPC Hydroxypropylcellulose

HPLC High Performance Liquid Chromatgraphy

HPMC Hydroxypropylmethylcellulose

ITC Isothermal Titration Calorimetry

IUPAC International Union of Pure and Applied Chemistry

KC Ketoconazole

LCT Long Chain Triglycerides

LD Laser Diffraction

LFCS Lipid Formulation Classification System

MCT Medium Chain Triglycerides

ME Microemulsion

MPS Mononuclear Phagocyte System

NaDC Sodium Desoxycholate

NBE New Biological Entity

NCE New Chemical Entitiy

NE Nanoemulsion

NS Nanosuspension

PDI Polydispersity Index

PK Pharmakokinetics

PSD Particle Size Distribution

PVP Polyvinylpyrrolidone

SDS Sodium Dodecyl Sulfate

SEDDS Selfemulsifying Drug Delivery System

SEM Scanning Electron Microscopy

SGF Simulated Gastric Fluid

SGFsp Simulated gastric fluid sine pepsin

SIFsp Simulated intestinal fluid sine pancreatin

SLS Static Light Scattering

SMEDDS Selfmicroemulsifying Drug Delivery System

TEM Transmission Electron Microscopy

XRD X-Ray Diffraction

1 Introduction

1.1 Nanoscalic drug delivery techniques in pharmaceutical development

„The compound has got a solubility problem? No, we could dissolve it in DMSO.“ Some formulation scientists in clinical or preclinical development might already have heard this from some colleague in the discovery function. In fact, an increasing number of new chemical entities shows extremely low aqueous solubility preventing the applicabilty in standard peroral dosage forms [1, 2, 3]. Merck Serono is not an exception for this industry-wide phenomenon. Figure 1.1.1 is giving a very explicit view on this: Over a time frame of 20 years the average solubilities of new development compounds dropped by several orders of magnitude. The reasons for this lie in the high specificity of combinatorial chemistry approaches which leads to compounds with extremely high lipophilicity and therefore low aqueous solubility. Most of these compounds belong to the Biopharmaceutical Classification System (BCS) class II, i.e. the compounds exhibit low aqueous solubility and high permeability across biological membranes such as the intestinal mucosa [4]. Often high permeability can level constraints in oral bioavailability due to low solubility, especially in cases where solubility is kinetically controlled or only low doses need to be applied. A couple of approaches to overcome solubility related issues are established in pharmaceutical development. Rabinow [1] describes a general decision tree on formulation measures appropriate for different substance characteristics (Fig. 1.1.2). The concept is taking into account an increasing level of technical effort (from bottom to top) which decreasing drug polarity (from left to right). Whereas for BCS class I (high solubility, high permeability) and III (high solubility, low permeability) it is often enough to investigate suitable salts or work with comparatively simple measures such as pH adjustement or the use of solvent/water mixtures, for BCS II (low solubility, high permeability) and IV (low solubility, low permeability) it may be required to use enabling technologies such as microemulsions, solid dispersions and nanosuspensions. Per definition these technologies on the one hand enable the galenic development of substances that were not made bioavailable via standard means such as tablets, capsules and oral surfactant solutions. On the other hand the technical effort that needs to be coped with is high with the consequence of significant consumption of material

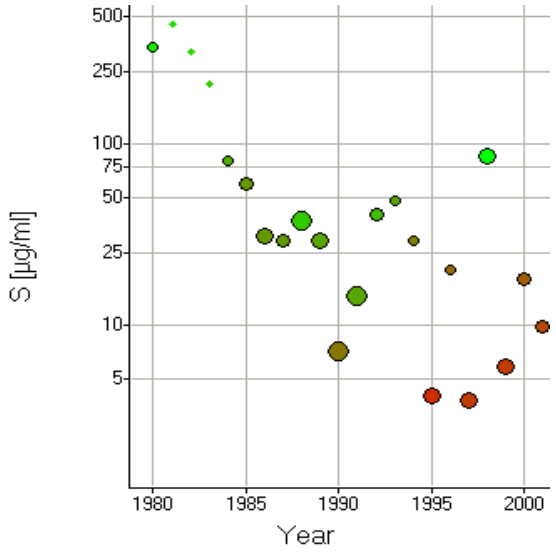

Figure 1.1.1: Aqueous solubility S versus time for Merck Serono preclinical compounds

and resources. In early pharmaceutical development this has very often to be balanced against short development timelines and limited availability of the active pharmaceutical ingredient (API) [5]. In most cases amounts of less than one gram of API can be provided. It is understood that formulation development in these cases cannot be performed on standard galenic equipment where batch sizes of $>$100 g are common. Therefore one of the major challenges is the setup of suitable small scale equipment for formulation processing. On the one hand the instruments must be able to cope with API amounts of less than 100 mg, on the other hand they should provide comparability or scalability at least to early clinical manufacturing processes. In the following four major approaches for nano drug delivery will be introduced. Although being of great interest for the targeted delivery of poorly soluble compounds liposomes and polymeric micellar systems will not be included within this work. The same applies to solid dispersion approaches for peroral bioavailability enhancement. Due to their complexity and the plethora of information already available a review of these methods would be beyond the scope of this work.

1.2 Nanosuspensions in pharmaceutical development

Nanosuspensions have emerged as an important tool in preclinical and clinical development. For the production of nanocrystalline API suspensions top-down and bottom up processes are discerned [6, 1, 7]. The most advanced nanosuspension production approach is marketed under the name „NanoCrystal® technology“. The technology is based on milling of poorly soluble actives in an aqueous dispersion medium via high-shear media mills [8]. The approach is scaled from milligram to upper kilogram scale per trial what underlines

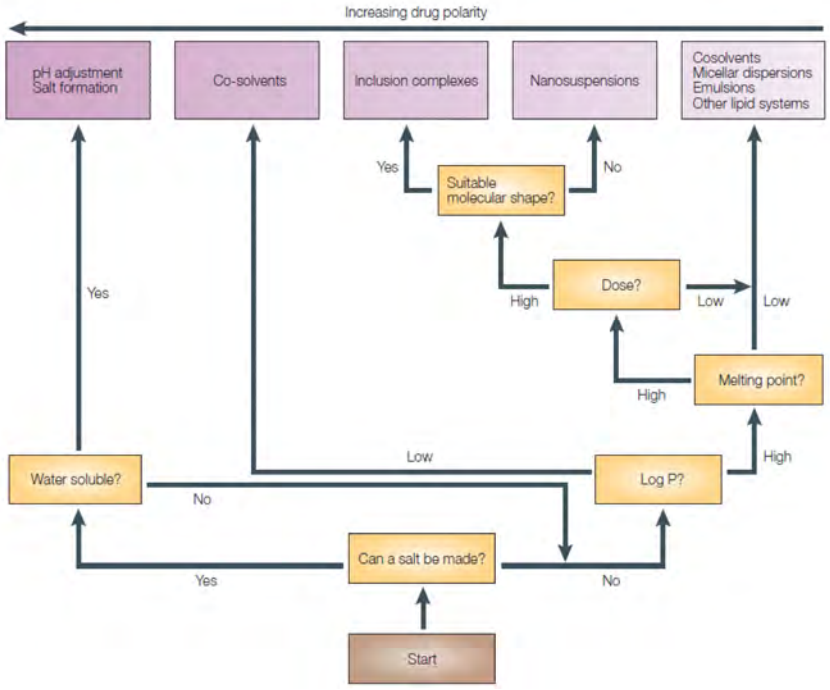

Figure 1.1.2: Decision tree for selection of formulations in early development (from [1])

the feasibility for early development as well as market supply. Apart from Nanocrystals the DissoCube® technology marketed by Skypharma deserves some attention. Instead of nanomilling high pressure homogenisation is applied to comminute micron sized drug particles in aqueous dispersion [9, 10]. Half a dozen products have been launched applying this technology generating a total revenue in the three digit million dollar range [11]. The respective brand names and manufacturers are listed in Table 1.1. Apart from marketed substances feasibility of nanomilling was shown on numerous examples in academia [12]. As for poorly soluble compounds often the solubility in surfactant and organic solvent vehicles is limited or the excessive use of solubilizers is not feasible due to toxicological reasons, the application of a fine dispersion together with the use of small amounts of wetting agents is often the only vehicle option. In contrast to solid dispersion formulations nanosuspensions are suitable for peroral as well as for parenteral use [13]. Nevertheless it has to be taken into consideration that a suspension instead of a real solution vehicle is applied. Potential implications of this can be e.g. undesired targeting of the MPS via the nanoparticles or insufficient dissolution of the particles in the GIT or parenteral compartments. The latter is especially of relevance if the active compound shows limited permeability through biological barriers and/or gets rapidly internalized into immunocompetent cells.

Brand name, drug substance	Manufacturing technology	Company	Approval
Rapamune®, Sirolimus	media milling	Wyeth	2001
Emend®, Aprepitant	media milling	MSD	2003
Tricor®, Fenofibrate	media milling	Abbott	2004
Triglide®, Fenofibrate	high pressure homogenisation	Shionogi	2005
Megace ES®, Megestrolacetat	media milling	PAR Pharmaceuticals	2005
InvegaSustenna®, Paliperidon palmitate	media milling	Janssen	2011

Table 1.1: Marketed products based on API nanocrystals

Different factors influence the milling performance in a ball milling process [14, 15, 16]. For planetary as well as for other ball milling systems, the effective energy input is of main importance. This is governed via apparative parameters (rotational speed, mill geometry) and setup parameters (type and size milling beads, bead fill level). Planetary ball mills are often equipped with zirconia milling beakers due to high resistance against abrasion. As a drawback zirconia shows extremely poor conduction of heat in comparison to other common materials such as stainless steel. This is critical because heat generated during the milling process can hardly be dissipated through the milling beakers. Cooling therefore occurs very slowly and is not effective enough to be done via air during milling. The problem can be overcome by two means: first the energy input can be controlled via factors such as rotational speed and intermittent milling to allow the sample to rest and cool. Second, depending on the design of the mill active cooling can be applied. Active cooling is especially possible in agitator ball mill systems. As these instruments can be run in continuous mode and therefore larger batch sizes can be realized this approach is most established in industry for wet milling applications [17, 10]. While the influence of parameters such as ball mill size and energy input is extensively investigated for inorganic substances [18, 19], only little work is so far done in pharmaceutical applications on organic substances. Main effort was so far on investigating and defining optimum stabilizers [20] for different model compounds and formulation variables [21, 22]. Scherliess investigated wet milling on an agitator ball mill and respective instrument factors for the model drug itraconazole [23]. While important work was done on the comparison of different processing parameters some aspects as product temperature and impact on product quality and processability were not covered. Also data were only generated on one model compound what only allows limited prediction for other APIs. Downscaling was investigated on 96w plate format in comparison to a planetary ball mill setting with good sucess [21]. In contrast the other route of scaling nanomilling from a planetary ball mill setup towards larger scales and /or a different milling setting is not tested so far. To provide a more profound insight into the principles of particle comminution in different mills some important aspects of grinding theory are presented as follows.

1.2.1 Grinding theory

The main objective for the modelling of impact mills with population balances here lay on a clear separation of the different influences of material properties, machine specific features and operating conditions in order to be able to interpret the results. Therefore it was assumed that the grinding process can be described separately by a machine and a material function [24, 19]. Hou et al. proposed mathematical modelling via the Taguchi method to describe and optimize milling processes [14]. In the following a practical and straightforward model to describe comminution in bead mills is presented. Kwade [25] and Blecher [26] introduced the parameters stress intensity BI and specific energy E_m for agitator ball mills . The authors defined the stress of milling beads as the product of agitator velocity v_t, diameter of milling beads $d_{MK}$and density of milling beads ρ_{MK}:

$$BI = d_{MK}^3 \cdot \rho_{MK} \cdot v_t^2 \tag{1.2.1}$$

The agitator velocity v [m/s] of agitator mills can be calculated from rotational speed n [rpm] by

$$v = \frac{r \cdot \pi \cdot n}{30} \tag{1.2.2}$$

Stress intensity and specific energy were shown to have direct impact on the comminution efficiency in stirring mills. Depending on material properties final product size is determined by the size of grinding beads as well as the specific energy input.

Considering the energy spectra in tumbling mills plethora of work has been published [27, 28] with many authors applying computer modelling such as the Discrete Element Method (DEM) [15, 16, 29, 30, 31]. Due to the complex motion patterns involved energy impacts are far less easy to determine and cannot be described via simple mathematical equations. Usually, the collision is described via compressive and frictional forces. If the number of milling bead collisions per second n and the relative velocity between colliding beads v_r is known by mathematical simulation, the net energy impact E_W can be expressed as

$$E_W = \sum \frac{1}{2W} \cdot m v_r^2 \tag{1.2.3}$$

where W is the mass of product [16]. Despite the complexity of grinding parameters in planetary ball mills work is published presenting scale-up strategies for this type of ball mill [16]. Taking a look at the forces that act on a single particle during grinding different mechanisms have been defined [32, 33, 34]. Abrasion, cleavage and fracture are the main identified modes that are displayed in Figure 1.2.1. Abrasion occurs when stress is applied tangentially as „shear stress“. Normally bimodal size distributions are obtained with one

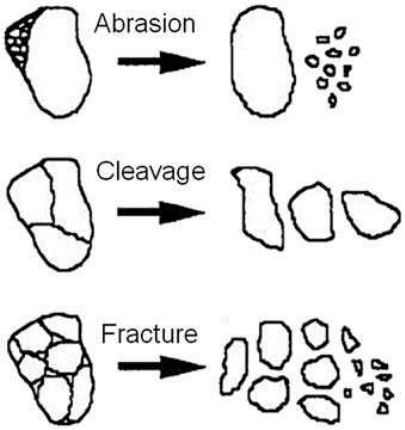

Figure 1.2.1: Mechanisms of particle fragmentation in an agitator ball mill (adopted from [33])

particle fraction being very small compared to another fraction where the particle size is close to that one of the unstressed particle. In contrast, fracture and cleavage lead to more pronounced particle comminution upon energy input. Cleavage is observed at slow energy inputs or compression leading to particles that normally show app. half the volume of the original particle. Fracture leads to finer particles in a range from 20-70% v/v of the original particle and is observed when intense impact stresses at high velocity are applied. Cleavage and abrasion were found to be the predominant mechanisms in a stirred media milling process [32]. Apart from that finding it is evident that the particle properties have major influence on the breaking behavior. Larger micron-sized drug crystals usually show a large number of crystal dislocations and offer therefore predetermined breaking points that make the crystals prone to cleavage and fracture upon stress. In contrast the smaller the particles the more important abrasion is for further particle comminution. Therefore cleavage and abrasion are found to be the important mechanisms for sub-micron suspensions. The short overview already reveals the complexity of grinding processes. As mentioned most of the research is so far done on metals and alloys rather than on more sensitive organic substances. Wet milling of pharmaceutical substances therefore deserves a more intense investigation.

1.2.2 Stabilisation of nanosuspensions

During particle comminution the surface area of the particulate phase will be dramatically increased resulting in a respective change in Gibbs free energy [20]. Consequently, the particulate system tends to minimize the total surface energy by surface area reduction, leading to agglomeration of the particles. The interaction between two particles is illustrated by the DLVO theory, which plots the total potential energy versus the interparticle distance

[10]. When distances between particles are becoming very small, attractive forces between particles prevail and agglomeration is induced. To overcome uncontrolled particle-particle interactions two types of stabilization mechanisms can be named. Electrostatic stabilization is provided by the physical adsorption of charged molecules on the nanoparticle surface. Particles in close vicinity are repulsed due to the electrostatic barriers. SDS, DOSS and NaDC are commonly applied electrostatic stabilizers [35, 36, 37]. In contrast, steric stabilization means the formation of a sterical barrier around the particles by adsorption of polymers onto the surface. Elastic and osmotic contributions are discussed for this type of stabilisation, mainly in the context of long-circulating liposomes or nanoparticles [38]. The elastic mechanism is based on the decreased volume for each polymer chain when two particles approach. Osmotically driven water influx between two particles occurs due to a local increase of polymer concentration when two particles get in closer proximity. Both mechanisms lead to repulsion of the nanoparticles and therefore to the stabilization of the dispersion. Typical steric stabilizers are the polymers HPC, HPMC and PVP with varying chain lengths and typical molecular weights between 15,000 to 50,000 Da [39, 40]. Other polymers with surface active properties are polysorbates [41], PEO-PPO-PEO block copolymers [42], TPGS and fatty acid esters of PEG [43, 44]. Often a combination of both stabilization approaches is advantageous for suspension stability in liquid state [22, 45, 46].

1.3 Emulsion systems

According to IUPAC (International Union of Pure and Applied Chemistry), aqueous emulsions are defined as dispersions of a non-water miscible liquid or liquid crystal in an aqueous liquid [47]. As the two liquids are immiscible in each other, an emulsifying agent, also called surfactant must be applied to stabilize the interface by formation of a monolayer of the amphiphilic agent between the two phases.

Compared to microemulsion phases extreme shear, well beyond the reach of ordinary mixing devices, must be applied to overcome the effects of surface tension to rupture the droplets into the nanoscale regime [48]. Emulsions of both the O/W and W/O type can be administered parenterally. While W/O or even O/W/O systems can solely be administered intramuscularily (i.m.), O/W systems can be administered by different parenteral routes (e.g. subcutaneous, intramuscular), but are predominantly given intravenously in parenteral nutrition [49]. A classification system to order different types of lipidic (and emulsion) systems according to their physchem characteristics and biopharmaceutical fate was introduced by Pouton in 2000 [50, 51]. Table 1.2 is giving an overview over the system, also referred to as the LFCS (Lipid Formulation Classification System). Type I formulations comprise oils that need to be digested to liberate the API, Type II formulations are

Table 1.2: The lipid formulation classification system LFCS (reproduced from [50])

Excipients in formulation	Content of formulation (%, w/w)				
	Type I	Type II	Type IIIA	Type IIIB	Type IV
Oils: triglycerides or mixed mono and diglycerides	100	40–80	40–80	<20	-
Water-insoluble surfactants (HLB < 12)	–	20–60	–	–	0–20
Water-soluble surfactants (HLB > 12)	–	–	20–40	20–50	30–80
Hydrophilic cosolvents (e.g. PEG, proylene glycol, transcutol®)	–	–	0–40	20–50	0–50

water-insoluble self-emulsifying drug delivery systems (SEDDS). Type IIIA systems denote SEDDS or SMEDDS with a lower fraction of water soluble ingredients, whereas TypeIIIB refers to microemulsifying systems with a higher fraction of hydrophilic solvents. The concept of SEDDS and SMEDDS will be discussed in more detail within the following section. Recently, the classification was expanded to Type IV systems which predominantly consist of hydrophilic surfactants and cosolvents. The main advantage of the latter over classic SMEDDS is the good solubilisation of hydrophobic, but not lipophilic drugs. On the other hand a poor local tolerability of the high surfactant concentrations in chronic use should be kept in mind [50]. While the last point is also true for Type III systems these efficiently facilitate drug uptake independent of the digestion of the lipids applied. Therefore these formulations help to level variability in drug uptake due to the food effect. The main drawback is the often observed loss in solvent capacity upon dispersion [52]. Type II systems in contrast can preserve the solubilisation upon dispersion, but are on the other hand more dependent upon digestion. The most unfavorable systems are classical oils/oil mixtures (Type I) which usually exhibit lowest solvent capacities and in which drug uptake is highly dependent on lipid digestion.

1.3.1 Microemulsion/S(M)EDDS

Microemulsions are optically transparent and stable mixtures of an oil, water, a hydrophilic surfactant and often a more hydrophobic cosurfactant [53]. Usually, these emulsions are in a size range from 20-100 nm droplet diameter. The most outstanding characteristic is that these systems form without significant mechanical stress only driven by the enthropy access liberated during hydration. Microemulsions find application in various industries, including consumer and industrial cleaning formulations, chemical reaction media, nanoparticle polymerization, and last but not least API delivery [54]. In pharmaceutical industry so called SMEDDS or SEDDS (Self Micro-Emulsifying Drug Delivery Systems) can be found. They denote the non-aqueous parts of a microemulsion incorporating the (usually) water-insoluble drug [55]. In contrast to microemulsifying systems SEDDS are leading to more coarse (>250 nm) and polydisperse emulsion systems. The nature of the DDS limits the

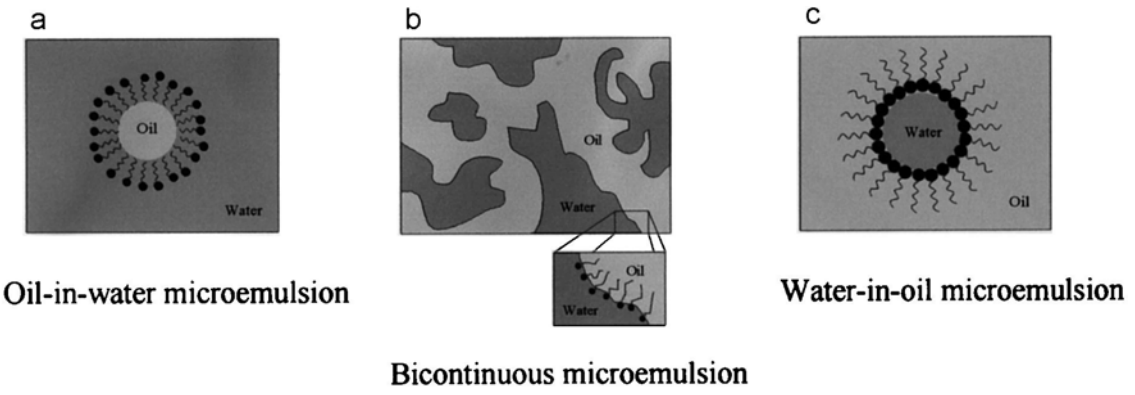

Figure 1.3.1: Representation of most common microemulsion structures a) o/w b) bicontinuous c) w/o microemulsion (copied from [53])

administration to the peroral route where a microemulsion is formed upon contact with the gastric or intestinal medium. S(M)EDDS are already well established on the pharma market with the most famous product Sandimmun Neoral® (Optoral® in Germany) by Novartis. Here the active ingredient ciclosporin is solubilized in a SMEDDS that is further formulated as a liquid filled capsule. Other examples are Norvir® (Abott, ritonavir), Agenerase® (GSK, amprenavir) or Accutane®(Roche, isotretinoin). All mentioned products are designed for peroral use. Apart from that topical and especially parenteral applications are described predominantly in academia [56, 57, 58].

Microemulsions generally undergo different states depending on the ratio of lipophilic to hydrophilic phases. Figure 1.3.1 schematically displays the most common states that microemulsion systems take at low (c) to high (a) levels of aqueous phase. When the amounts of water and lipids are similar bicontinuous states can be oberserved exhibiting a fluctuating surfactant-stabilized interface with a curvature of zero [53]. The in-depth investigation of microemulsion formation was done on several techniques, among them viscosity measurements, conductivity measurements, static and dynamic light scattering, small angle neutron scattering (SANS), small angle x-ray scattering (SAXS) and electron microscopy (cryoTEM, freeze fracture TEM).

Especially structural investigations benefit from the application of neutron or electron scattering techniques such as SANS and SAXS. The distribution of different oils in the spherical droplet could be followed [59] as well as the distribution of the surfactant [60]. Sommer et al applied SANS and SAXS methods to show the effect of a PEGylated surfactant Brij®700 on the formation and structure of a model microemulsion [61].

1.3.2 Nanoemulsions

In contrast to microemulsions nanoemulsions are kinetically stable oil droplets in the submicon size range stabilized via one or more surfactants [62]. Normally surfactants are added

only in the one digit volume percent range, so the absolute content of amphiphilic substances is far lower than in microemulsions. Another important aspect is that nanoemulsions require significant energy input for yielding nano-sized oil droplets [63]. Most commonly applied are high-shear mixing and homogenizing devices, but also ultrasound or extrusion techniques are described [48, 64]. Similar as microemulsions a large variety of analytical techniques are described to characterize nanoemulsions, among them light scattering and electron microscopy methods [64]. For pharmaceutical drug delivery systems nanoemulsions are used as carrier for lipophilic drugs (e.g. Diazepam® Lipuro) and are widely used in the field of parenteral nutrition (e.g. Lipofundin®). Other than in technical applications only a very limited number of oil phases and surfactants are applied in the pharmaceutical field. Most widely used are soybean oil and medium chain triglycerides (e.g. Miglyol®812). Egg or soy derived phosphatidylcholines and sodium oleate are the most common surfactants [65] although also other ionic and nonionic surfactants are described [64]. For pharmaceutical applications nanoemulsions contain usually 10-20% (v/v) oily phase, oil contents higher than 50% are often critical due to the viscosity and the resulting limited syringeability [62]. When comparing nanoemulsions to other lipidic drug delivery systems (microemulsions, liposomes) several advantages are to be listed. First, due to the high amount of oil higher drug loads are feasible in comparison to liposome bilayer vesicles. Second, nanoemulsions are far better tolerated in-vivo than microemulsions as only low fractions of surfactants are required to produce nanoemulsions. As a potential disadvantage the limited physical and chemical stability of nanoemulsions upon heat and freezing must be mentioned. This is in some cases overcome by lyophilisation in presence of suitable cryoprotectants.

1.4 Inclusion complexes

When talking about inclusion complexes for enhancing solubility of sparingly soluble APIs usually cyclodextrins are used. Cyclodextrins (CD) are cyclic oligosaccharides consisting of α-1,4-glykosidic glucose molecules [66]. CDs are produced by enzymatic degradation of starch in bacterial media (e.g. bacillus macerans). The type of binding leads to a toroidal structure with a central hydrophobic cavity. CDs are classified in:

- α-Cyclodextrin: n = 6 glucose units (cavity cross section/-height: 4.7..5.3/7.9 A)
- β-Cyclodextrin: n = 7 glucose units (cavity cross section/-height: 6.0..6.5/7.9 A)
- γ-Cyclodextrin: n = 8 glucose units (cavity cross section/-height: 7.5..8.3/7.9 A)

The size of the hydrophobic „bird's nest“ defines to a large extent the suitability for different substances and size classes. Apart form this steric aspect the interaction between host

molecule (API), guest molecule (CD) and a solvent must lead to a favorable net energy force that facilitates the inclusion of the host molecule. Main forces are the displacement of water from the CD cavity, the resulting increase in hydrogen bonds within the cavity, a reduction in host-water repulsion forces and increase in hydrophobic interactions after insertion of the host. However not always the interaction can be described as inclusion type but also distinct interactions between moieties of guest and host can lead to solubilisation (non-inclusion type) [67]. Regarding the complexity of these interactions it gets clear that the resulting binding constants betwen API and CD are influenced by various parameters such as salt content, pH, buffer composition, temperature and the concentrations of the components [68]. Numerous examples for solubility enhacement of new APIs are described, in most cases optimum solubility is achieved in β-cyclodextrins [69, 70][71, 72, 73]. Mostly used CDs are substituted β-cyclodextrins, such as HP-ß-CD (e.g. Kleptose®) and sulfobutyl ether ß-cyclodextrin (Captisol®) [74] which display very high water solubilities $> 500\,\mathrm{mg/mL}$ and are well tolerated excipients for peroral and parenteral use [75, 66]. In contrast underivatized β-CDs are not suitable for parenteral use due to their low solubilisation capacity and toxic side effects, esp. hemolysis and nephrotoxicity [5]. Different preparation techniques can be applied for producing binary mixtures of APIs and CDs. Mixtures can be kneaded in aqueous or dry state, processed in polar organic solvents or via supercritical fluids or simply mixed in aqueous environment. The latter is the most commonly used technique for preclinical vehicles as it allows - after removal of excess API - the direct administration of a solution via parenteral or peroral route. The ease of processing and the administration in liquid or solid dosage form e.g. after freeze drying make CDs a versatile tool in preclinical formulation development. As a drawback the interaction between an API and a cyclodextrin is highly specific and so is the factor of solubility enhancement. In daily practice only a minor fraction of compounds profits from solubilisation in modified β-cyclodextrins.

1.5 Aim of the thesis

The work focusses on the the development and characterisation of nanoscale drug delivery systems in preclinical pharmaceutical development. The primary scope is set on peroral formulations that also allow technical applicability in parenteral settings. Prerequisites were the application of commercialized equipment and excipients to guarantee potential implementation in Merck Serono standard processes. The formulation processes should be applicable to small molecules with different physicochemical properties. Therefore formulation work is - where applicable - performed on three BCS II class model compounds fenofibrate, griseofulvin and ketoconzole. The compounds cover a wide range of melting points (80°C - 220°C) and logP (2.18 - 5.2) values and are poorly soluble in aqueous media. Hence they present

ideal candidates to test the suitability of formulation approaches for new chemical entities from the Merck pipeline. Starting from the formulation decision tree proposed by Rabinow [1] inclusion complexes, nanoemulsion, nanosuspension and microemulsion techniques will be evaluated. Due to the extensiveness of these research topics only single aspects are highlighted for lipidic systems as well as inclusion complexes. Special focus will be set on nanomilling of solid APIs as this approach provides potential to be a versatile technology operating with minimum amounts of pharmaceutical excipients. Miniaturisation is one of the important factors to operate with minimum API amounts that are available in early preclinical development so scale is sized down towards 10-20 mg range. On the upper end the two-digit gram scale will be investigated for the nanomilling approach. The developed formulations are to be tested in-vitro and in-vivo regarding their biopharmaceutical performance in comparison to microparticulate formulations to assess the benefits and limitations of these drug delivery approaches.

2 Materials and methods

2.1 Materials

2.1.1 Drug substances

2.1.1.1 Fenofibrate

Fenofibrate (1-methylethyl 2-[4-(4-chlorobenzoyl)- phenoxy]-2-methylpropanoate) is a lipid lowering agent and belongs to the chemical class of fibrates. Fibrates are applied when triglyceride plasma levels are to be lowered and when CSE inhibitors are not tolerated. Fenofibrate (Fig. 2.1.1 a) is a prodrug and gets rapidly hydrolyzed to fenofibric acid (Fig. 2.1.1 b) in-vivo[76] [77]. The metabolite causes the clinically relevant effects, such as reductions in total plasma cholesterol, lowdensity lipoprotein cholesterol, triglycerides, and very low-density lipoproteins and increases in high-density lipoprotein cholesterol and apolipoproteins. The described effects are based on activation of peroxisome proliferator-activated receptor-α (PPARα) [78].

Chemical and physical properties: Fenofibrate is a highly lipophilic molecule (logP = 5.2) with the formula $C_{20}O_4H_{21}Cl$ and a molecular mass of 360.83 g/mol [76][79]. The white crystalline powder displays a melting point of 80°C and an aqueous solubility of 0.3 µg/mL [80][81]. The API was obtained by Smruthi Organics (Smruthi Organics Limited, India) in Ph.Eur. quality.

Dose: 160 - 400 mg per day

Brand names: Lipidil®, Tricor®

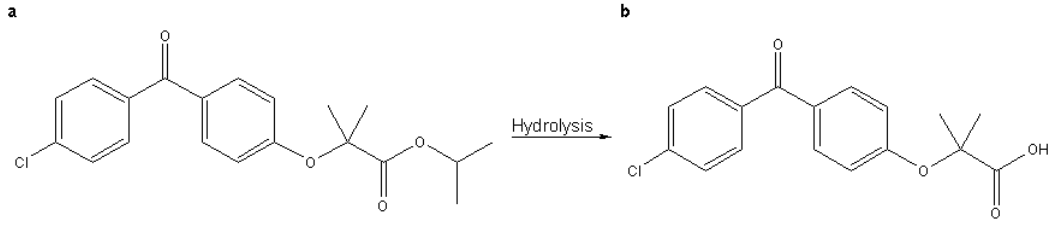

Figure 2.1.1: Structure a) fenofibrate and b) fenofibric acid

2.1.1.2 Griseofulvin

Griseofulvin (2S,6'R)- 7-chloro- 2',4,6-trimethoxy- 6'-methyl- 3H,4'H-spiro [1-benzofuran-2,1'-cyclohex[2]ene]- 3,4'-dione) is an oral antimycotic from the class of benzofuranes (see Fig. 2.1.2). It shows antibiotic action on dermatophytes like Microsporum Trichophyton species but no effect on candida and yeast . Griseofulvin binds to cellular tubulin and disturbs microtubuli function during mitosis thus locking the cell proliferation in the metaphase [82][76]. Consequently, GF acts fungistatic on proliferating mycotic cells.

The API was obtained by Fagron (Fagron GmBH, Germany) in Ph.Eur. quality.

Chemical and physical properties: Griseofulvin (M_w = $C_{17}H_{17}ClO_6$) is a white powder with a molar mass of 352.77 g/mol and a logP of 2.18. The melting point is 218-220°C, aqueous solubility is determined at 8.64 µg/mL at 25°C [81].

Dose: 50 - 150 mg/kg per day in animals, 0.5 - 1.0 g per day in humans

Brand names: Griseo-CT®

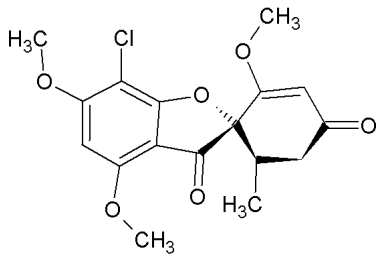

Figure 2.1.2: Structure of griseofulvin

2.1.1.3 Ketoconazole

Ketoconazole (1-[4-[4-[[(2R,4S)-2-(2,4-dichlorophenyl)-2-(imidazol-1-ylmethyl)-1,3-dioxolan-4-yl]methoxy]phenyl]piperazin-1-yl]ethanone) is an antimycotic from the class of azoles[83]. It is highly effective against systemic mycosis, candida albicans infections of oral and GI tract and dermatophytes [84] and was the first antimycotic for oral application. KC inhibits the enzyme lanosterol demethylase which catalyses the conversion of lanosterol in 14alpha-demethyl-lanosterol. The latter is a precursor of ergosterole which is the main component of fungal cell walls. Inhibition of 14 -demethylation leads to a depletion in ergosterol and to an increase in 14-methyl steroles in the mucotoc membrane. The resulting increase in membrane fluidity leads to inhibition of membrane bound enzymes and consequently to inhibtion of growth [85][86].

The API was obtained by Fagron (Fagron GmBH, Germany) in Ph.Eur. quality.

Chemical and physical properties: Ketoconazol (M_w= $C_{26}H_{28}Cl_2N_4O_4$) is a lipophilic (logP = 4.43), white powder with a molar mass of 531.43 g/mol, a melting point of 150°C and an aqueous solubility of 8.6 µg/mL [81]. The calculated logP value is 4.19 - 4.3, the

pKa values of the weak base are reported as 3.29 and 2.55. It is a derivative of imidazole and belongs to the chemical group of azoles. A racemic mixture of (2S,4R)-form und (2R,4S)-form is applied.

Dose: 200 - 400 mg per day orally

Brand names: Ket®, Terzolin®, Nizoral®

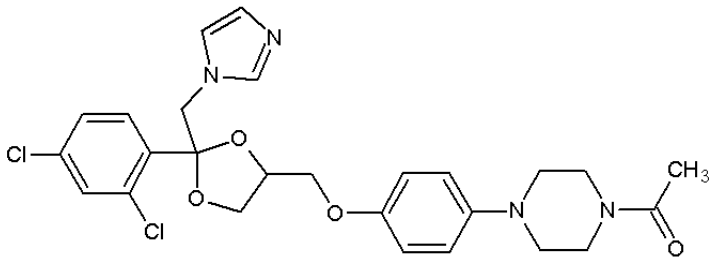

Figure 2.1.3: Structure of ketoconazole

2.1.2 Excipients and reagents

All excipients were of pharmaceutical (Ph.Eur., USP) or LC-analytical (purity >99%) grade if not mentioned otherwise. This also applies to solvents that are not listed specifically in this work.

2.1.2.1 Cyclodextrins

Kleptose® (HP-β-Cyclodextrin)

Kleptose®HP was purchased by Roquette (Roquete Freres, France). The white powder shows excellent solubility in aqueous media (>500mg/mL). The degree of substitution is generally between 5.25 - 6.65, a maximum of 1% β-cyclodextrin is not substituted . The applied batch is characterized by a molecular weight of 1399g/mol.

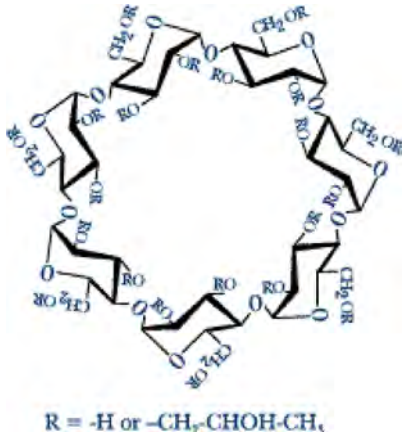

Figure 2.1.4: Structure of Kleptose®HP [87]

Captisol® (SBE-β-Cyclodextrin)

Captisol®is a sulfobutylether derivative of β-cyclodextrin and was a donation from Ligand Pharmaceuticals (Ligand Pharmaceuticals Inc., USA). The white granulates provide a water solubility of up 1.5 g/mL [88]. The molecular weight of the provided batch was 2163 g/mol. Captisol carries 6-7 sulfobutyl groups per molecule and contains one sodium ion for each level of substitution.

2.1.2.2 Long chain and medium chain triglycerides

Long chain triglycerides (LCT) and medium chain triglycerides (MCT) mainly differ in their fatty acid components. While the former contain fatty acid chains with 14, 16, 18, 20 and 22 carbon atoms and sometimes with double bonds, the latter are composed of saturated fatty acids with chains containing 6, 8, 10, or 12-carbon atoms [89]. Soybean oil is obtained from natural sources by solvent extraction of cracked soybeans with hexane and further refined or sometimes hydrogenated. The major unsaturated fatty acids in soybean oil are oleic acid, linoleic acid and linolenic acid, the last one being highly prone to oxidation. The semi-synthetic neutral oil Miglyol®. 812 is yielded from esterification of glycerol with fatty acids obtained from the hydrolysis of coconut oil followed by the fractionation of the free fatty acids. The main fatty acids in MCT are caprylic acid and capric acid.

2.1.2.3 Sucrose esters

Sucrose esters are nonionic surfactants based on sucrose. Due to the high functionality of the sugar molecule one or more hydroxy moieties can be esterified with medium or long chain fatty acids (Fig. 2.1.5). This bears the advantage that HLB values between 1 and 16 can be adjusted. On the other hand sucrose esters show poor purity and also monoesters are usually mixtures of monoester and polyesters [90]. Sugar esters were obtained by Mitsubishi Kagaku (Mitsubishi-Kagaku Foods Corporation, Japan) in Pharma grade quality. Esters with high HLB vales (HLB = 16) were applied, esterified C12, C14 or C18 fatty acids, namely lauric acid (L1695), myristic acid (M1695) and stearic acid (S1670). The esters contain 95% or 70% monoester, respectively.

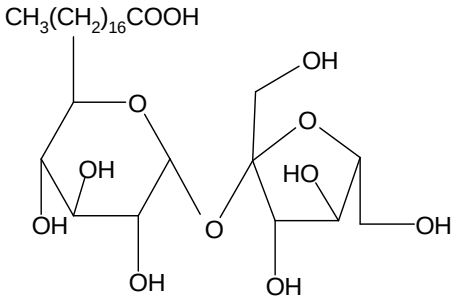

Figure 2.1.5: Chemical formula of sucrose monostearate

2.1.2.4 Excipients for use in nanosuspensions, nanoemulsions and SMEDDS

The following table (Tab. 2.1) lists polymers, cosolvents and surfactants applied in experiments for the formulation of the nanoscalic DDS investigated within this work.

Table 2.1: Excipients for use in nanoscalic DDS within this work

Commercial name	Substance/ IUPAC name	Supplier	Handling instructions	HLB value
Aerosol OT (AOT)	Dioctyl sulfosuccinate sodium salt (DOSS), Sodium 1,4-bis(2-ethylhexoxy)-1,4-dioxobutane-2-sulfonate	Sigma Aldrich		32
Capryol	Propylene glycol monocaprylate	Gattefossé		6
Cremophor RH 40	Macrogol-glycerol hydroxystearate 40	BASF	melt at 60°C & mix before use	14-16
Lutrol F 108	Poloxamer 338 (Poloxamer = Polyoxyethylene-polyoxypropylene block copolymer)	BASF		>24
Kollidon K12	Polyvinylpyrrolidone	BASF		
Kollidon K17	Polyvinylpyrrolidone	BASF		
Lutrol F 127	Poloxamer 407	BASF		18-23
Lutrol F 68	Poloxamer 188	BASF		>24
Methocel E5 Premium LV	Low viscosity hydroxypropylmethyl cellulose	DowWolff		
Miglyol	Medium chain triglycerides, MCT	Merck Schuchardt		
Soybean oil	Long chain trigylcerides, LCT	Caelo		
Ryoto Sugar ester: L-1695	sucrose laurate with 80% mono ester; 95% Purity of combined fatty acid	Mitsubishi-Kagaku		16
Ryoto Sugar ester: M1695	sucrose myristate 95% Purity of combined fatty acid	Mitsubishi-Kagaku		16
Ryoto Sugar ester: S-1670	Sucrose stearate with 75% mono ester; 70% Purity of combined fatty acid	Mitsubishi-Kagaku		16
Sodiumdeoxycholate	Sodiumdeoxycholate	VWR Prolabo		16
Sodiumdodecylsulfate	Sodiumdodecylsulfate (SDS)	Merck		40
Solutol HS 15	Polyethylene glycol-15-hydroxystearate	BASF	melt at 60°C & mix before use	14-16
Tween 20	Polysorbate	Merck		16,7
Tween 80	Polysorbate	Merck		15

2.2 Analytical Methods

2.2.1 Solubility and phase solubility tests

Solubility trials were conducted in 500 µL GC vials (VWR, Germany) equipped with polystyrene stoppers. 20 mg API were weighed into the vials on a Sartorius microbalance and the respective formulation or vehicle added via suitable Gilson® positive displacement pipettes. A magnetic stir bar was added into each vial and solubility tests performed for 24h at 25°C or 37°C with stirring at 1000 rpm. Temperature was controlled in a customized water bath, GC vials were fixed by customized plastic housings. Phase solubility trials were performed accordingly in the small scale test setup. API and cyclodextrins were directly weighed into GC vials and the respective medium (FaSSIF, FeSSIF) added. First, an excess of API of 5 mg was weighed in each GC vial equipped with a magentic stirring bar. An amount of cyclodextrin corresponding to 0 to 50mM CD was then added to the vials. Finally, 300µL of aqueous medium (water, FaSSIF, FaSSIFblank, FeSSIF, FeSSIFblank) were added to each vial. Media were produced according to the protocol of the inventors [91]. SGFsp and SIFsp were produced according to the USP protocols [92].

2.2.2 High Performance Liquid Chromatography (HPLC)

HPLC measurements were performed on a Merck Hitachi®(Hitachi Corp., Tokyo, Japan) apparatus, consisting of a D-7000 interface, two L-7400 pumps, a L-7400 UV detector, a L-7360 column oven and a L-7250 autosampler. An Agilent Zorbax Eclipse® C18 (4.6 x 50 mm, 3.5 µm) column was used. The run conditions were as shown in Table 2.2:

Table 2.2: HPLC conditions for the three test compounds

Mobile phase A	acetonitrile/water 5/95 (v/v) pH 2.9
Mobile phase B	acetonitrile/water 95/5 (v/v) pH 2.9
Detection wavelength	fenofibrate, fenofibric acid 288 nm
	griseofulvin 293 nm
	ketoconazole 210 nm
Injection volume	20 µL
Extraction medium	API, suspensions, cyclodextrins: acetonitrile/water 80/20 (v/v)
	emulsions, S(M)EDDS: THF/water 90/10 (v/v)
Flow rate	3.0 mL/min

Calibration for the three model compounds and fenofibric acid was performed in a concentration range of 0.2, 1.0, 10, 50, 100 and 200 µg/mL. All samples were prepared in triplicate and two injections were performed per vial. Good linearity with R^2 of 0.9988 to 0.9995 was obtained for all test substances.

2.2.3 Rheology

Rheologic experiments were conducted on a Brookfield DV-III Ultra (Broookfield® engineering laboratories Inc., Middleboro, USA) cone-plate rheometer, equipped with a Brookfield® TC-502 cryostat. CPE-40 (viscosity working range 0.15 - 3,065 mPas) and CPE-52 (4.6 - 92,130 mPas) type cones were applied depending on the expected viscosity range of the test system.

Data was analysed via Rheocalc® software V.3.1-1, applying appropriate analysis models.

2.2.4 Imaging methods

2.2.4.1 Optical light Microsopy

Microscopic pictures were taken by a Olympus® BX-60 (Olympus Deutschland GmbH, Hamburg, Germany) light microscope, equipped with Olympus® objectives (5x, 10x, 20x, 40x, 60x, 100x magnification) and a Sanyo® VCC-2973 colour CCD camera. Data analysis was performed via analySIS® 5.0 software (Soft Imaging System GmbH, Münster, Germany).

2.2.4.2 Transmission electron microscopy (TEM)

Transmission elctron microscopy was performed on a Tecnai 12® (FEI Corp., Hillsboro, USA) under cryo and non-cryo conditions. The conditions were as follows: Voltage 120 kV, spotsize 4-5, objective aperture 15 µm, sample dilution (if not stated otherwise) 1:200.

CryoTEM samples were prepared by plungefreezing the liquid samples that were dispersed on carbon-sputtered copper grids in liquid propane by using a Vitrobot®(FEI Corp., Hillsboro, USA).

2.2.4.3 Scanning electron microscopy (SEM)

SEM pictures were recorded on a Zeiss Leo® 1455 (Carl Zeiss, Germany) at 5 kV after pretreatment of the samples via the negative staining technique. Negative staining denominates that the sample of interest is immersed and dyed in a medium containing atoms with higher electron absorption than the sample. Thereby the contrast between the sample and the surrounding medium is enhanced. Sample preparation was as follows: One drop of undiluted nanoemulsion and one drop of a solution of phosphotungstic acid (1% w/v) were

mixed on a glass plate and directly transferred on a copper grid. Excess of the sample was carefully removed with pulp and the grid was dried for app. 3 min at ambient temperature before starting the measurement. 10 pictures were recorded per preparation.

2.2.5 Particle size analysis

2.2.5.1 Dynamic light scattering (DLS)

DLS, also known as photon correlation spectroscopy (PCS), was measured on a Zetasizer Nano ZS.(Malvern Ltd. Malvern, UK) with data treatment performed on Malvern DTS 5.0 software. The principal of dynamic light scattering is based in the Brownian motion of particles within a dispersion medium. Small isometric particles cause different fluctuations in the scattering pattern recorded over a distinct period of time in comparison to larger particles. These intensity shifts are recorded within a DLS measurement. Autocorrelation of the raw data -under assumption of spherical and evenly composed particles - yields a mean particle diameter. In addition the computed size distribution is expressed as the Polydispersity Index (PDI) with an high PDI value meaning higher heterogeneity of the sample.

Nanoemulsions and Nanosuspensions: DLS measurements of nanosuspensions containing 50-200mg/mL API were performed at dilutions of 1:200 applying bidistilled water as dispersion medium to exclude multiple scattering of the samples and to adjust a signal rate of 200-400 kcps. Measurements were performed in disposable semi-micro polystyrene cuvettes (VWR International, LLC, Vienna, Austria). Three measurements were taken per run with 10 runs per measurement at a temperature of 25°C. Data treatment was performed applying the „multiple purpose“ algorithm and the physical parameters of the respective drug compound and water. Attenuator settings and measurement position were set to automatic mode and the results are reported as intensity weighed mean hydrodynamic size (Z average).

Microemulsions: Microemulsions were not to be measured on high dilutions and had to be corrected for viscosity. Viscosities were determined via cone-plate rheometer (see 2.2.3)

2.2.5.2 Static light scattering (SLS)

The method of SLS, also referred to as laser diffraction (LD) is based upon the principle of smaller particles scattering light into different angles than larger particles. By detecting the intensity of light emitted in different directions by photo detectors one can correlate to the size distribution of spherical solid-body particles. Particles smaller than 1 µm in diameter are described by the Mie theory for what knowledge of refractive indices of dispersed

Table 2.3: Substance parameters for DLS and SLS experiments

	Fenofibrate	Griseofulvin	Ketoconazole	Miglyol
Refractive index	1.51[1]	1.5403[2]	1.456[3]	1.450[4]
Absorption, empirically set to	0.01	0.01	0.01	0.01

[1]measured internally
[2]reference from [93]
[3]reference from [94]
[4]reference from [95]

substance and dispersant is crucial. For absorbing particles larger than 5 µm the Fraunhofer approximation is applied.

Measurements were conducted on a Retsch Partica Horiba® LA-950V2 (Retsch Technology GmbH, Haan, Germany) with Horiba NextGen® software v5.20. Particle sizes distributions were calculated as volume fraction considering 15 iterations.

Samples were diluted in a liquid sample cell with bidistilled water as dispersant until appropriate transmission (60-80 % of blue laser light) was obtained. In all cases Mie theory was applied for data treatment. For refractive indices of test substances see Table 2.3. All sample dilutions and measurements were performed in triplicate.

2.2.5.3 Small angle neutron scattering (SANS)

Small angle scattering (SAS) is the collective name given to the techniques of small angle neutron (SANS), X-ray (SAXS) and light (LS, includes both Static SLS and Dynamic DLS) scattering. In each of these techniques radiation is elastically scattered by a sample and the resulting scattering pattern is analyzed to provide information about the size, shape and localisation of specific components of the sample. In SANS measurements are based upon the scattering and absorption of neutrons by materia. In contrast to SLS a focused neutron beam is scattered by nanosized structures according to their size and elemental composition. The reason for that is that neutrons can interact with atoms via dipole-dipole interaction resulting in magnetic scattering and nuclear scattering [96][97].

SANS measurements were carried out at the SANS facility of SINQ at Paul Scherrer Institute, Switzerland, using a neutron wavelength of λ=1.3 nm and two sample detector distances of 9 and 12 m. The range of momentum transfer $0.01 < Q$ (nm-1) < 0.5 was covered. The momentum transfer Q is defined in the usual way as $Q = 4\pi/\lambda \sin(\theta/2)$, where θ is the scattering angle. All measurements were performed at 21$\pm$1°C. The intensity data were corrected for background and transmission and for non-uniform detector efficiency by referring to the incoherent scattering of a water sample. Picture 2.2.1 is giving a schematic overview over the single components necessary in a SANS measurement setup. Neutrons of distinct velocity are gated in the velocity selector and directed towards uniform

flight behavior in a collimator with adjustable length. Scattered neutrons are trapped within an evacuated flight tube and recorded via a 2D beam stopper. In order to be able to monitor and analyze samples with non-uniform or changing sample composition a customized rotating cuvette was designed (Fig. 2.2.2). The cuvette consists of a stainless steel housing and two quartz glass windows. In the experimental setup for SANS studies on a microemulsion the SMEDDS preconcentrate was inserted with a 21G needle into the cuvette through an sealable orifice, the respective aqueous (D_2O, H_2O) media also added via a needle, and the cuvette locked. First data points were recorded after 30s. If not stated otherwise, scattering data were recorded every 30s up to a total measurement time of 15 min. Data analysis was performed via SASfit® software (SINQ, PSI, Switzerland).

SANS measurements were performed on the model microemulsion described under section 3.2. In a first set of experiments 0.25%, 0.5%, 4%, 10%, 15%, 20% (w/w) microemulsion was dispersed in H_2O and D_2O in order to get information on changes in the scattering pattern of the microemulsion droplets. As for concentations of $\geqq$10% a concentration influence on data treatment must be considered it was decided to start into deeper investigation with a max. solid content of 4% and 10%. As multiple scattering also affected sample readout in te 10% samples data interpretation was solely performed at 4% solid content.

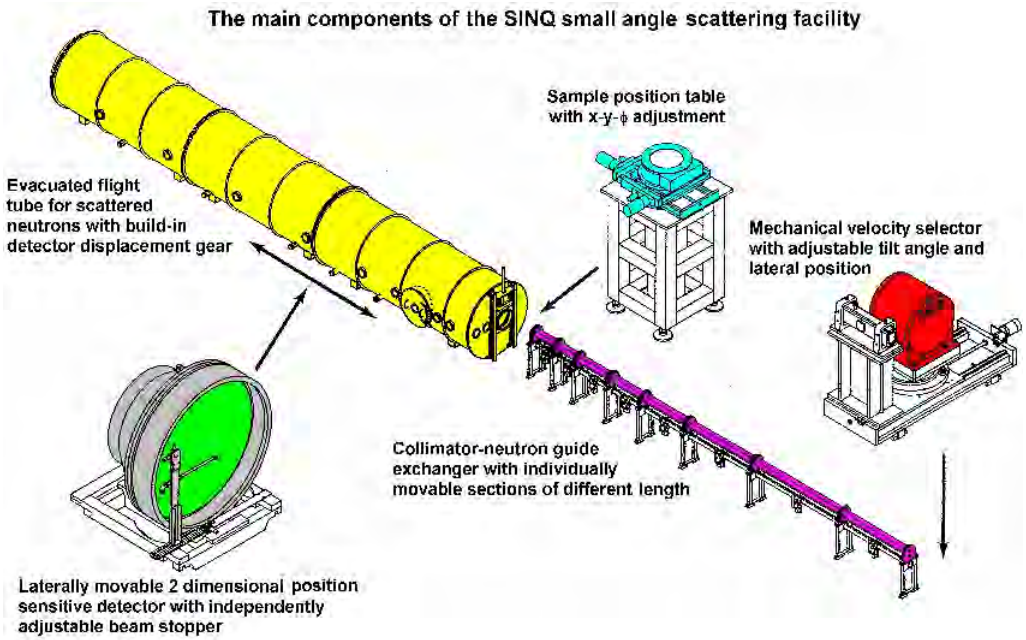

Figure 2.2.1: Schematic view of experimental setup of the SINQ SANS facility

Structural properties and computational model

Molecular modeling and calculation of relevant structural parameters was performed via Chemsketch and SASfit software, respectively (Tab. 2.4).

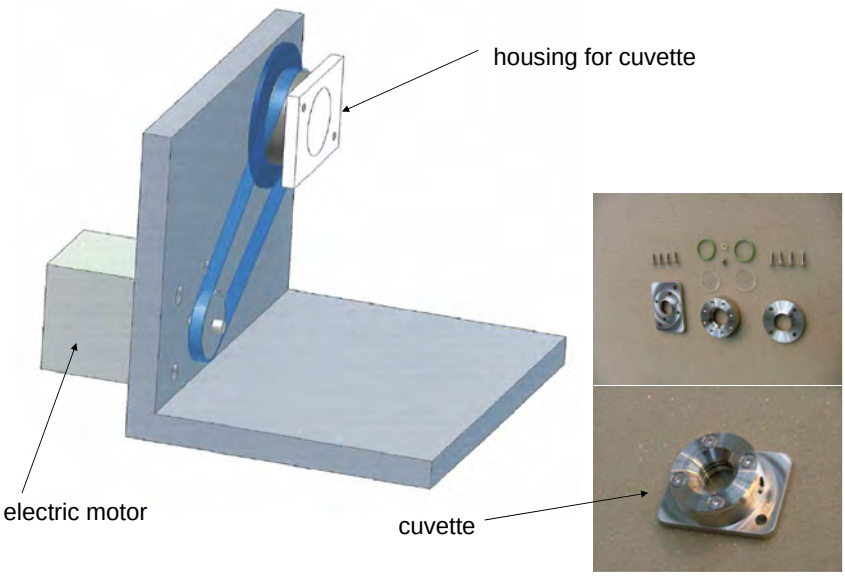

Figure 2.2.2: Schematic view and photographs of a rotating cuvette

Table 2.4: Physical properties of ME ingredients relevant for neutron scattering, values for Solutol® were estimated on basis of a mean of all described surfactant species found in the composition (calculated via Chemsketch or SASfit)

	Molecular formula	Density [g/cm^3]	SLD [cm^{-2}]	SL [cm]	Volume per molecule [A^3]
Solutol total molecule	C50H100O19	1.04	4.28E+09	6.87E-12	1605
Solutol hydrophilic part	C33H65O17	1.13	6.95E+09	7.49E-12	1086
Solutol lipophilic part	C26H53O2	1	-2.00E+09	-1.37E-12	660
Miglyol	C28H54O6	0.942	2.21E+09	1.90E-12	805.38
Capryol	C11H22O3	0.938	2.31E+09	8.26E-13	358
D_2O	D2O	1.1	6.33E+10	19.145	30.23

Among the relevant parameters scattering lengths SL, scattering length densities SLD, molecular and molar volumes need to be listed. The samples of interest are spherical in shape and unimodal in size distribution or follow a log-normal size distribution. The assumption was made that the oily droplets behave similar to polymeric micelles where the lipophilic part of the molecule is densely aggregated within the spherical core. The two following models proposed by Pedersen and modified by Kohlbrecher [98, 99] were applied:

SPHERE+Chains(RW)

The model is based on the assumption of a polymeric micelle with a solid core and hydrophilic parts of the polymer forming a corona or brush on the spherical particles. For calculation the scattering length densities of Miglyol® and PEG660 were chosen as the hydrophobic and hydrophilic „blocks“. The scattering intensity is then composed via the general equation:

$$I_{misc} = N_{agg}^2\beta_{core}^2 P_{core}(q) + N_{agg}^2\beta_{brush}^2 P_{brush}(q) + 2N_{agg}^2\beta_{core}\beta_{brush}S_{brush-core}(q) + N_{agg}(N_{agg}-1)\beta_{brush}^2 S_{brush-brush}(q) \quad (2.2.1)$$

The sphere model is described as

$$P_{core}(q, R_{core}) = \Phi^2(qCore) \quad (2.2.2)$$

$$\Phi(qR) = 3\frac{sin(qr) - qRcos(qR)}{(qR)^3} \quad (2.2.3)$$

$$P_{brush}(q, R^3) = 2\frac{exp(-x) - 1 + x}{x^2} \quad (2.2.4)$$

$$S_{brush-core}(q, R_{core}, R_g, d) = \Phi(qR_{core})\Psi(R_g)\frac{sin(q[R_{core} + dR_g])}{q(R + dR_g)} \quad (2.2.5)$$

$$\Psi(qR_g) = \frac{1 - exp(-x)}{x} \quad (2.2.6)$$

$$S_{brush-brush}(q, d, R_g, R_{core}) = \Psi^2(qR_g)(\frac{sin(q[R_{core} + dR_g])}{q(R + dR_g)})^2 \quad (2.2.7)$$

with

$$N_{agg} = n_{agg}S \quad (2.2.8)$$

The surface S of the core is given by $S = 4\pi R^2_{core}$ what in comb ination with the core

volume V leads to the calculation of excess scattering lengths β

$$\beta_{core} = \frac{V(1 - x_{solv,core})}{N_{agg}}(\eta_{solv} - \eta_{core}) \tag{2.2.9}$$

$$\beta_{shell} = V_{brush}(\eta_{brush} - \eta_{solv}) \tag{2.2.10}$$

Units that are not explained in the previous text are listed in the following legend:

V_{brush}: molecular volume the diblock copolymer part forming the corona

ηcore: scattering length density of the diblock copolymer part forming the core

ηbrush: scattering length density of the diblock copolymer part forming the corona

ηsolv: scattering length density of the solvent

N_{agg}: aggregation number

$x_{solv,core}$: volume fraction of solvent in the micellar core

R_g: radius of gyration of the block unit in the corona

R_{core}: radius of the micellar core

n_{agg}: grafting density (number of copolymer molecules Nagg per surface are S, nagg = Nagg=S)

d: non-penetration of the chains into the core is mimicked by d~1 for $R_{core} >> R_g$

Solutol Capryol Miglyol micelle (SCMM)

Similar to the previous model a spherical particle with an hydrophilic shell composed of PEG chains is assumed. The model takes into consideration the specific physicochemical characteristics of the components and in addition their relative amount in the particles. As a simplification it is assumed that the core of the micelle consist of Miglyol only with a radius R. The core is than surrounded by a shell of thickness R_{sh} consisting of Capryol® and the lipophilic part of Solutol® (Figure 2.2.3). The small hydrophilic part of Capryol® is ignored and accounted to the volume of the shell. To model the micelle a form factor of Jan Skov Pedersen has been slightly modified.

It is assumed that the Miglyol core has a lognormal size distribution:

$$N(R, \sigma, R_0) = \frac{1}{R\sqrt{2\pi\sigma^2}} exp\left[-\frac{1}{2}\left(\frac{ln(R) - ln(R_0)}{\sigma}\right)^2\right] \tag{2.2.11}$$

For the surfactant molecules it is assumed that they have a specific aggregation number density n_{agg} (number of surfactant molecules per surface area) which is independent of the size of the Miglyol® core. On the other side the ratios between $x_{Solutol}$:$x_{Miglyol}$:$x_{Capryol}$ is known. The volume of the Miglyol® core is simply

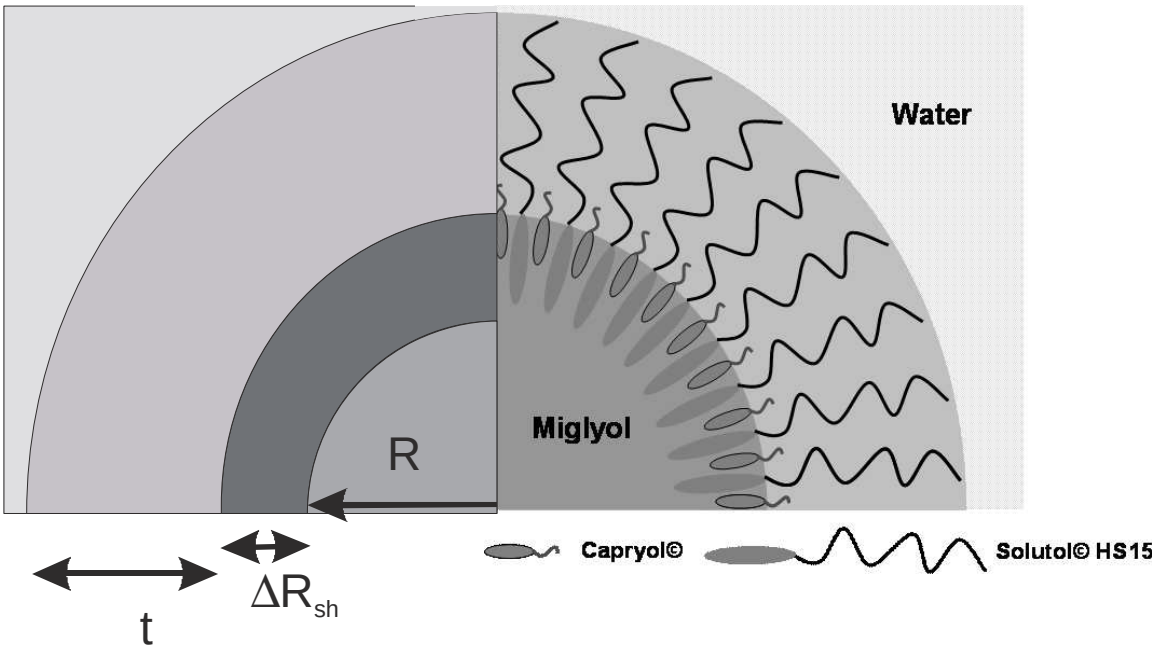

Figure 2.2.3: Schematic representation of SCMM model for SANS data evaluation

$$V_{Miglyol} = \frac{4}{3} R_{Core}^3 \tag{2.2.12}$$

The volume of Solutol® and Capryol® for a micelle is than given by surface of the Miglyol® core $S_{Miglyol} = 4\pi R_{Core}^2$, the specific aggregation number $n_{Soltutol}$and $n_{Capryol}$, the molecular volume of the surfactant molecules $\nu_{Solutol}$ and $\nu_{Capryol}$. The overall volume of the surfactant molecules in a micelle is then given by

$$V_{surfactants} = S_{Miglyol}(n_{Solutol}\nu_{Solutol} + n_{Capryol}\nu_{Capryol}) \tag{2.2.13}$$

As the ratio of Miglyol and the surfactants are known, the following ratio needs to be fulfilled

$$\frac{S_{Miglyol}(n_{Solutol}\nu_{Solutol} + n_{Capryol}\nu_{Capryol})}{V_{Miglyol}} = \frac{x_{Solutol} + x_{Capryol}}{x_{Miglyol}} \tag{2.2.14}$$

$$\frac{n_{Solutol}\nu_{Solutol}}{n_{Capryol}\nu_{Capryol}} = \frac{x_{Solutol}}{x_{Capryol}} \tag{2.2.15}$$

From this two equations the specific aggregation numbers $n_{Solutol}$ and $n_{Capryol}$ are given by

$$n_{Solutol} = \frac{1}{\nu_{Solutol}} \frac{V_{Miglyol}}{S_{Miglyol}} \frac{x_{Solutol}}{x_{Miglyol}} \tag{2.2.16}$$

$$n_{Capryol} = \frac{1}{\nu_{Capryol}} \frac{V_{Miglyol}}{S_{Miglyol}} \frac{x_{Capryol}}{x_{Miglyol}} \tag{2.2.17}$$

As the micelles have a size distribution in the core radius R_{core} and we assume a size independent specific aggregation number the ratios in equation 2.2.14 have to be therefore generalised by integrating over the size distribution. To calculate the corresponding total volume of the Miglyol core and the corresponding surface one can make use of the analytical solvable integral for the nth-moment of the lognormal distribution (Equ. 2.2.15).

$$\int_0^\infty N(R, \sigma, R_0) R_n dR = e^{\frac{n^2\sigma^2}{2}} R_0^n$$

The corresponding total volume of the Miglyol core and its total surface are given by

$$V_{tot,Miglyol} = \int_0^\infty N(R, \sigma, R_0) \frac{4}{3}\pi R^3 dR = \frac{4}{3}\pi e^{\frac{9\sigma^2}{2}} R_0^3 \tag{2.2.18}$$

and

$$S_{tot,Miglyol} = \int_0^\infty N(R, \sigma, R_0) 4\pi R^2 dR = 4\pi e^{2\sigma^2} R_0^2 \tag{2.2.19}$$

This results in

$$n_{Solutol} = \frac{1}{\nu_{Solutol}} \frac{V_{tot,Miglyol}}{S_{tot,Miglyol}} \frac{x_{Solutol}}{x_{Miglyol}} \tag{2.2.20}$$

$$n_{Capryol} = \frac{1}{\nu_{Capryol}} \frac{V_{tot,Miglyol}}{S_{tot,Miglyol}} \frac{x_{Capryol}}{x_{Miglyol}} \tag{2.2.21}$$

Knowing the specific aggregation numbers $n_{Solutol}$and $n_{Capryol}$ of the surfactant molecules next the thickness of the shell $\triangle R_{sh}$ as a function of the radius needs to be calculated. For simplicity it is assumed that Capryol® is completely part of the shell between R and $R + \triangle R_{sh}$. Secondly it is assumed that only the lipophilic part $\nu_{lipo,Solutol}$ of the Solutol® molecules ($\nu_{Solutol} = v_{hydro,Solutol} + \nu_{lipo,Solutol}$)is extended into this shell. The volume V_{sh} of the shell between R and $R+\triangle R_{sh}$.and which should not contain any solvent is therefore given by

$$V_{sh} = \frac{4}{3}\pi \left([R + \triangle R_{sh}]^3 - R^3 \right) = 4\pi R^2 \nu_{lipo,Solutol} n_{Solutol} + \nu_{Capryol} n_{Capryol} \tag{2.2.22}$$

The shell thickness therefore reads as

$$\triangle R_{sh} = \sqrt[3]{R^3 + 3Rn_{Solutol}\nu_{lipo,Solutol} + 3Rn_{Capryol}\nu_{Capryol}} - R \tag{2.2.23}$$

The hydrophilic part of the Solutol® molecule with the molecular volume of $\nu_{hydro,Solutol}$ is pointing into the solvent to form the hairy outer shell of the micelle. The radius of gyration R_g of the individual hydrophilic Solutol® parts will be a fitting parameter. The aggregation number of Solutol® molecules as a function of the Miglyol® core radius $N_{Solutol,agg}(R)$ is simply

$$N_{Solutol,agg}(R) = n_{Solutol} S_{Miglyol} = n_{Solutol} 4\pi R^2 \tag{2.2.24}$$

Now all parameters are known to calculate the form factor of a spherical shell grafted with the hydrophilic part of the Solutol® surfactant molecules with a radius of gyration R_g. The form factor of homogeneous spheres with Gaussian chains attached has been given by J.S. Pedersen [98] and only needs to be generalised by replacing the form factor of a homogeneous sphere by that one of a spherical shell.

$$I(q) = F_{sh}^2(q) + N_{Solutol,agg}\beta_{brush}^2 P_{brush}(q) + 2N_{Solutol,agg}\beta_{brush} P_{brush-core}(q) + N_{Solutol,agg}\left(N_{Solutol,agg} - 1\right)\beta_{brush}^2 S_{brush-brush}(q) \tag{2.2.25}$$

The form factor amplitude of a Gaussian chain is defined as

$$P_{brush}(q) = 2\frac{exp\left[-x\right] - 1 + x}{x^2} \tag{2.2.26}$$

with $x=R^2_g q^2$

The form factor amplitude of the spherical shell forming the core is

$$F_{sh}(q) = \triangle\eta_{sh}\frac{4}{3}\pi\left(R + \triangle R_{sh}\right)^3 3\frac{sin(q(R+\triangle R_{sh})) - q(R+\triangle R_{sh})cos(q(R+\triangle R_{sh}))}{q(R+\triangle R_{sh}))^3} - \triangle\eta_{core}\frac{4}{3}\pi R^3\frac{sin(qR) - qRcos(qR)}{(qR)^3} \tag{2.2.27}$$

The interference term between spherical shell and the Gaussian chains can be calculated by

$$S_{brush-core}(q) = F_{sh}(q)\psi(qR_g)\frac{sin(q[R+\triangle R_{sh}+dR_g])}{q[R+\triangle R_{sh}+dR_g]} \tag{2.2.28}$$

and the self term by

$$S_{brush-brush}(q) = \psi^2(qR_g)\left[\frac{sin(q[R+\triangle R_{sh}+dR_g])}{q[R+\triangle R_{sh}+dR_g]}\right]^2 \tag{2.2.29}$$

with the form factor amplitude of a chain

$$\psi(x) = \frac{1 - exp(-x)}{x} \tag{2.2.30}$$

The scattering contrasts $\triangle\eta_{core}$ and $\triangle\eta_{sh}$as well as the excess scattering length $\beta_{brush}$of the hydrophobic part of the Solutol® chain are given by

$$\triangle\eta_{core} = \eta_{Miglyol} - \eta_{solv} \tag{2.2.31}$$

$$\triangle\eta_{sh} = \left[\eta_{lipo,Solutol}\frac{x_{Solutol}}{x_{Solutol} + x_{Capryol}} + \eta_{Capryol}\frac{x_{Capryol}}{x_{Solutol} + x_{Capryol}}\right] - \eta_{solv} \tag{2.2.32}$$

2.2.6 X-ray diffraction (XRD)

Samples have been prepared in a combinatorial 96-well-plate, comprising an X-ray amorphous foil as bottom. Measurements were performed in transmission geometry with Cu-$K_{\alpha 1}$ radiation on a Stoe StadiP 611 Combi diffractometer. Scans were acquired using an Imaging Plate PSD detector, covering 0-72° 2θ simultaneously, with a step width of 0.03° 2θ, and a total measurement time of 20 minutes. The detector was arranged in mid-symmetrical alignment to the samples, resulting in 2 diffraction subranges 0-36°, simultaneously collecting intensities diffracted to the left and the right 0-36° angular range. The resulting scan file was folded from the 2 diffraction ranges.

2.2.7 Zeta potential measurements

Zeta potential was measured using a Zetasizer Nano ZS (Malvern Ltd. Malvern, UK) and transparent Malvern folded capillary cells. The measurement is based upon the M3-PALS technique. Phase analysis light scattering (PALS) is a variation of laser doppler velocimetry
.

Samples were diluted 1:100 - 1:200 with NaCl solution (0.1 mM) to obtain transparent systems with low electric conductivity (approx. 50 µS/cm). Sample dilutions as well as measurements were done in triplicate with automatic selection of run numbers. For data treatment the Smoluchowski approximation for aqueous systems was applied.

2.2.8 Differential scanning calorimetry (DSC)

DSC measurements were performed on Mettler Toledo DSC 821e equipped with a Mettler Toledo TSO801RO sample robot (Mettler Toledo, Giessen, Germany). Device control and data analysis was done by Mettler Toledo STARe version 8.10 software. If not described

otherwise, 100 µl alumina pans (Mettler Toledo, Giessen, Germany) were blank weighed, filled with about 50µl of the respective test system via a 100µL Gilson Microman® positive displacement pipette (Gilson Inc., Middleton, USA), dried - if water containing systems were to be investigated - under ambient conditions, sealed and weighed on a microbalance (Sartorius ME5, Sartorius AG, Göttingen, Germany).

Nanosuspensions: Samples were heated with 10 K/min from 20°C to 250°C

SMEDDS: Samples were heated from -50 to +50°C with 2 K/min several times

2.2.9 Karl-Fischer titration

Water content in sold samples was determined via Karl Fischer titration via a DL39 titrator (Mettler Toledo, Giessen, Germany). 200mg of samples were weighed correctly and dissolved within 240 s in methanol. Titration was done in triplicate per sample system. Calibration was performed on 1% water with an maximum accepted standard deviation of 0.6 %.

2.2.10 Isothermal titration calorimetry (ITC)

ITC measurements were performed on a iTC200 (MicroCal™, Europe, UK) applying 1.43 mL teflon cell and a standard glass hamilton dosing syringes (285 µL fill volume) at 200 rpm agitation speed and without agitation. Microemulsion preconcentrate that was equilibrated by a water bath was dosed in intervalls of 10 min into 1.00 ml purified water equilibrated at 37°C. Injection volumina varied from 0.5 - 10 µL preconcentrate. injection volumina of $>$ 5µL generated signals too large to measure. The heat generated upon dilution of preconcentrate and formation of microemulsion droplets was recorded as µcal/s and plotted against time. Samples at 25°C were too viscous to be measured reproducibly. Experiments were therfore performed at 37°C and 47°C.

2.2.11 Rheology

Rheological properties were determined via a Brookfield® LVDV-III Ultra cone-plate-rheometer (Brookfield, Lorch, Germany). The CPE-40 cone was applied using different shear gradients to investigate the behavior of nanosuspensions upon shear stress. All measurements were done in triplicate at 25°C. Maximum shear gradients of 200 s^{-1} were applied.

2.2.12 Nanoindentation

Nanonindentation experimenbts were performed on a TriboIndenter® nanoindentation instrument (Hysitron, Minneapois, USA) pictured in Fig. 2.2.4. Berkovich geometry was

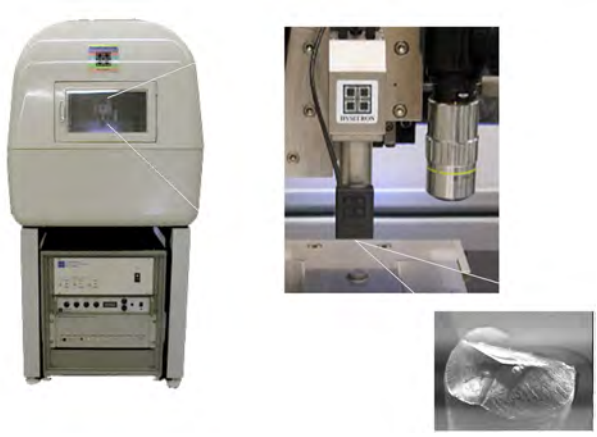

Figure 2.2.4: Experimental setup nanoindentation experiments

used for the indentation tip. Force-displacement curves were recorded for a maximum indentation depths of 1000nm. 25 indents were recorded per each measurement condition and averaged. Models developed by Olliver and Pharr [100] were applied to calculate material hardness and elastic modulus of the test material. API crystals were grown at ambient temperature in supersaturated organic solutions of the respective API. 100 mg/mL API were dissolved in the respective solvent in 15 mL glass beakers and the solvent evaporated slowly over several days. Evaporation was controlled via tuning the size of the vessel orifice via aluminum foil. FF was dissolved in toluene, GF and KC in methylene chloride. The same organic solvents were applied as during the purification steps of the synthesis in order to generate crystals with structure and dislocations comparable to the product applied in nanomilling.

2.2.13 DoE data analysis

Design of experiments trials for optimisation of a wet milling process were planned and analyzed via Cornerstone® software (camLine, Petershausen/Germany). D-optimal design was chosen for setting experimental parameters. Regression analysis was performed via fully quadratic model, including power transformation for the responses „particle size“ and „sdv particle size“.

2.2.14 Cell permeation experiments

2.2.14.1 Cell culture

Caco2 cells were seeded at 100000 cells/well in 12-well Transwell® plates (Type 3401, Corning Inc., Corning, USA) with 0.4 µm polycarbonate filter and 1.12cm^2 area. DMEM supplemented with 100 IU/mL penicillin, 100 µg/mL streptomycin, 1% non-essential amino

acids and 10% FBS was used for cell culture in an atmosphere of 5% CO_2 and 90% relative humidity. Cells were used on day 20 - 22 after seeding on passage 45 - 60. For cell splitting approx. 90 % confluent cell layers were trypsinized with trypsin/EDTA solution (0.25%/0.02%) and seeded again at 300,000 cells/20mL in T-75 culture flasks.

2.2.14.2 Test protocol

To mimic drug concentrations relevant in the small intestine formulations were diluted to a concentration of 0.5 mM in the donor compartment. Transport media and formulations were equilibrated to 37°C prior to dilutrion. Dilution was done directly before pipetting into the donor compartment. Samples for HPLC analysis were withdrawn directly after applying the drug containing dilutions (t=0min) and after 30, 60, 90 and 120 min. For each sample point 0.5 mL of acceptor medium (HBSS containing 10mM HEPES pH7.4) were withdrawn and replaced by fresh acceptor medium.

2.2.14.3 TEER measurements

Transepithelial electrical resistance (TEER) was measured via a chopstick electrode (Millicell ERS, Millipore, Bedford, USA). TEER values were taken in culture medium as described earlier. For permeation tests only wells with TEER $> 600\ \Omega/cm^2$ were used. Before starting the experiments the wells were incubated for 20 min. in transport medium, i.e. FaSSIF or FaSSIFblank pH 6.5 (600 µL) on the apical side, HBSS containing 10mM HEPES pH7.4 (1.5 mL) on the basolateral side. Teer values were taken at the start (t=0 min) and the end (t=120 min) of the experiments.

2.2.15 Animal studies

2.2.15.1 Preparation of test formulations

Nanoscopic test carriers were manufactured as described in the respective section. Prior to administration the formulations were diluted to a concentration of 0.6214 mg/mL (corresponding to 145 mg API per 70 kg body weight) with bidistilled water. The drug substance reference formulation was manufactured as follows: 0.5 g Methocel K4M, 0.055 g Tween 20 and 62.14 mg fenofibrate were weighed into a glass beaker. About 80 ml were added and the mixture was stirred for 4 hours. The mixture is transfered quantitatively into a 100 mL volumetric flask and the flask filled up to mark.

2.2.15.2 Sample collection

1.0 ml of each of the 6 test formulations was administered to fasted, male Wistar rats (300 g) by gavage. 4 animals were treated per formulation. Blood samples were withdrawn 0,5, 1, 2, 3, 8, and 24 h after administration. For sample collection 100 µL blood was taken at each sample point from the eyeground of a rat and added to 20 µl EDTA-solution (12 mg/mL in water). Rats were anesthesized before every treatment with isoflurane. The mixture was centrifuged for 6 min in a Eppendorf® 5415D centrifuge (Eppendorf AG, Hamburg, Germany) at 16,100 g. The supernatant plasma was transferred into 500 µl Eppendorff® caps and stored at -25°C until analysis. Rats were fed after the 8 h sample collection.

2.2.15.3 LC-MS analysis

50 µL plasma samples were spiked with 100 µL internal standard mycophenolic acid (10 mg/L in methanol) and extracted two times with n-butyl chloride. The organic phases were pooled and dried under nitrogen in an evaporator (Fa. Liebisch, Germany). The sample was then dissolved in eluent A.

Samples were analyzed via LC-MS applying the conditions summarized in Tab. 2.5.

MS conditions were as follows:

Table 2.7: MS detector conditions for the detection of fenofibric acid and internal standard (mycophenolic acid)

substance	eduction [m/z]	production [m/z]	Dwell time [s]	Cone [V]	Collision [V]
Fenofibric acid (FFA)	317.2	231	0.3	60	15
Mycophenolic acid	319.1	191	0.3	45	21

2.2.15.4 Data treatment

Calculation of AUC, Cmax and Tmax was done on Topfit® Modeling Software. AUC was determined according to the trapezoidal method. Statistical tests as well as part of the figures were done on SigmaPlot® 10.0 (Systat Software Inc., USA). Other drawings and figures were created via Microsoft Excel®.

Table 2.5: LC conditions for MS analysis of fenofibric acid plasma samples

Eluent A	25mM ammonium acetate buffer/methanol 40/60 (v/v) pH 3,6		
Eluent B	methanol		
Gradient	time [min]	A (%)	B (%)
	0	30	70
	2.1	30	70
	3.1	0	100
	5.1	0	100
	5.2	30	70
	7.5	30	70
Instrument	Agilent 2200 series HPLC (Agilent, Germany)		
	Quattro-Ultima detector (Waters, Eschborn, Germany)		
	Prontosil C18 column (10x4,6mm ; 3µm)		
Extraction medium	25 mM ammonium acetate buffer/methanol 40/60 (v/v) pH 3.6		
Flow rate	0.7 mL/min		
LOQ	10 µg/L		
Method linearity	0 µg/L -1000 µg/L VK:5 % (50 µg/L)-8 % (10 µg/l)		

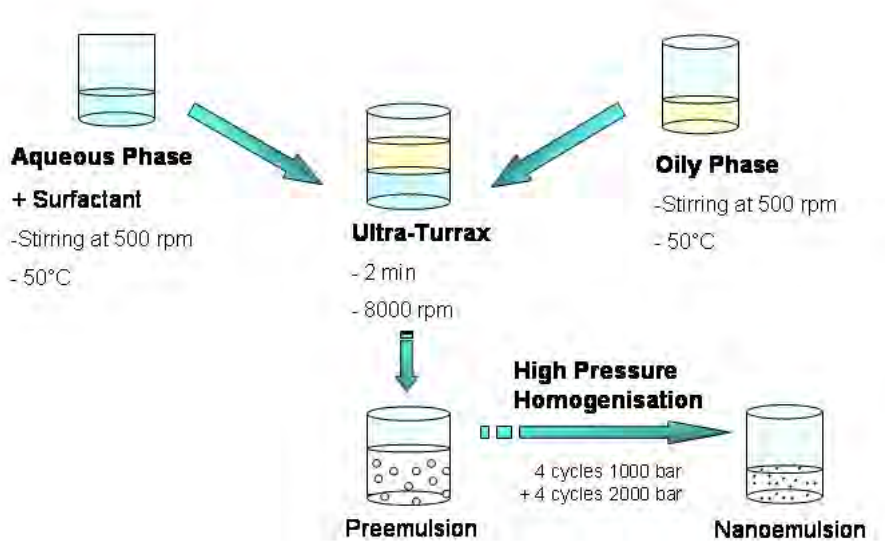

Figure 2.3.1: Preparation scheme of nanoemulsions via high presure homogenisation process

2.3 Manufacturing methods

2.3.1 High pressure homogenisation

High pressure homogenisation was performed on a Avestin Emulsiflex-C3 (Avestin Inc. Ottawa, Canada) applying standard in house air pressure supply (max. pressure 6 bar) for gap tuning.

Preparation of nanoemulsions containing 20 mg/mL fenofibrate (50 mL batch):

2.00 g of fenofibrate were weighed into glass beaker and 20 mL of Miglyol added. The mixture was stirred on a magnetic stirrer at 50°C until all solid was dissolved and 50°C reached. 1.00 g of surfactant is weighed in another glass beaker and 40 mL of bidistilled water added. The mixture is stirred at 50°C until a clear solution is obtained. Then 10 mL of the ff-containing oil is added to the aqueous solution and the mixture is homogenized with an Ultra Turrax (IKA T-25, IKA Werke GmbH, Staufen, Germany) at 8000 rpm for 2 min. The obtained coarse emulsion is homogenized with the high pressure homogenizer for 4 cycles at 1000 bar and 4 cycles at 2000 bar (see Fig. 2.3.1). An equivalent procedure was applied for API free nanoemulsions except for that no fenofibrate was added to the Miglyol.

2.3.2 Lyophilisation

2.3.2.1 Lyophilisation of nanoemulsions

Freezedrying of nanoemulsions was performed on a Tiny-LYO® (HOF Sonderanlagenbau, Germany) according to the protocol shown in 2.8. 2.0 mL emulsion were filled in a 30 mL lyophilisation vial (Schott, Germany) and a cap was mounted. After secondary drying the vials were closed under vaccuum. Then the process chamber was flushed with nitrogen.

Table 2.8: Protocol for lyophilisation of nanoemulsions

	Time [min]	Temperature [°C]	Pressure [bar]
Load	5	20	ambient
Freezing	210	-50	ambient
Primary drying	7200	-40	0.5 E-3
Secondary drying	2880	20	0.25 E-3

2.3.3 Wet milling

Two types of labscale bead mills were applied for wet grinding experiments. For small scale experiments (150 mg - 4.00 g slurry mass) the planetary ball mill Fritsch Pulverisette P7 classic line (Frisch GmbH, Idar-Oberstein, Germany) equipped with 12 mL zirkonium oxide milling jars was used (Fig. 2.3.2). Experiments in a larger scale (60g - 250 g slurry mass) were conducted on an agitator ball mill from WAB, type Dynomill RL (Willy A. Bachofen AG, Muttenz, Switzerland). Product cooling in agitator ball milling processes was accomplished by an air-cooled cryostat (Lauda WK4600, Lauda GmbH, Germany).

Standard grinding media for wet-milling applications were applied from different manufacurers. Zirkonium Silicate beads (0.1-0.2 mm, 0.2-0.3 mm and 1 mm diameter) were purchased from Fritsch, but substituted against low abrasion beads from Sigmund Lindner (ZYP 0.1-0.2 mm, 0.2-0.3 mm) for product contamination issues. For comparison to standard Zirkonia media new types of hardened polystyrene beads were purchased from Glen Mills (Glen Mills Inc. Clifton, USA) and Norstone (Norstone Inc., Wyncote, USA). Table 2.9 gives an overview over grinding media applied and their physical characteristics.

Table 2.9: Grinding media for wetmilling applications

	Glenmills GM2	Norstone Nor80150	Fritsch Zirconium silicate	Sigmund Lindner SiLi ZYP*
Size range [µm]	150-250	80-150	100-200/200-300/1000	100-200/200-300
Density [g/cm3]	1.05	1.05	6.07	6.06
Hardness [HV or GPa]	9.49 GPa	7.58 GPa	13.0 HV1	1,200 HV/215 GPa

*[101]

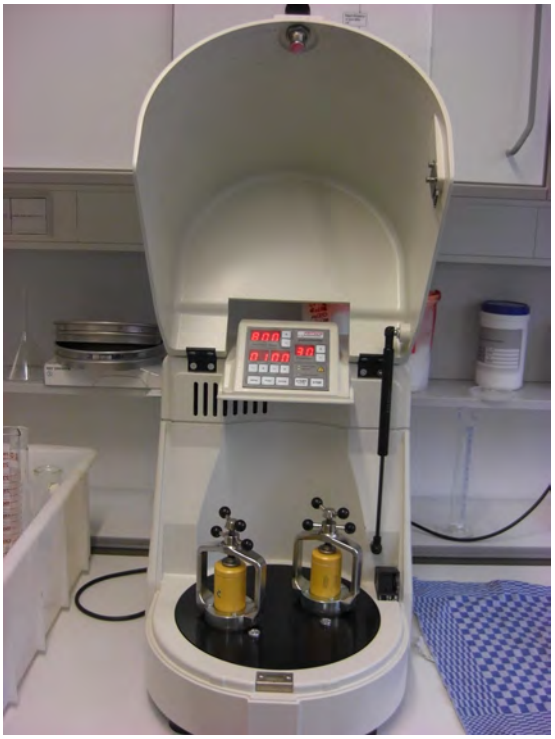

Figure 2.3.2: Fritsch Pulverisette P7 classic line® planetary ball mill

Milling procedure on planetary ball mill:

Respective milling beads are directly weighed into the jars. The required amounts of stabilizer and drug substance are weighed on a precision balance and added to the jars. Finally, an appropriate amount of bidistilled water is fillied into the jars to yield target drug concentration of the suspension. Due to excessive heat impact during the milling trials all tests on the planetary mills are run in a cycle mode, i.e. pauses are inserted. A milling protocol is applied where 30 s of millling is alternated by 30 s of rest in order to cool the sample. If not stated otherwise this milling protocol is applied.

Milling procedure on agitator ball mill:

The required amount of milling beads is to be inserted into the milling chamber during mounting the mill. A slurry containing the respective drug substance and stabilizers is prepared by weighing the API and stabilizers into a glass beaker, adding the required amount of bidistilled water and stirring the dispersion on a magnetic stirrer until all stabilizer is dissolved. The Dynomill RL (Fig. 2.3.3) is equipped with a 79.6 mL silicium carbide milling chamber and a patented Dyno accelerator® instead of standard agitating discs for effective high energy milling. If not stated otherwise batch sizes of 100 g suspension were applied. All samples were measured within one hour after preparation.

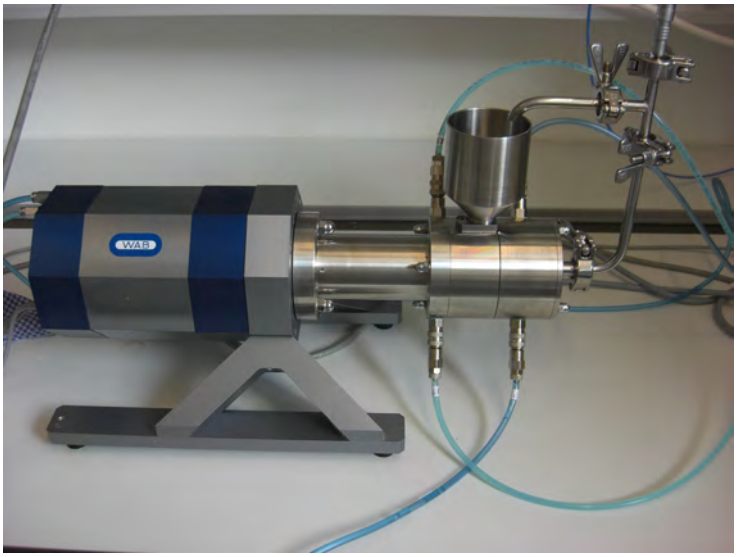

Figure 2.3.3: WAB Dynomill RL® agitator ball mill

3 Results

3.1 Cyclodextrin inclusion complexes

Interactions between cyclodextrins and guest molecules are intensively investigated in literature. As pointed out in the introduction section various factors have been described to influence the loading efficiency of these complexes, e.g. preparation technique, temperature, pH, ionic strength etc. Aim of this study was to compare different preparation techniques for two beta-cyclodextrins widely used in early formulation development. Furthermore the influence of biorelevant media on the complexation behavior should be investigated. In terms of reducing the amount of variables test samples were prepared in a molar ratio of 1:2 (API:cyclodextrin). The ratio was chosen to enable also non-inclusion related interactions between the host and the guest molecule via offering a surplus of host. Water was chosen to minimize the effect of ionic strength and pH on inclusion efficiency.

3.1.1 Influence of Tween® 20 on cyclodextrin inclusion

Several authors have shown the interference of surfactants and cyclodextrins in the solubilisation of drug substances. Enhancing as well as solubility decreasing effects are described for several CD-surfactant multicomponent mixtures. To elucidate the influence of surfactants on the binding efficiency of the three test substances different amounts of Tween® 20 were added to 50 mM cyclodextrin solutions in PBS pH 7.4. Tween® 20 was chosen as a model surfactant because of its frequent utilisation in preformulation development as a single solubilizer or in combination with others. At Merck Serono, Tween® 20 is one of the most common additives to facilitate wetting and dispersion of poorly soluble compounds. Concentrations below and above the CMC of Tween® 20 ($c = 0.1\,mg/mL$) were chosen to detect potential competitive or synergistic mechanisms either hindering the interaction between API and cyclodextrin or enhancing total solubility.

It is remarkable that within the concentraton range of Tween 20 tested no significant ($p < 0.1$) influence on the solubilisation of the three APIs could be detected (Fig. 3.1.1). It is questionable wether a small effect can not be detected due to the poor reproducibility of measurements. Unfortunately, reproducibility could not be enhanced with the small scale

methods applicable in preformulation development. In any case Tween® 20 did not have any major impact upon solubility for the tested substances.

3.1.2 Studies on inclusion in biorelevant media

Interactions between model compounds and the biorelevant media FaSSIF and FeSSIF were studied according to the method proposed by Higuchi et al [102]. An excess of API was incubated with different amounts of hydroxypropyl-beta-cyclodextrin (0 - 50 mM) in the respective medium at 37°C for 48 h. The resulting phase solubility curves are compared with the solubilisation behavior in pure water. Figure 3.1.2 depicts the solubility of the three model compounds in water, FaSSIF and FeSSIF, respectively.

It can be clearly seen that the solubility behavior is affected differently for different drug compounds. Whereas the total solubility of ketoconazole is highly enhanced in presence of FeSSIF the solubility of griseofulvin drops to a level 70 fold below maximum solubility at 50 mM CD in water in presence of bile salts, lecithin and buffer components. Maximum solubility is again increasing in FeSSIF, but still around 8 fold below the water/kleptose solubility. It can be stated that phase solubility of griseofulvin is highly affected by components of the biosimulating media as the increase of cyclodextrin concentration is not transferred into significantly higher drug solubility in these media. Regarding shape and slope of the curves one can detect flat slopes for griseofulvin and fenofibrate with increasing cyclodextrin molarity in all tested media except for water whereas for ketoconazole one can see a shift of solubility onset from 0 mM cyclodextrin in water to around 10mM in FaSSIF and FeSSIF. Generally, the solubility enhancement is highest for ketoconazole. Being a weak base the compound exhibits pH dependent solubility in the pH range investigated (5 to 6.5) with increasing solubility at lower pH values.

To elucidate whether the dramatic changes in phase solubility are due to surface active substances (sodium taurocholate, lecithin) FeSSIFblank, i.e. buffer without the surface active substances was used for phase solubility trials. Figure 3.1.3 displays the results in FeSSIF buffer. Generally, solubilities are higher in FeSSIF because of the presence of surface active ingredients. More remarkably, the shape of the plot for ketoconazole is hardly affected, only absolute values are higher for FeSSIF as compared to FeSSIFblank. The interference in solubility enhancement at 10 mM CD is therefore rather influenced by the presence of salts and pH than by surface active components.

Several mathematical parameters to compare the efficiency of complexation are used in literature. One very common is Eq. 3.1.1 where $K_{1:1}$is the stability constant between a drug substance and a CD and depicted in M^{-1}, $S_0$the intrinisic solubility without CD, and Slope the slope of the line that is obtained when plotting the molar concentrations of CD and drug substance in a diagram [70]. $K_{1:1}$is valid when one drug molecule (D) forms a

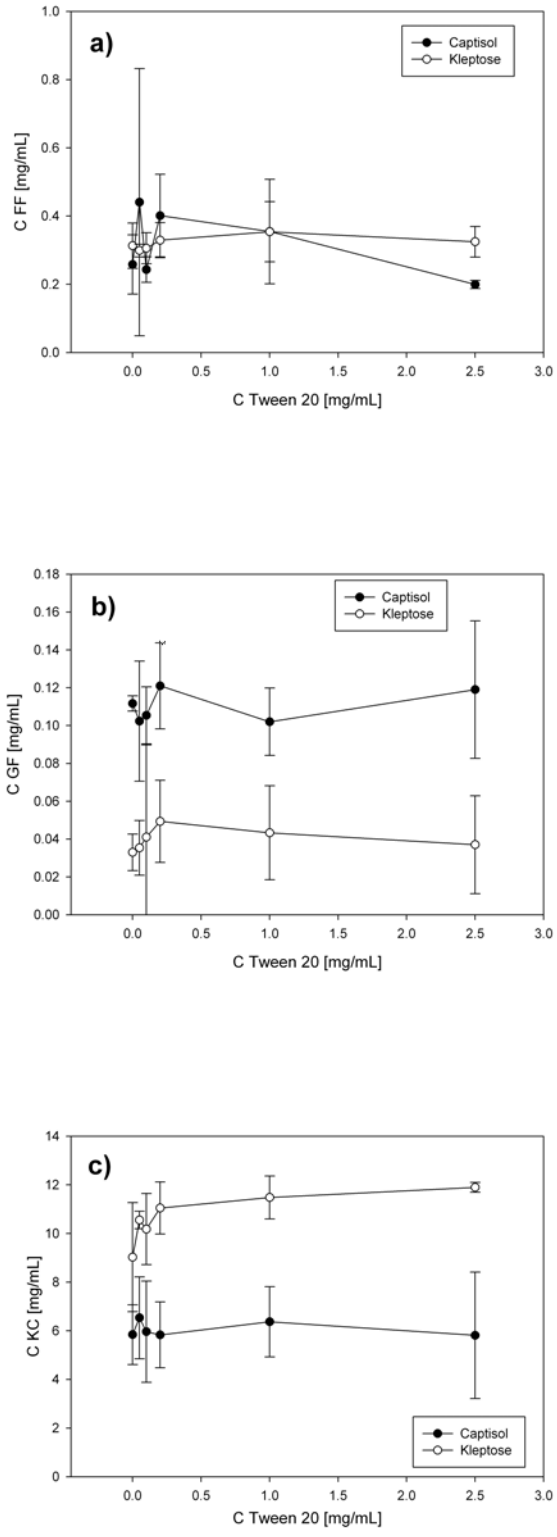

Figure 3.1.1: Influence of Tween® 20 on solubility of model compounds a) fenofibrate b) griseofulvin c) ketoconazole in cyclodextrins, mean±sd, n=6. Solubilities were determined after 24h strirring in the presence of either 50mM Captisol® or Kleptose® in PBS pH 7.4.

complex with one cyclodextrin molecule (CD). In ideal solvents S_0 should correspond to the solubilty given by the intercept of the y - axis in phase solubility plots. Very often this is not the case as it can easily be seen in the lines in Figure 3.1.2. In consequence this leads to wrong estimations of the stability constants that are not comparable to e.g. other CD types. Loftsson is therefore proposing a parameter that is independent from substance solubility characteristics [103, 70]. The so called complexation efficiency (CE) is describing either the slope of the phase-solubility profile or the complex to free cyclodextrin concentration ratio (Equ.3.1.2). [D/CD] is the concentration of dissolved complex, [CD] the concentration of dissolved CD. CE-values can be used to compare the solubilizing effects of various cyclodextrins, to calculate the drug/cyclodextrin complex: free cyclodextrin molar ratio and to study the influence of different pharmaceutical excipients (also bile salts and lecithins) on the solubilization.

$$K_{1:1} = \frac{Slope}{S_0(1 - Slope)} \tag{3.1.1}$$

$$CE = S_0 K_{1:1} = [D/CD] \,/\, [CD] = \frac{Slope}{1 - Slope} \tag{3.1.2}$$

Table 3.1 depicts the CE values for the three drug substances and Kleptose® in different media. For ketoconazole one can clearly detect complexation enhancing effects due to incubation medium. Interestingly, CE is similar in FaSSIF and FeSSIFblank which indicates that pH as well as surfactants have enhancing effects. Griseofulvin is giving an opposite picture. Complexation efficiency is obviously lowered in presence of lower pH (see Figure 3.1.3). The reason for this is unclear as griseofulvin is a neutral substance and solubility should be pH-independent. A high content of sodium taurocholate + lecithin is then again fostering inclusion again in the FeSSIF medium when comparing the solubilities to the ones measured in the pure FeSSIFblank buffer medium. Fenofibrate shows the lowest interaction with the CD. Despite being a neutral compound, slight solubility enhancement effects can be seen when comparing FeSSIFblank and water as dispersion media. An increased surfactant content is then suppressing the inclusion again as lower CE values for FeSSIF indicate (Table 3.1).

Table 3.1: Complexation efficiencies for drug-Kleptose complexes in different media

API	water	FaSSIF	FeSSIF	FeSSIFblank
Fenofibrate	0.0021	0.0048	0.0037	0.0045
Griseofulvine	0.1745	0.0009	0.0047	0.0007
Ketoconazole	0.0556	0.1770	0.3492	0.1675

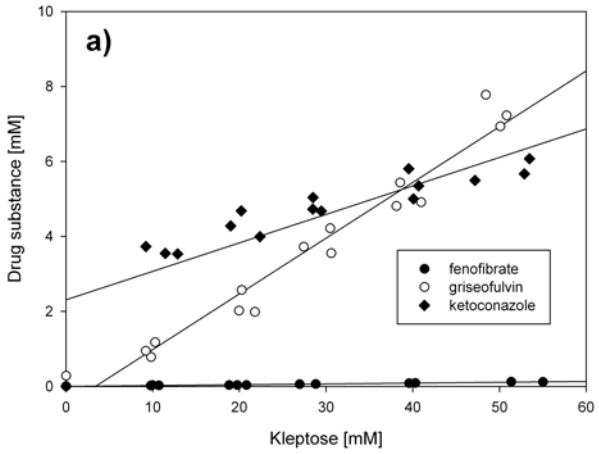

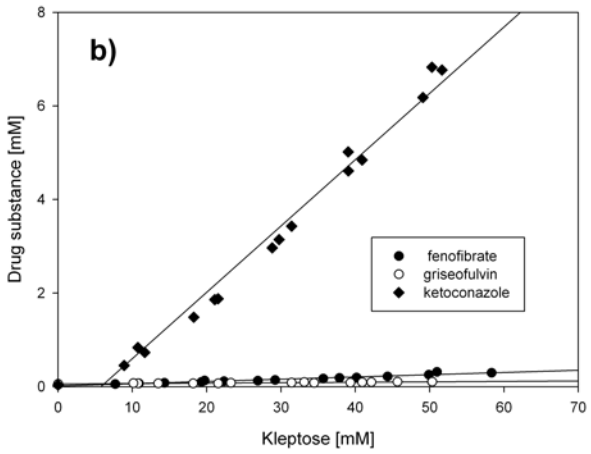

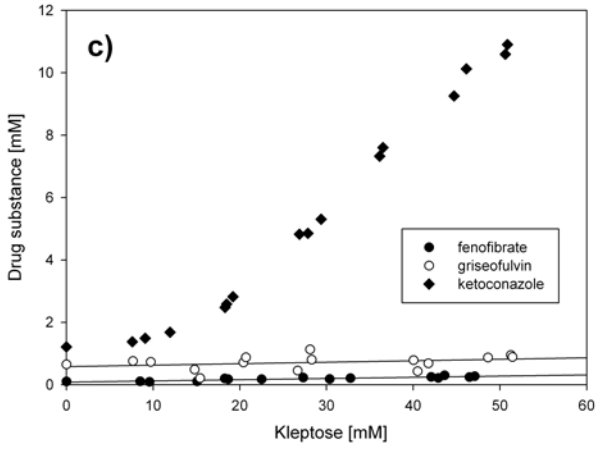

Figure 3.1.2: Phase solubility plots for fenofibrate, griseofulvine and ketoconazole in a) water, b) FaSSIF and c) FeSSIF (37°C, n=3, all values plotted)

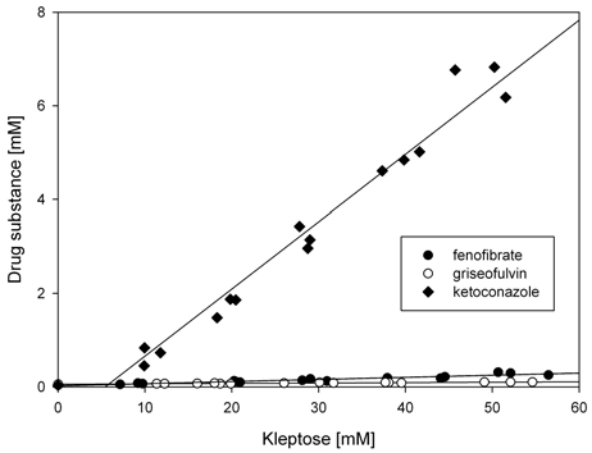

Figure 3.1.3: Phase solubility in FeSSIFblank (37°C, n=3, all values plotted)

3.2 Investigation of a model microemulsion

In preclinical development at Merck several SEDDS and SMEDDS systems were developped during the time frame of this work. Within the scope of the thesis emphasis was put on one system that attracted special interest due to the slow emulsification kinetics when dispersed in aqueous media. This microemulsion preconcentrate consisted of 60% (w/w) Solutol® HS15, 20% /w/w) Capryol® 90, 20% (w/w) Miglyol® 812. In the following different aspects of physicochemical characterisation of this model microemulsion will be presented, the system will be denoted with the acronym ME.

3.2.1 Solubility in surfactants and oils

Solubility tests were performed as described in section 2.2.1. High solubilities were found in both soybean oil as example for a long chain triglyceride mixture as well as in medium chain triglycerides (Miglyol® 812). Notably fenofibrate exhibits high solubility in oils as well as in surfactants with a clear trend towards higher solubility in more lipophilic vehicles. Solubility of the SMEDDS mixture described above was determined to be 132.5±6.3mg. Solubility enhancement is therefore obviously synergistic, as adding the solubilities in the respective components lead to a lower „theoretical“ solubility value.

3.2.2 Drug loading of model microemulsion

Drug loading was performed via mixing the respective model drug (600mg/3mL) in liquid preconcentrate at 25°C under stirring via a magnetic stirrer (500 rpm). After 24 h of stirring the respective samples were centrifuged and the supernatant assessed via HPLC. The highly

Table 3.2: Solubility of FF in different surfactants and oils, mean±sd, n=3

Excipient	Solubility [mg/g]
Migyol 812	105.6±4.4
Soybean oil	87.3±8.1
Labrasol	85.3±4.7
Solutol HS15	87.2±10.2
Cremophor RH40	80.1±8.7
Capryol 90	121.1±1.4

Table 3.3: Solubilities of different model drugs in ME SMEDDS, n=3, mean±sd

API	FF	GF	KC
Conc [mg/mL]	134.1±0.6	6.5±0.9	17.1±0.6

lipophilic model drug fenofibrate displays expectedly highest solubility within the lipidic matrix, solubilities of GF and KC are determined to significantly lower levels.

3.2.3 Physical characterisation of ME

One characterisation of microemulsions is the titration of the main relevant components in a phase diagram and the respective analysis of the physical state of the mixture. Normally the latter is done optically after a suitable equlibration time. For the model system tested a ternary phase diagram with the three parameters Surfactant/Cosurfactant, MCT and water was investigated. The ratio between surfactant (Solutol®) and cosurfactant (Capryol® 90) was kept constant at a level of 3:1 (w/w) because preliminary tests revealed that physical stability and formation of Type III systems were compromised when lower ratios were applied and MCT was introduced into the composition. On the other hand higher S/CoS ratios between 5:1 and 8:1 rather led to the formaton of turbid emulsions when introducing significant amounts of Miglyol 812. The chosen composition (Fig. 3.2.1) is stable upon dispersion over a wide range of water content, starting from app. 50 % (w/w) water. It must be noted that also below this threshold optically clear systems are obtained which - due to the aqueous fraction and the absence of measurable particles within DLS measurements - are rather to be attributed to bicontinuous microemulsion phases. The results further indicate that microemulsion systems are obtained at different water:SMEDDS ratios with lipid:surfactant ratios of up to 1:3.

Stability of microemulsion droplets in biosimulating media was assessed using DLS measurements. In a first set of experiments size distributions and surface charges of microemulsion droplets in water, SGFsp and SIFsp were measured after 2h incubation at 37°C (Tab.3.5). It can be clearly seen that low pH exerts a negative influence on PSD of the the droplets. Also in SIF at a pH 6.8 the morphology is affected, notably the size of

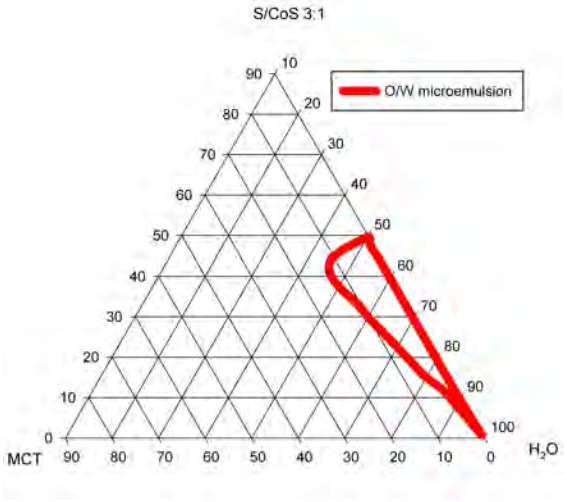

Figure 3.2.1: Phase diagram for ME at 37°C, S/CoS ratio depicted in w/w

Table 3.4: Size distributions of model microemulsion in FaSSIF and FeSSIF, mean±sd of three preparations

	Z-ave 0h [nm]	PDI 0h	Z-ave 2h [nm]	PDI 2h	Z-ave 24h [nm]	PDI 24h
Water	23.6±0.2	0.031±0.004	22.7±0.3	0.027±0.004	23.8±0.5	0.032±0.004
FaSSIF	52.2±2.6	0.36±0.06	45.2±1.2	0.36±0.04	24.0±4.0	0.22±0.08
FeSSIF	30.2±9.1	0.39±0.16	22.4±2.0	0.32±0.04	35.6±5.5	0.3±0.07

particles decreases concomitant with an increase in PDI. Despite large deviations in terms of salt content and pH zeta potentials do not significantly vary between the three test media.

In another set of experiments the influence of biorelevant media containing bile salts and lecithins is investigated (Tab. 3.4). PSD was measured after 0, 2 and 24 h. In comparison to pure FaSSIF (73±0.6 nm, PDI 0.16±0.01) and FeSSIF (34.7±0.2 nm, PDI 0.15±0.01) mean particle sizes shift towards smaller particles with broader size distributions which is most probably due to the mixing of the different size fractions. Notably, PSD substantially decreases in FaSSIF whereas size distributions in water as well as FeSSIF stay constant.

3.2.3.1 Light microscopy

As already mentioned macroscopic studies on the model emulsion revealed a slow emulsification process upon the addition of aqueous media. When analyzing the process via

Table 3.5: Size distributions and zeta potential of model microemulsion in different aqueous media after 2h, dilution 1:10, mean±sd of three preparations

Dispersant	Z-ave [nm]	PDI	Zeta potential [mV]
Bidistilled water	24.1±0.3	0.031±0.006	-30.8±2.9
SGFsp	35.8±0.8	0.189±0.057	-29.5±2.8
SIFsp	17.8±0.2	0.160±0.006	-26.5±2.5

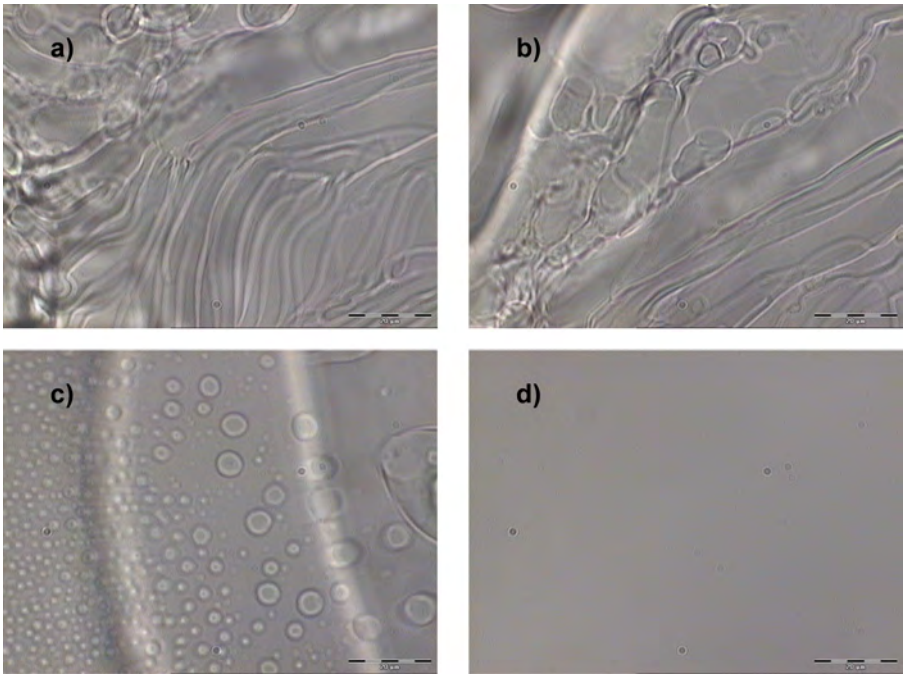

Figure 3.2.2: Monitoring different stages of ME emulsification in water: a) directly after addition of H_2O b) 2 min c) 5 min d) 10 min, 100µL of preconcentrate were placed on a glass slide and 1 mL of water added directly besides the oily droplet, microphotographs were recorded at 100x magnification, size bar represent 20µm

light microscopy different stages until obtaining a clear isotropic solution can be detected. Figure 3.2.2 is depicting different stages in a 10 min. dispersion process without agitation in bidistilled water. A drop of preconcenrate was placed on a glass slide and one mL of water right at the left side of the oil droplet. The mass ratio between ME preconcentrate and SGF was 1:10. The focal plane was adjusted for each photograph. Picture a) is showing the interfacial region between aqueous and lipidic phase. The visible structure is non-ordered and suggests bicontinuous phase behavior due to the unshaped surface curvature. Droplet-like structures are dissociating from the interface after approx. 2 min after combining the two phases (b). In picture c) clearly droplet structures can be distinguished. As the flow direction is from the right to the left side of each photograph (from oily to aqueous phase), a decrase in droplet size is visible with increasing aqueous dilution. Droplet sizes decrease further until a optically transparent solution is obtained after app. 10 min (d). The results suggest a kinetically driven formation of microemulsion droplets as indicated in the clear isotropic solution obtained after 10 min. dispersion time.

3.2.3.2 Transmission electron microscopy

Cryo TEM micrographs were recorded readily formed microemulsions in distilled water, SGFsp and SIFsp. Simulated media were chosen to investigate the structure upon changes in salt and pH in the test medium. The preconcentrate: medium ratio was 1:10 in all

pictures. Figure 3.2.3 is depicting the morphology of particles in the three different media. The pictures reveal spherical to aspherically shaped particles and different degrees of dispersity depending on the dispersant applied. Whereas monodisperse emulsions are obtained in water, more irregular shaped particles are visible when applying SGF (see B). In SIF comparatively large particles of around 50 nm can be detected asides small particles in the 15-20 nm range. Larger particles show an aggregate or fused droplet like appearance in SGF and SIF containing media. The findings correlate well with the obtained DLS data shown in Table 3.5.

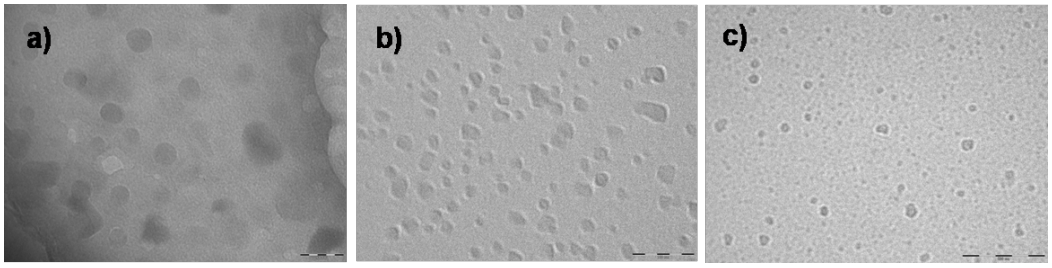

Figure 3.2.3: CryoTEM micrographs of me in a) water b) SGF c) SIF (please note different scale bars: a) 50 nm, b) and c) 200 nm)

3.2.4 SANS studies on kinetic behavior of model microemulsion

Fig. 3.2.5 and 3.2.6 are giving an overview over the intensity profiles of Solutol® 10% and ME 10% in D_2O. As expected the size and scattering profile significantly differs between the two types of samples. For an adequate data treatment several structure models have been probed and several assumptions needed to be made. For model dependent calculations form factors considering a hard sphere droplet, a micellar structure with a rigid core (Sphere+Chains model) and a customized form factor were applied. The two latter are assuming a hydrophilic droplet shell originating from the PEG660 part of Solutol® and a hydrophobic core composed of the oily components Miglyol®, Capryol® and the hydrophobic part of Solutol® (Fig. 3.2.4). Depending on the model the oily core is considered to be more or less homogeneous for neutron scattering which means that oily core and oily surfactant interface are considered to be one non-distinguishable sphere, denominated as R0. In the other case a Miglyol® core is assumed that can be discerned from an surfactant shell composed of Capryol® and the lipophilic part of Solutol®. Considering the findings in TEM where rather monodisperse and homogeneous distributions were found in the water samples particle sizes were assumed to follow a log-normal distribution. Additionally correction for sample setup and background noise was done.

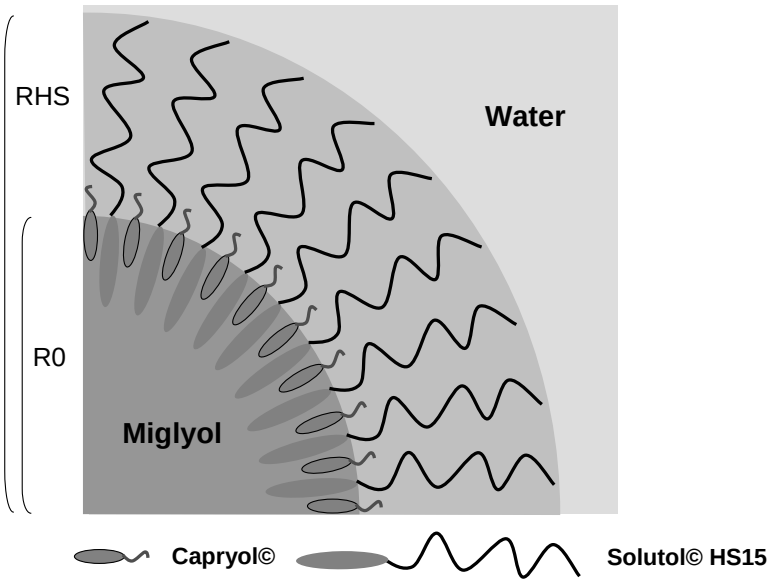

Figure 3.2.4: Composition of ME droplets, assumption on distribution of surfactant and cosurfactant at the oil-water interface, R0 denominates the radius of the lipophilic core, RHS is the hard-sphere repulsion radius of the droplet

In the following results are shown for 4% and 10% preconcentrate volume in D_2O. Figure 3.2.5 is giving the scattering vector Q versus scattering intensity I graphs for different time points after adding 10% Solutol to D_20. The first measurement was recorded after 30s, the last sample point defined after 20min. Scattering profiles tend to show more variation and noise at 30s and 120s especially at lower scattering angles. Profiles at 600 and 1200s are less noisy which can be easily explained by the fact that micelles are completely formed at these later time points and no larger Solutol droplets are present parallel to readily formed micelles. This fact also corresponds to the higher intensity recorded with increasing dissolution time: The increase in intensity is caused by a higher number of particles in the aqueous environment over time. When comparing the profiles for 4% and 10% microemulsion preconcentrate (Fig. 3.2.6 and 3.2.7) one can see similar trends towards higher particle intensity with increasing measurement time. Furthermore, the graphics reveal a different size and inner structure of Solutol micelles in early (30s) as well as at late (10min) measurement time points. The results indicate that no isolated Solutol micelles are detectable during the measurement. Taking a closer look at the Porod regions at scattering vectors of around 0.5 differences between 4% and 10% profiles can be identified. Whereas 4% samples show a flat decline of the scattering curve, samples with 10% preconcentrate

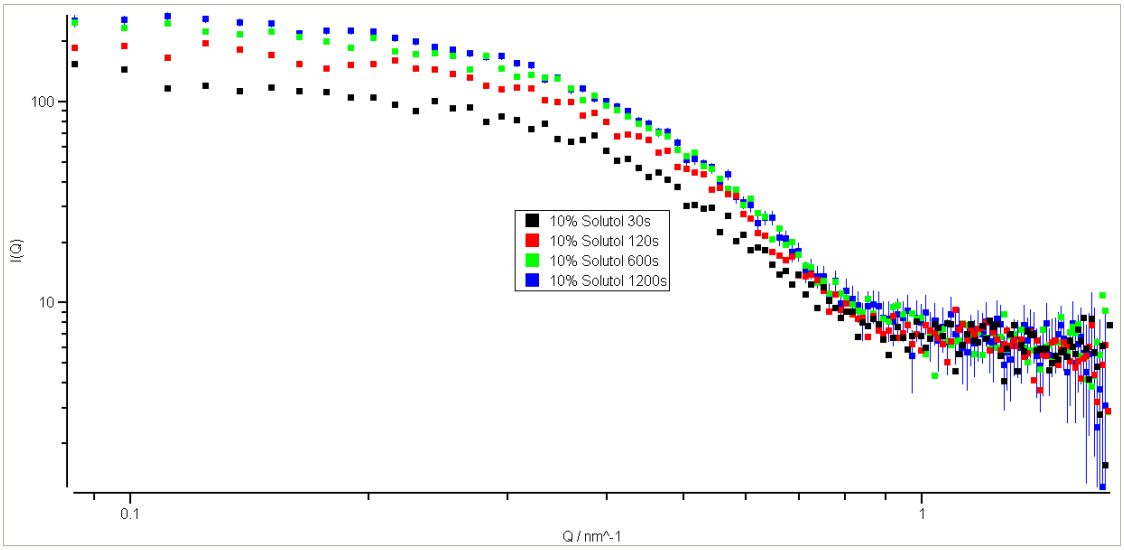

Figure 3.2.5: Scattering profiles of 10% Solutol® in water at different time points, 400 rpm spin

show a second maximum at 0.5nm^{-1}. When evaluating this maximum with a TeybnerStrey model for bicontinuous structures data suggest the copresence of bicontinuous structures with a breadth of app. 12 nm parallel to the detectable micellar structures. Naturally, intensities are higher in the 10% samples due to the higher load of lipid mass.

As outlined in the materials and methods section different models can be applied when assessing the scattering curves. As a more straightforward approach first a sphere model assuming structures similar to polymer micelles was applied. Figure 3.2.8 is giving a time resolved view on the most important fitting parameters on a 20 min time scale. Different developments can be seen for the two preconcentrate concentrations. At 4% solid fraction an increase in the hard sphere radius can be observed concomitantly with an decrease in $f_p$over time. The time scale for levelling of these two parameters is around 300s. Notably, core radius and radius of gyration stay constant over time what leads to the assumption that no re-ordering or size increase takes place in the oily core of the droplets. Remarkably, volume fractions f_p are overstimated both for 4% and 10% samples.

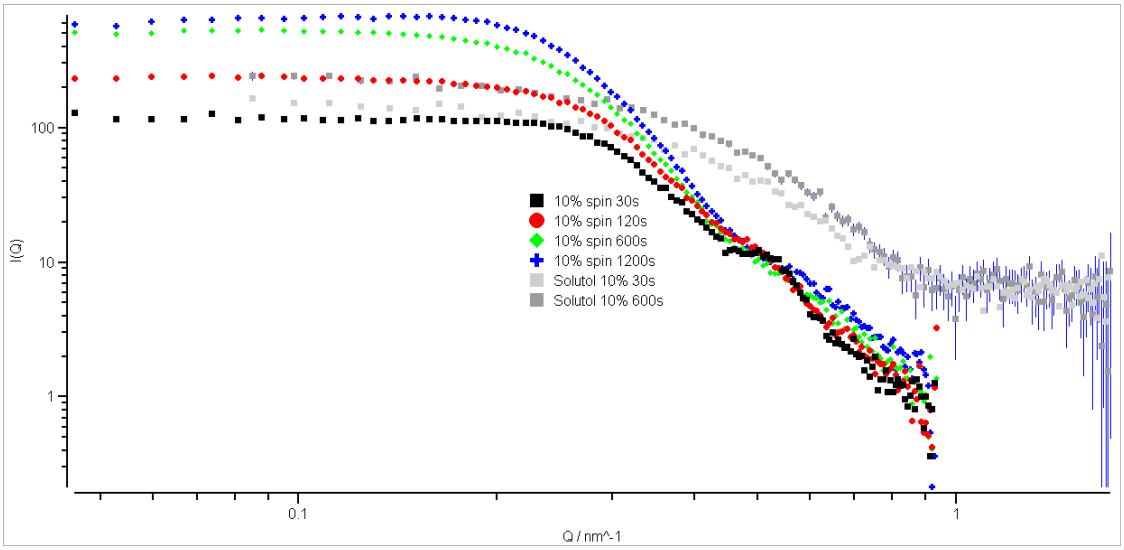

Figure 3.2.6: Scattering profiles of 10% ME in D_2O at different time points, 400 rpm spin, an increase of intensity with increasing time following dilution is visible, scattering patterns dramatically differ from that of pure Solutol micelles at all measurement time points, at Q=0.5 an addtional peak is suggesting the presence of addtional structures, most likely bicontinuous type

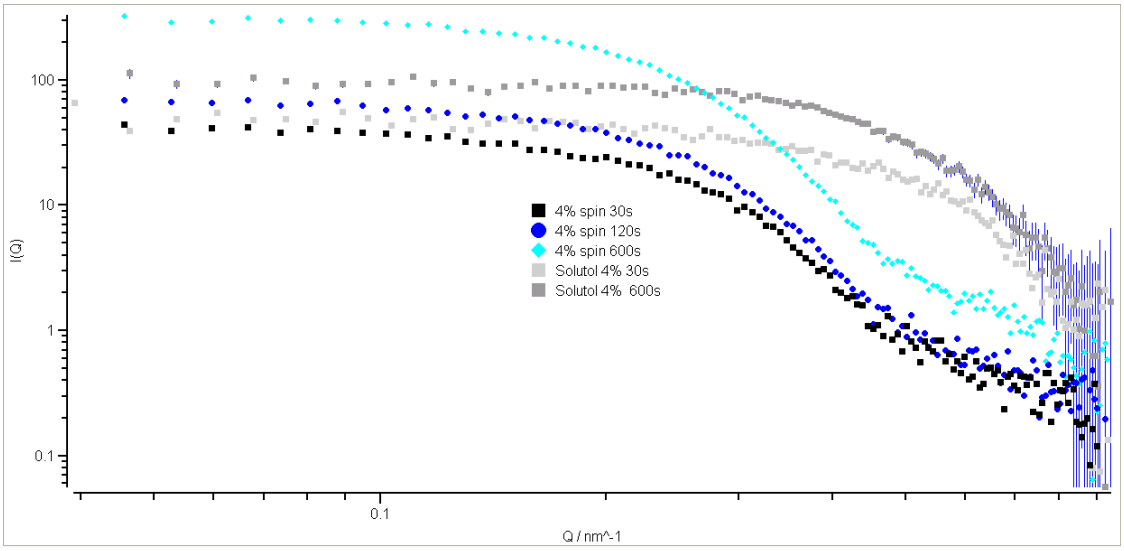

Figure 3.2.7: Scattering profiles of 4% ME in D_2O at different time points, 400 rpm spin, an increase of intensity with increasing time following dilution is visible, scattering patterns dramatically differ from that of pure Solutol micelles at all measurement time points

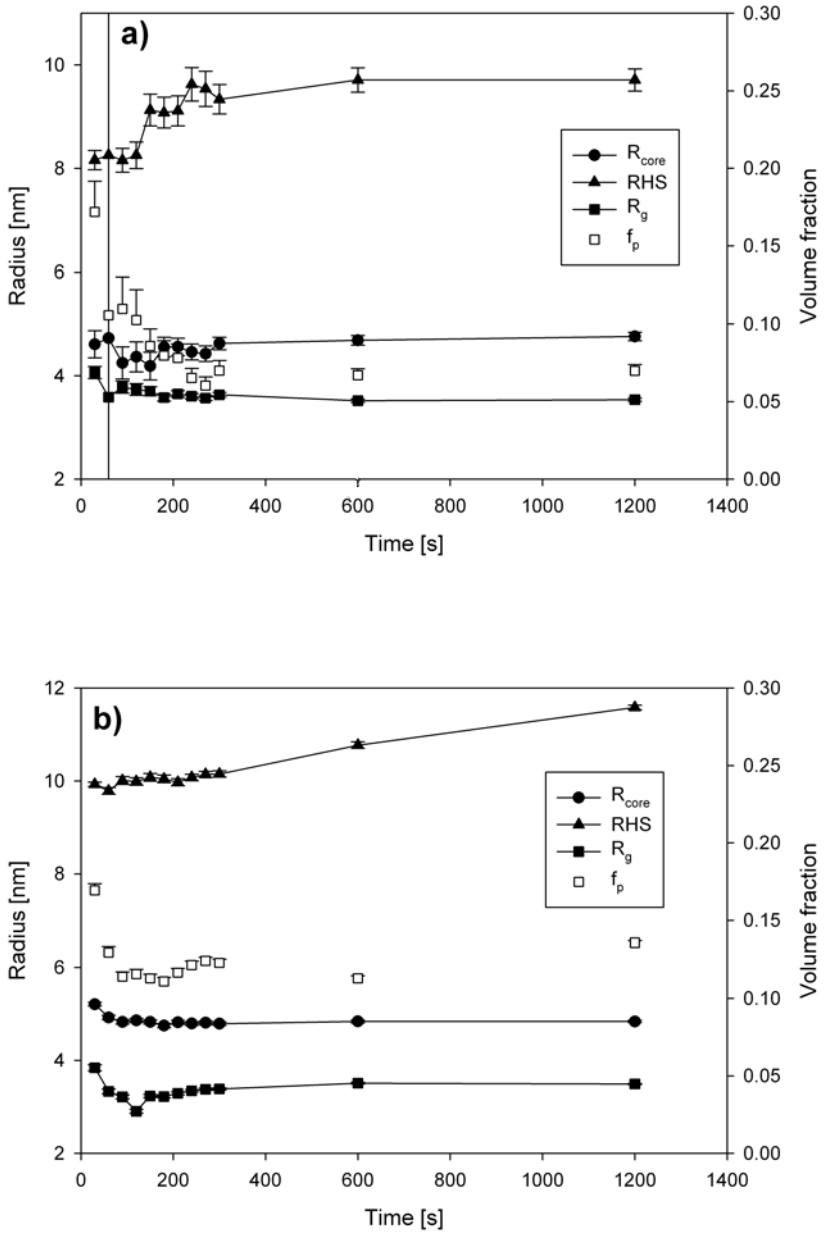

Figure 3.2.8: Fitting parameters for a) 4% preconcentrate in D_2O and b) 10% preconcentrate in D_2O at 400 rpm spin, results are shown for core radius R_{core}, radius of gyration R_g, hard sphere repulsion radius RHS and volume fraction f_p, fitting was done via the SPHERE+Chains(RW) model, mean+confidence interval

In the following scattering profiles were investigated via a more sophisticated model taking into consideration volume fractions and scattering parameters of the single components. The model is denominated as SolutolCapryolMiglyolMicelle (SCMM) and described in the materials and methods section. Due to the potential bias of the 10% preconcentrate samples via a supposed bicontinuous structure, only 4 % preconcentrate samples were simulated via this

	30s	300s	600s
x(Solutol)	0.119129 ± 129.473	0.566812 ± 419.621	0.661081 ± 186.239
x(Capryol)	0.737591 ± 800.8	0.222696 ± 328.477	0.241281 ± 67.9949
x(Miglyol)	0.172153 ± 186.944	0.214589 ± 317.881	0.243753 ± 68.6582

Table 3.6: Relative composition x of microemulsion droplets at different time points during emulsification, 4% preconcentrate at 400Hz spin, fitted value±confidence interval based on SCMM model, all other parameters in the model were fixed at values displayed in fig. 3.2.9

model. Figure 3.2.9 is giving the respective time resolved radii and sigma values for a 1200s monitoring. For this setting the volume fraction $f_p$was assumed to be constant at 3.6% as it is the case in reality. Here the following trend is visible: Whereas R_g remains constant over time, an increase of $R_{core}$and RHS is detectable within the first 200s of the emulsification process. Interestingly, all measurement points can be calculated by assuming a composition of 58% Solutol®, 21% Capryol® and 21% Miglyol®. On the other hand it gets evident from Figure 3.2.7 that fitting quality is rather poor for the first 4 measurement points. Only for RHS the conclusion can be drawn that the mean radius is significantly increasing. For the core and gyration radii observed changes are not to be regarded as significant. Also the size distribution sigma shows large confidence intervals indicating the scattering signals not solely originating from one spherical particle species. The results further indicate a superior goodness of fit for later time points during the measurement process. This corrobrates the assumption that at time points >200s microemulsions exhibit a uniform composition as hypothesized in the SCMM model.

In a third step the composition of the microemulsion droplets was fitted at constant radii and volume fraction. It was investigated if the data fit can be improved by adjusting the relative composition of the three components of the emulsion droplets. Fitting was terminated after 100 iterations. Table 3.6 is displaying the dimensionless volume fractions x at different time points. Two facts need to be discussed. First, the quality of fit is poor at all chosen data points despite meaningful correlations are obtained for fitting the dimensions of the spherical particles. Second, despite the compromises in prediction it might be suggested that the composition of particles in the beginning differ to some extent from the final particle composition after 5 min or 10 min. A more precise computation of the relative fractions is most probably hampered 1) by the similarity in scattering length of the the three different lipophilic species, namely Miglyol®, Capryol® and the lipophilic tail of Solutol® and 2) the comparatively low contrast within the hydrophilic shell of the droplets in relation to the lipophilic core.

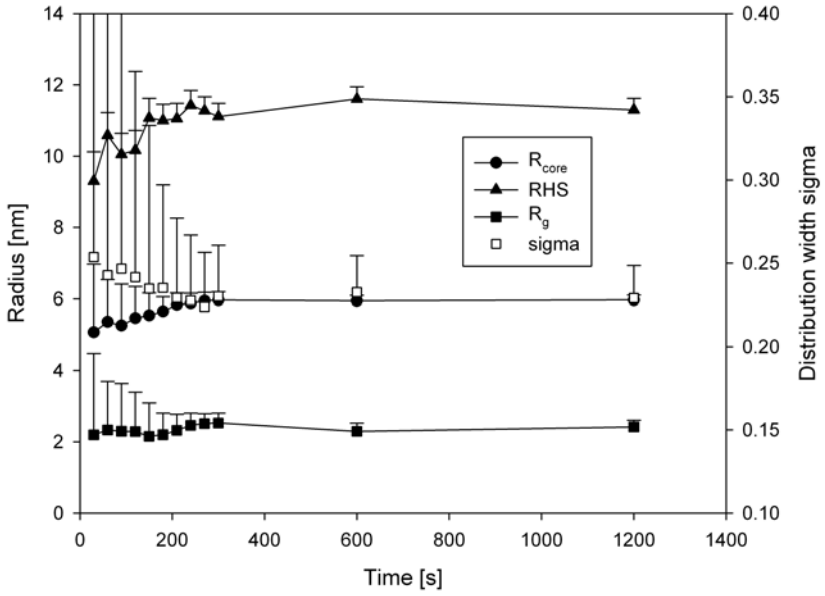

Figure 3.2.9: Fitting parameters for 4% preconcentrate in D_2O at 400 rpm spin applying the SCMM model, results are shown for core radius R_{core}, radius of gyration R_g, hard sphere repulsion radius RHS and the particle size distribution width sigma, mean+confidence interval

3.2.5 ITC studies on microemulsions

ITC was assessed as a tool to potentially resolve the kinetics of a microemulsion formation process as it is capable of recording the resulting heat signals upon dispersion in a time resolved manner. Nevertheless accurate dosing of the preconcentrate was critical and could not be accomplished at 25°C (results not shown). Also at 37°C no reproducible signals were obtained. Fig. 3.2.10 is depicting the power signal versus time for 20 consecutive injections. It can be seen that signal intensity varies and no clear trend in the decay of the signal towards base line can be obtained. Indeed, the application of very small injection volumina of the viscous agent is critical in ITC. A lack of reproducibility could therefore be expected. Higher injection volumes in contrast lead to signal intensities beyond the limit of detection and were therefore not feasible either.

In another set of experiments the kinetics was further slowed down by not agitating the preconcentrate-water mixture. Fig. 3.2.11 is displaying three consecutive injections of the preconcentrate. Signal intensities increase with every injection, in contrast the time to reach baseline equilibrium decreases with every injection. In addition, endothermic signals are observed after the first two injections. It must be noted that also the effects observed here lack in reproducibility and effects were only observed in two of three experiments. Interpretation must therefore done with caution.

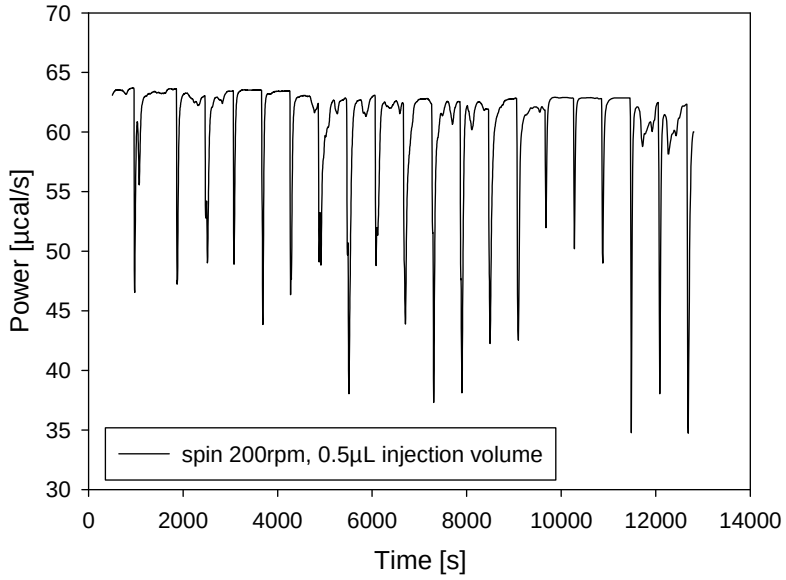

Figure 3.2.10: Microemulsion preconcentrate injected in H_20 at 37°C, the sample was stirred at 200 rpm, injection volume 0.5 µl each, injection interval 900 s

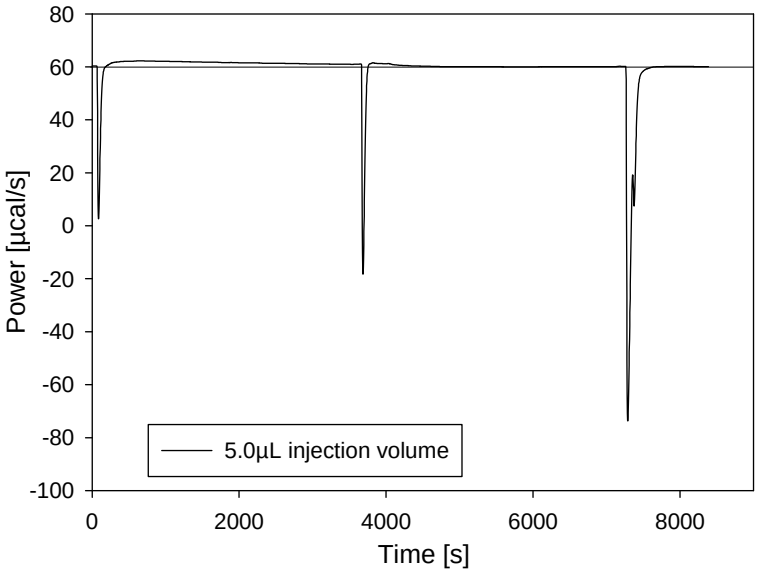

Figure 3.2.11: Microemulsion preconcentrate injected in H_20 at 37°C, sample not stirred, injection volume 5.0 µl each, injection interval 3600 s

3.3 Nanoemulsions

Pharmaceutical nanoemulsions are suitable carrier systems for the administration of highly lipophilic drugs. The use ranges from parenteral nutrition to the application in mucosal or parenteral vaccination. Due to their versatility in applications nanoemulsions display an ideal liquid carrier system for preclinical formulation development. Many preparation techniques are well described and investigated [104]. Therefore it is not within the scope of this work to investigate preparation techniques for nanoemulsions but to compare surfactants that are well established in the pharmaceutical field with novel sucrose esters. These were presented in detail in the introduction and are hitherto mainly applied in the food and cosmetics area. Nevertheless US Drug Master Files exist for SE Pharma grades [105]. Because applicability of these esters in parenteral medication is still unclarified and some issues might arise with regard to the hemolytic activity of sucrose esters, the focus of this work is set on peroral application. Therefore tasks relevant for parenteral drug delivery such as sterile filtration were not adressed. Instead shelf life stability and processability to the dry state (lyophilisation) were investigated and the results compared to excipients commonly applied in the pharmaceutical field. Furthermore the formulation feasibility with the lipophilic model drug fenofibrate was assessed. Fenofibrate was used as it offered the highest solubility in long and medium chain trigylcerides of all three model substances (see 3.2.1).

3.3.1 Physicochemical characterisation of nanoemulsions

3.3.1.1 Standard nanoemulsions

As shown in Figure 3.3.1 the particle sizes of standard emulsions range between 150 nm and 270 nm and increase with increasing fatty acid chain length and oil content. Emulsions applying lecithin exhibit larger particle size and broader PSD in comparison to Solutol® and Cremophor® emulsions. Furthermore, higher particles sizes are obtained when 1) applying long chain instead of medium chain triglycerides and 2) applying a higher of oil/surfactant ratio (10:1 versus 5:1).

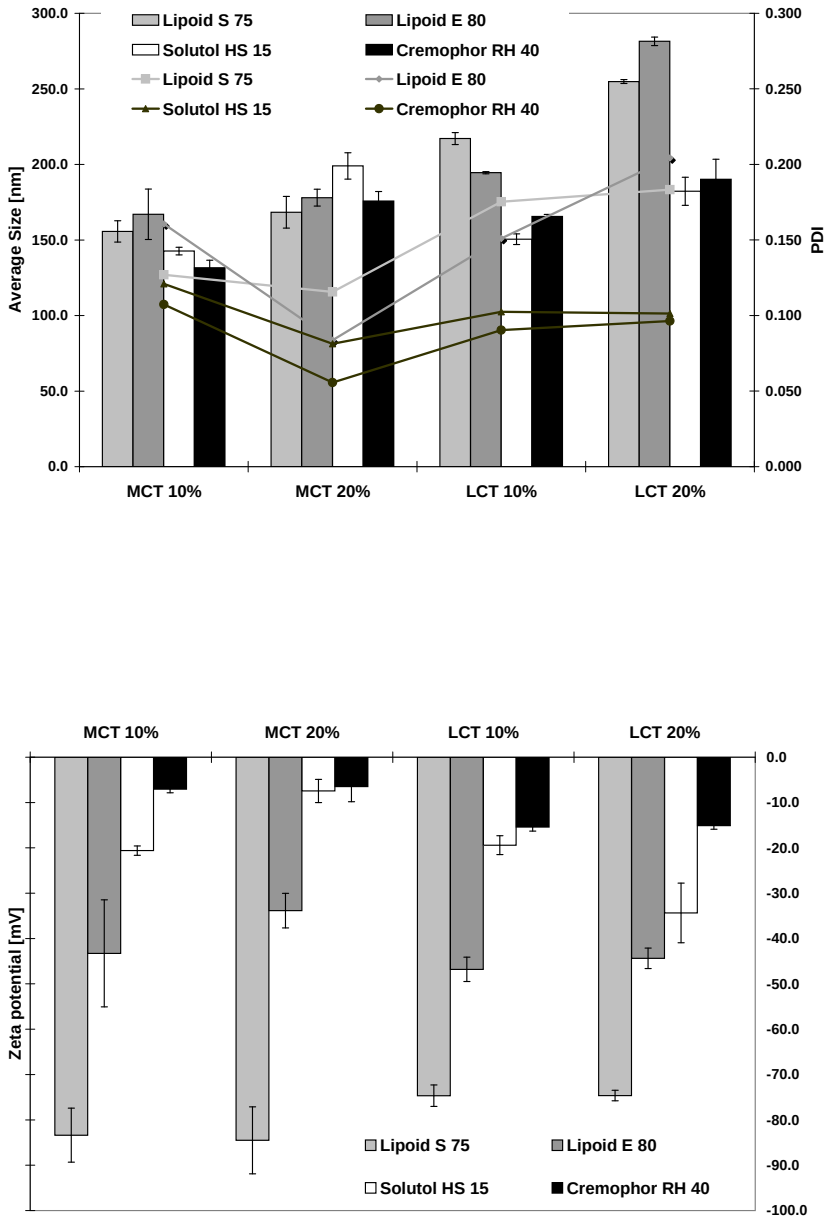

Figure 3.3.1: Average sizes and zeta potentials of nanoemulsions applying different types and amounts of oils (MCT: Miglyol 812, LCT: soybean oil) and different commonly used surfactants, mean±sd, n=3

3.3.1.2 Emulsions containing sucrose esters

Particle sizes of nanoemulsions containing sucrose esters (Figure 3.3.2) are smaller in comparison to the standard tensides (100 to 163 nm). Again average particle sizes are increasing

with increasing oil content and fatty acid chain length. Remarkably, there is also a dependence between particle size and fatty acid chain length of the sucrose ester. If the fatty acid compositions of oil and surfactant are similar the process is resulting in smaller emulsion droplets. The PDI of the emulsions ranges in values of around 0.2 and is thus only sligthly larger in comparison to the reference standard surfactants. One reason for that might be the lower purity of sucrose esters in comparison to tensides from synthetic source. That might also explain the higher PDI values for the emulsions containing lecithins from natural source.

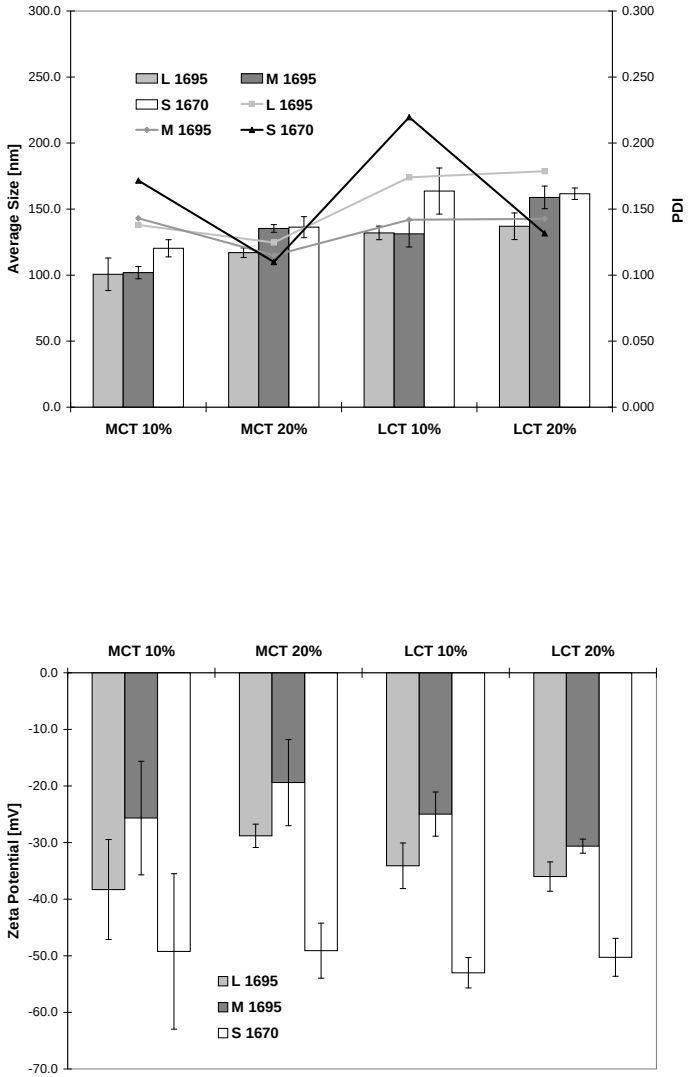

Figure 3.3.2: Average sizes and zeta potentials of nanoemulsions applying different types and amounts of oils and different sucrose esters, mean±sd, n=3

3.3.2 Storage stability of nanoemulsions

To compare the physical stability of nanomulsions without drug payload with samples incorporating the model drug fenofibrate (see 3.3.3) the section only focusses on samples applying 10 % MCT as oily phase. The respective results for the other lipids can be found in the annex. Shelf life stability was assessed for up to 3 months at 25°C. In Figure 3.3.3 PSD and zeta potential values are depicted. Apart from outliers in Lipoid® E80 samples (2 weeks storage) only minor increases in particle size in the range of approximately 10 % can be detected. Regarding zeta potential only Cremophor® RH 40 showed a pronounced decrease in zeta potential after 12 weeks. Storage stability of sucrose ester nanoemulsions is comparable to that of standard surfactants (Fig. 3.3.4). Size increases approx. 20 nm over time in all tested sucrose esters with higher vatiability in measured values at the 8 and 12 weeks timepoints. Also zeta potential values are highly variable, especially for the sucrose stearate samples. Due to the high standard deviations of measurement values no general trend in altering zeta potential values can be obtained.

3.3.3 Drug loading of nanoemulsions

3.3.3.1 Standard nanoemulsions

Drug loading of nanemulsions was assessed by applying the lipophilic model drug fenofibrate according to the protocol described in 2.3.1. Miglyol® 812 (MCT) was assessed as lipophilic carrier phase in a concentration of 10% (w/w) due to the preferrable PSD and stability of the drug-free compositions. The emulsions were assessed for PSD and zeta potential and for physical stability for up to 3 months storage at 25°C. Generally, particle sizes increase approx. 60 nm when fenofibrate is incorporated into the oily phase (Figure 3.3.5) in comparison to unloaded nanoemulsions. Zeta potential values decrase until 4 weeks storage in Lipoid® E80 samples from app. -38 mV to -60 mV and stay constant afterwards. A tendency towards decreasing zeta potential values can also be seen in Cremophor® RH40 samples. The results are very similar as values obtained for emulsions without drug load.

3.3.3.2 Sucrose ester nanoemulsions

As it can be seen in Figure 3.3.6, PSD and PDI show only minor changes towards values with the exception of L1695. Here after 12 weeks substantial increase in PSD can be observed in two of three samples ($p<0.05$). It can be speculated that this increase might be due to microbiological contamination as no additional preservative is added to the storage samples. In all other tested formulations the size increases for about 40% which is in good accordance to nanoemulsions without drug load. Zeta potential values show tendency towards lower

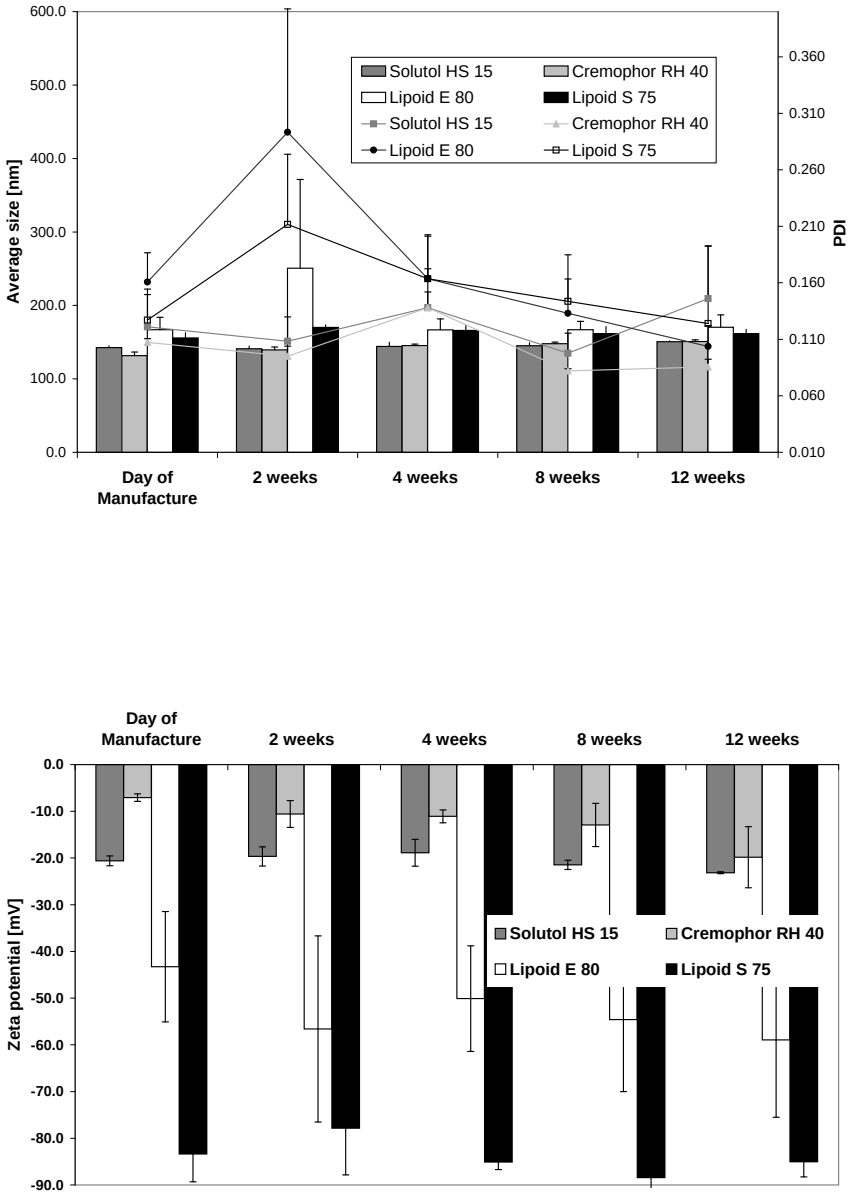

Figure 3.3.3: PSD and zeta potentials for 3 months storage at 25°C applying 10 % MCT and 2 % surfactant, mean±sd, n=3

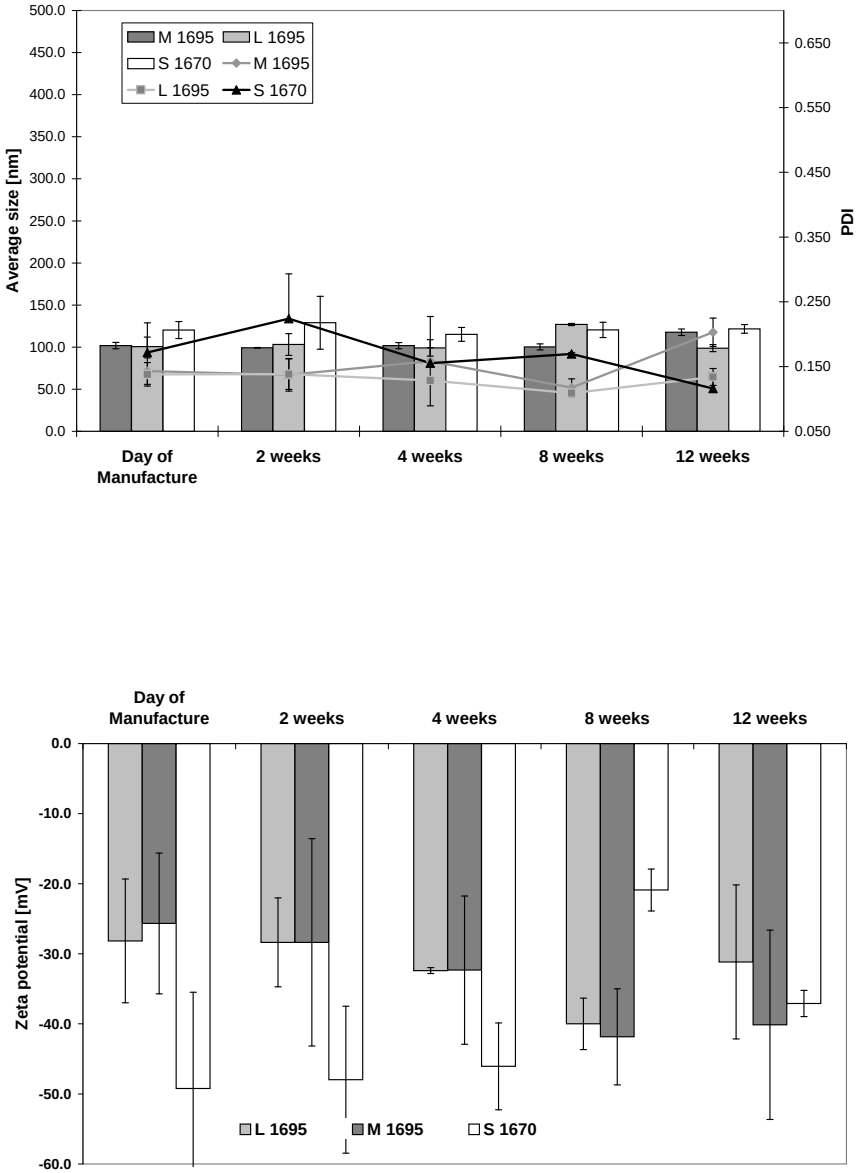

Figure 3.3.4: PSD and zeta potential of sucrose ester nanoemulsions for 3 months storage at 25°C applying 10 % MCT and 2 % surfactant, mean±sd, n=3

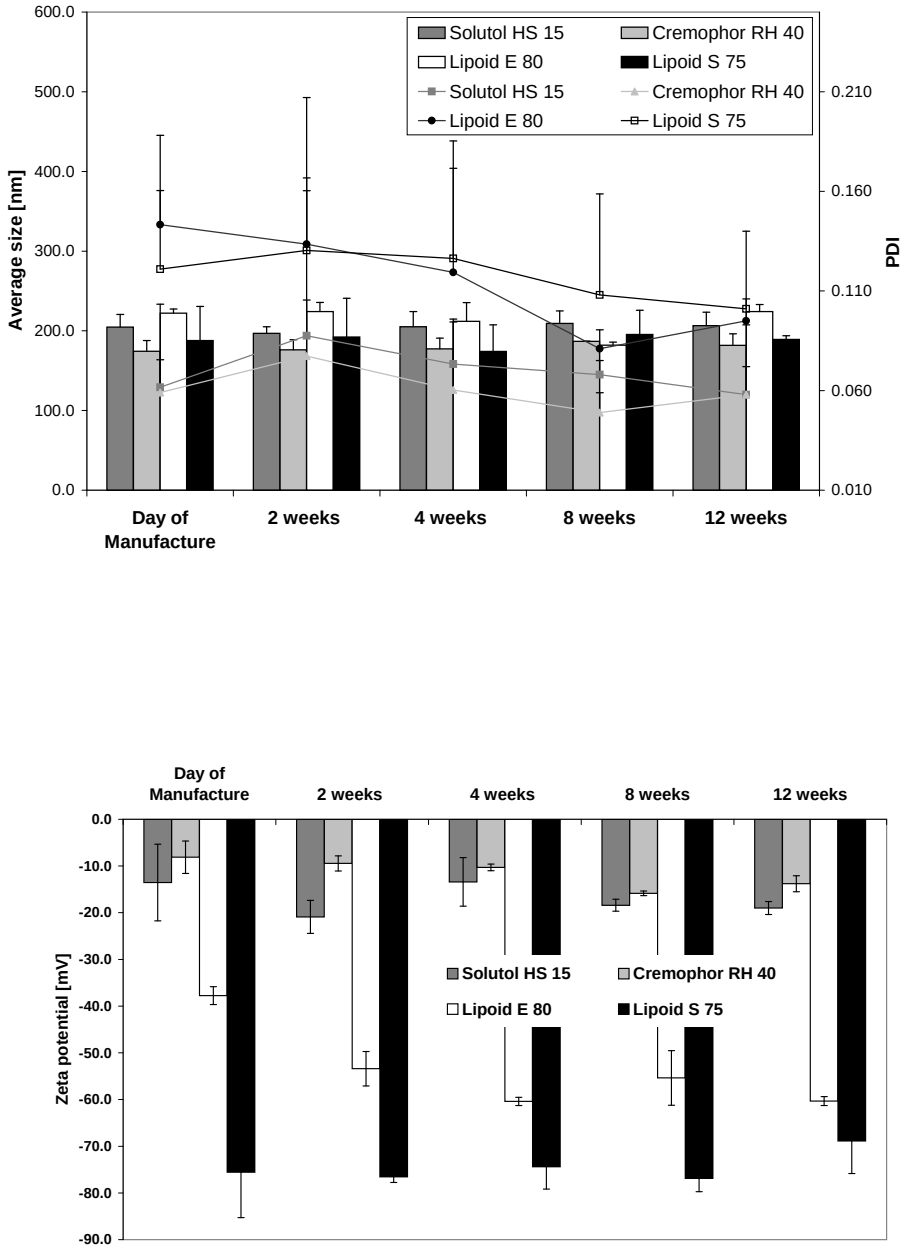

Figure 3.3.5: PSD and zeta potential over 3 months for a formulation containing 10 % MCT, 10 mg/g fenofibrate and different standard surfactants, mean±sd, n=3

values for L1695 and M1695 containing emulsions until 4 weeks storage, but the trend is not significant. Afterwards values are constant. Emulsions formulated with S1670 do not show significant changes in zeta potential over storage time, the other two sucrose esters show increased variance in surface potential. Values are not substantially different to unloaded emulsions indicating that stability and surface potential are largely unaffected by the drug payload.

3.3.4 Electron microscopy of sucrose ester nanoemulsions

Scanning electron microscopy was performed exemplarily on an emulsion containing 2% L1695 and 10% MCT. As described in the methods section negative staining was performed and the emulsion dried for several minutes at ambient conditions. Figure 3.3.7 shows the narrow size distribution of droplets in the 100 nm range. The data are in good accordance with the values determined via DLS. Remarkably, 3D structure of the emulsion droplets was preserved during the water evaporation. No destruction of the primary structure can be seen. This is remarkable because emulsions are knwon as systems with a soft interface that do not possess a robust inner structure. Upon removal of the aqueous dispersing medium one would expect a collapse of oil droplets and subsequently fusion of the oily drops to a homogeneous oily phase.

3.3.5 Lyophilisation of nanoemulsions

When preparing the emulsion samples for electron microscopy it was seen that by simple drying the three dimensional structure of the droplets could be partly conserved (see 3.3.4). It is therefore obvious to test the activity of sucrose esters as lyoprotectants for the emulsions described within this chapter. The formulations containing sucrose esters were compared to standard emulsions (with Cremophor®, Solutol®, phosphatidylcholines) and the marketed nanoemulsion Lipovenös® PLR 10 %.

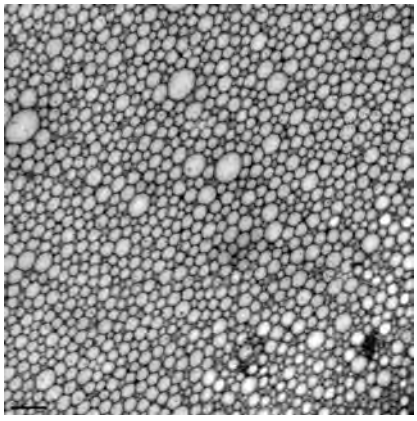

Figure 3.3.7: SEM picture of a nanoemulsion containing 2 % L1695 and 10% MCT (scale bar 200 nm)

In a first trial emulsions containing M1695 2 % or L1695 2 % were lyophilized to detect the influence of fatty acid chain length on freeze drying. Reconstitution was assessed visually and worked best with L1695, therefore this sucrose ester was applied for further trials. To determine the influence of the

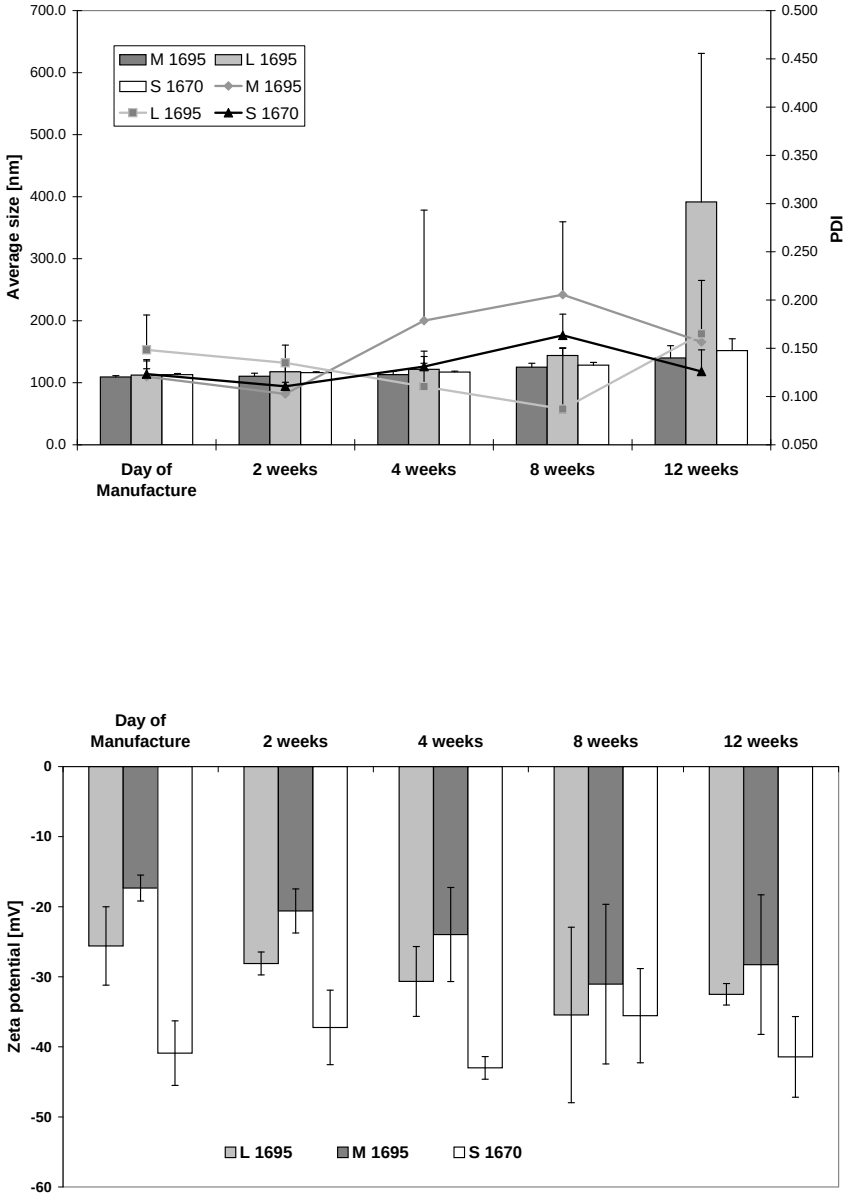

Figure 3.3.6: PSD and zeta potential over 3 months for a formulation containing 10% MCT and 10 mg/g fenofibrate, mean±sd, n=3

Table 3.7: Composition and results of freeze drying of sucrose ester nanoemulsions (L1695, 10 % MCT)

Content sucrose ester (% w/w)	Size [nm] and PDI before lyo		Size [nm] and PDI after lyo		Residual moisture (%)
2	100.6	0.138	-	-	-
5	107.0	0.155	135.0	0.160	0.623
7.5	109.6	0.206	134.0	0.167	0.430
10	112.6	0.198	129.9	0.187	0.422

content of sucrose ester emulsions were prepared according to the compositions listed in Table 3.7. DLS data before and after freeze drying indicate that lyophilisation is possible with a sucrose ester content $\geq$ 5%. The lyo cakes containing 2% L1695 collapsed during secondary drying and were not further investigated. Particle sizes increase by about 30% after the drying in DLS readout. This is acceptable as the PSD is still sufficiently narrow and the particles in a $<$ 200 nm range. When assessing the PSD via light microscopy one can detect larger fractions of coarse emulsion particles in the 50µm range, especially when applying 5% of L1695 (Fig. 3.3.9). Notably less differences can be seen before and after freeze drying when 5% and 10% surfactant are applied. Structure seems to be more conserved at 7.5% and 10% surfactant although DLS measurements are not indicating this in the small particle measurement range. Besides these observations it must be pointed out that the freeze drying process was not optimized for the systems tested. Results are therefore likely to improve with refined drying conditions. Residual moisture shows tendency to decreasing values with increasing sucrose ester content.

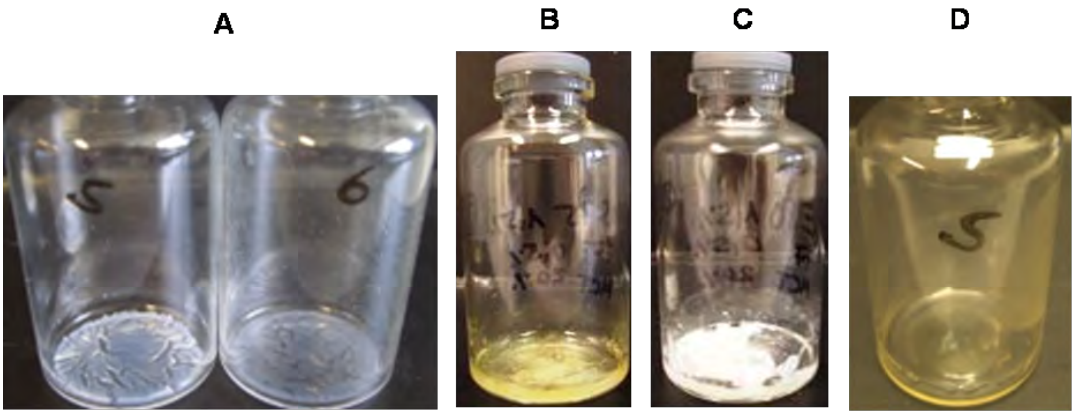

Figure 3.3.8: Standard nanoemulsions after lyophilisation. All samples collapsed during freeze drying. A) Solutol® and Cremophor®emulsions B) Lipoid® E80 C) Lipoid®S75 D) Lipovenös®PLR10%

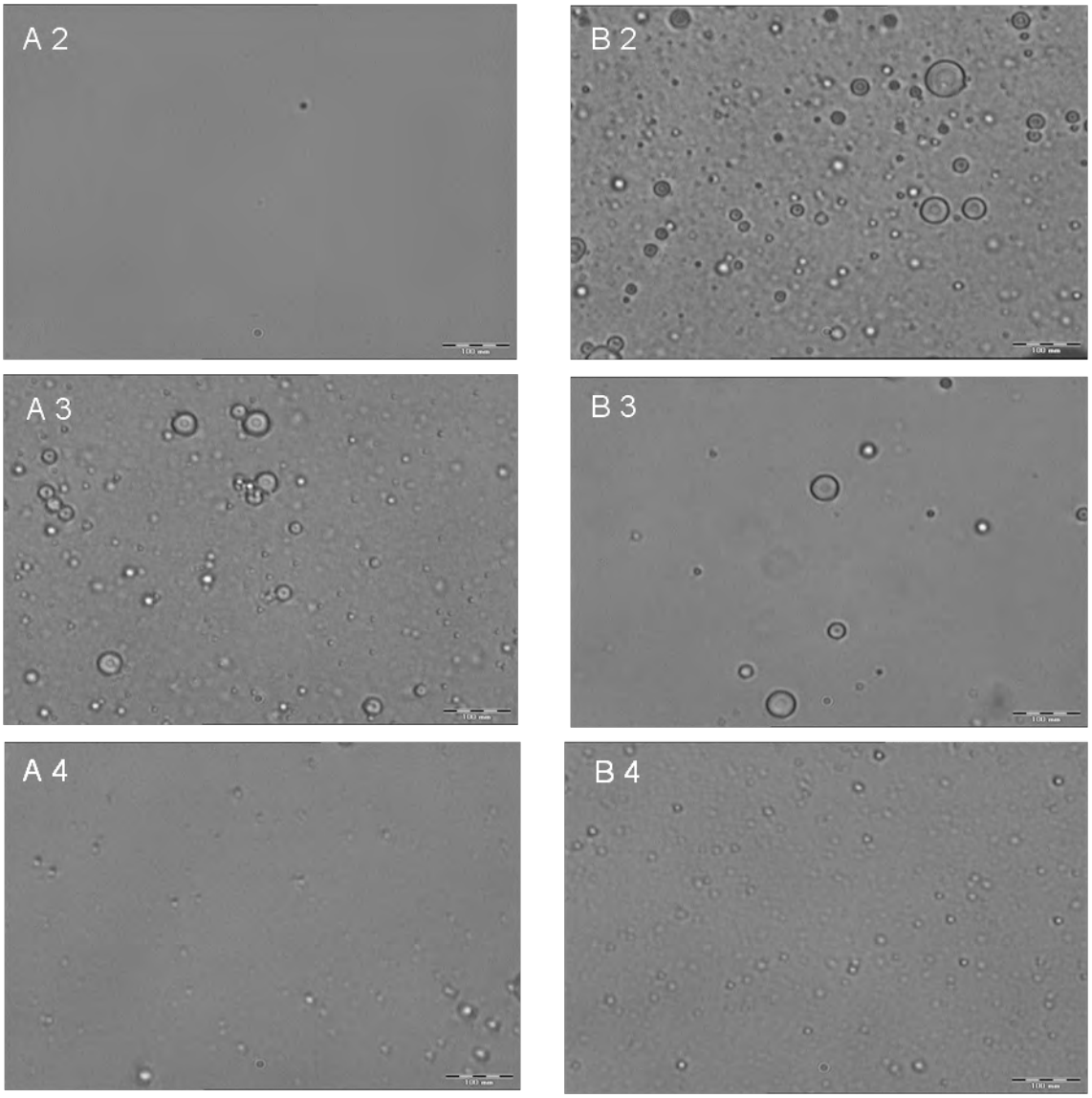

Figure 3.3.9: Light micrographs of sucrose ester nanoemulsions (L1695, 10 % MCT) before and after freeze drying. A2 - A4: before freeze drying, 5 %/7.5 %/10 % L1695 B2 - B4: after freeze drying, 5 %/7.5 %/10 % L1695, scale bar: 100 µm, please note that only oversized droplets can be seen that are not captured via the DLS measurement, while distinct differences can be seen at 5% sucrose ester the particle size distribution is rather unaffected at higher sugar ester content

3.4 Nanosuspensions

Within this section the preparation of pharmaceutical nanosuspensions will be covered. The most common technique to manufacure pharmaceutical nanosupensions is media milling. Therefore, the feasibility and relevant processing parameters of two different types of ball mills will be investigated.

3.4.1 Process development on planetary ball mills

Investigation of milling parameters was in most cases performed on suspensions of FF stabilized with Docusate-Na (DOSS). Main readout was comminution performance, measured as average particle size via DLS. DLS was prefered over SLS because dynamic light scattering can be performed with extremely low amounts of sample down to 1 µL when diluting the sample in water or buffer. In SLS generally larger sample amounts are necessary.

3.4.1.1 Rotational speed and size milling beads

Two different sizes (1.0 mm and 0.2-0.3 mm) of zirconia milling beads were applied to test the milling performance on a FF nanosuspension containing 25% FF and 5% DOSS. 0.6 mL suspension was applied togeter with a bead filling level of 40 % (v/volume milling vessel). The results are shown in Figure 3.4.1. It can be clearly seen that by applying 1mm beads low particle size distributions can be obtained already at applying 500 rpm whereas for 0.2 - 0.3 mm beads milling performance is dramatically increased at higher rotational speed. Remarkably not significant differences in comminution can be detected for 1mm beads in a range of 500 - 800 rpm. In contrast, size reduction and reduction of PDI correlates with increased rotational speed for 0.2 - 0.3 mm beads. At 800 rpm smaller particle sizes and PDI are obtained for the small beads. The results indicate that for larger milling beads a sufficient energy input for comminution is already obtained at low rotational speeds whereas for smaller milling beads larger kinetic energies ar required for size reduction. As soon as energy input is sufficient smaller bead sizes seem to be preferable because smaller particle sizes and PDI can be achieved.

3.4.1.2 Influence of bead filling level

Several authors describe the optimum bead fill levels for planetary ball mills at approximately 40 % bead bulk volume per volume milling vessel [28, 27]. It must be noted that background experiments for this assumption were mainly done on dry grinding samples. In order to determine the optimum bead fill range for the three model compounds bead filling levels from 40 up to 90 % were investigated. Figure 3.4.2 is displaying the results for 25 % drug

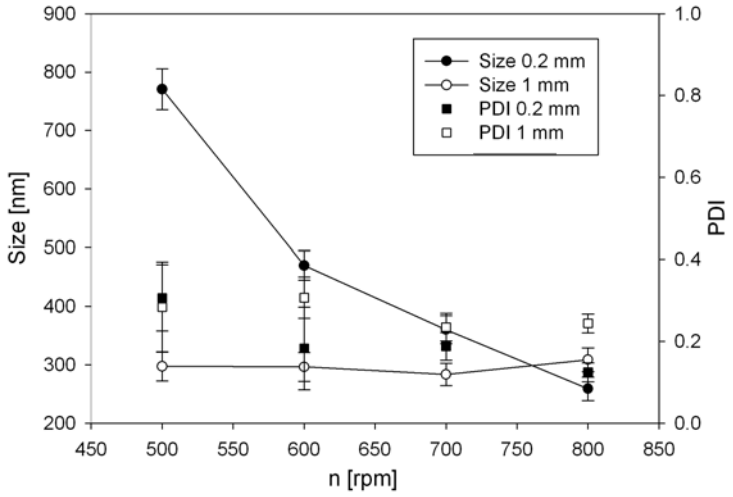

Figure 3.4.1: Particle size reduction depending on bead size and rotational speed, 30 min, 40 % bead fill level, mean±sd, n=3

suspensions stabilized with 5 % DOSS. It can be seen that the influence of bead fill levels is obviously dependent on the applied drug substance. While for FF higher levels are beneficial particle sizes of <200 nm can be obtained already with 40 % milling beads for GF and KC. Generally, higher fill levels are beneficial for milling performance. This is easily explainable via grinding theory as a higher number of milling beads is causing a higher number of collisions per time unit. As a practical disadvantage it has to be mentioned that separation of grinding media and drug product gets more demanding with increasing media fill level. For easy withdrawal of samples via a syringe or pipette tip a fill level of 60 % should not be exceeded.

3.4.1.3 Processing time

Grinding time is often reported to be in the hour to day range form milling processes on planetary ball mills [10, 13, 106]. Often grinding is performed at low rotational speeds with the consequence of prolonged processing times. On this experimental setup the relevant processing time for particle comminution is investigated for two model drugs (FF, KC) at high rotational speed (800 rpm). In order to prevent excessive heating of the drug formulations the protocol was designed as such that 30s of milling were alternated by 60 s of pause. The final product temperature did not exceed 35°C after the milling run. Zirconia milling beads at a filling volume of 40 % (volume/per volume milling vessel) with a size of 0.2-0.3 mm were used. The suspension slurry was adjusted to a total mass of 600mg and

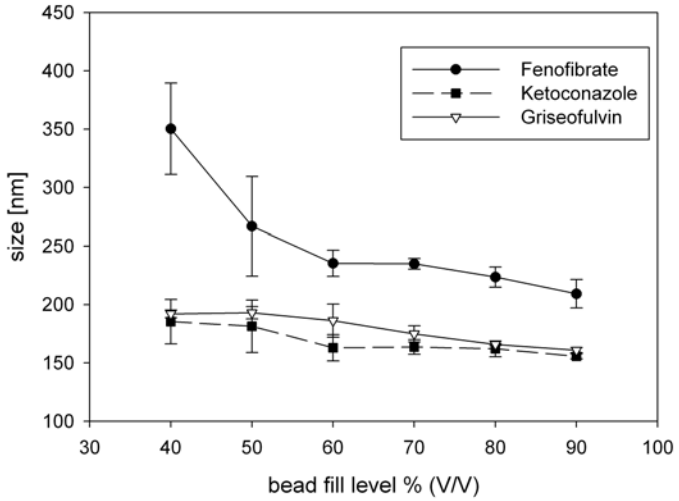

Figure 3.4.2: Influence of the bead filling level on grinding performance, 0.2-0.3 mm zirconia beads, 800 rpm, 30 min processing time, 1 g suspension, mean±sd, n=3

contained 25 % (w/w) API and 5 % (w/w) DOSS as stabilizer. The rest of the sample mass consisted of bidistilled water. Figure 3.4.3 demonstrates that for the given high rotational speed the milling process reaches minumum particle size and PDI already after 60 min (net processing time without adding pauses). Further processing does not decrease particle size, in contrast particle and PDI increase are observable for processing times > 120 min.

3.4.1.4 Influence of API concentration in slurry

The influence of the slurry density adjusted via the amount of drug substance suspended in aqueous medium is investigated on the model drug fenofibrate. Varying concentrations from 10 to 60 % (w/w) drug substance in sample slurry mass were applied in 600mg sample mass. The suspension was stabilized in a 5:1 ratio with DOSS. The bead fill level of 0.2-0.3 mm zirconia beads was 60 %, a process time of 60 min was applied. Figure 3.4.4 is displaying the respective impact on resulting particle sizes. It can be seen that optimum comminution conditions are achieved within a range of 20-40 % drug substance content. At lower and higher levels particle sizes tend to increase again, and more remarkably PSD is increasing and showing high variations.

3.4.1.5 Downscaling

In early development phases supply of drug substance is the most limiting factor for the number of milling trials that can be performed within a feasibility study. Usually only few tens to hundreds of mg are available. It is therefore of outmost importance to downscale the apparative setup as far as possible. The approach of this work is to use standard

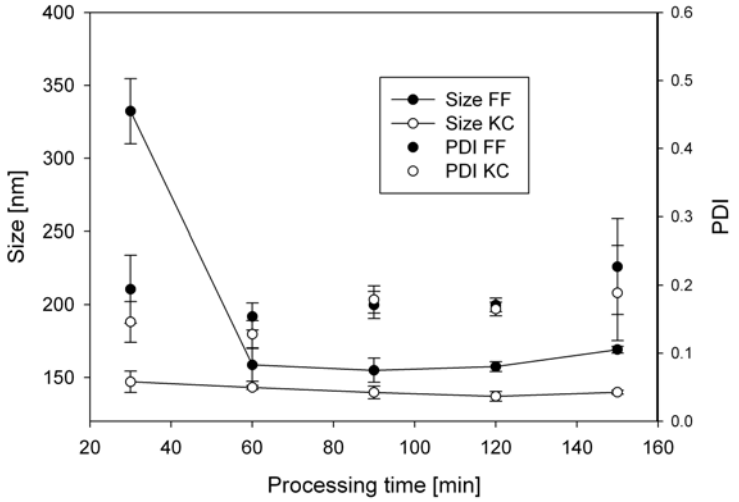

Figure 3.4.3: Influence of grinding time on particle sizes of FF and KC suspensions, 800 rpm, 0.2 - 0.3 mm zirconia beads (40 % v/v), mean±sd, n=3

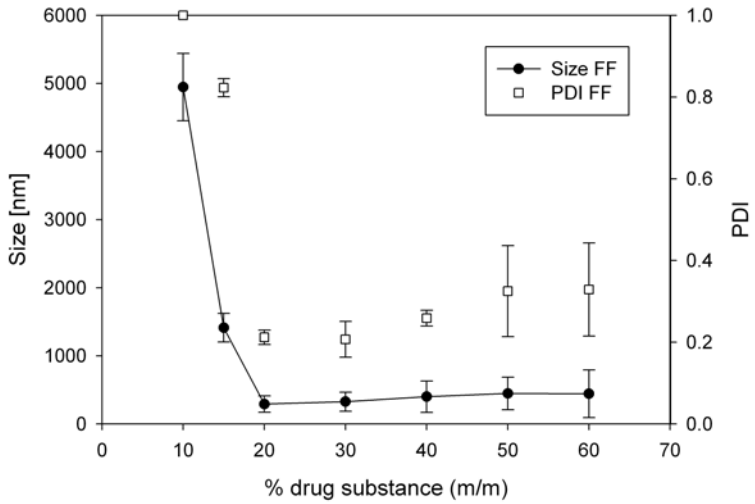

Figure 3.4.4: Different FF concentrations in aqueous suspensions and the influence on grinding performance, mean±sd, n=3

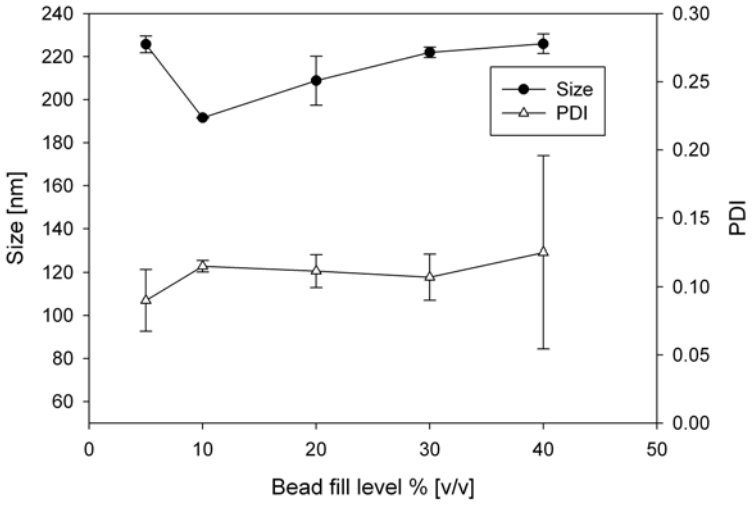

Figure 3.4.5: Downscaling of bead fill concomitantly with reduction of slurry weight, FF and DOSS were used as API and stabilizer, the mill was run at 800 rpm for 30 min with 30 s of run time followed by 30 s pause, mean±sd, n=3

equipment available and to decrease the batch size in the commercial setting as far as possible. The question herein is if small sample amounts (down to 15 mg API) could also be processed in a comparably large milling beaker (12mL). The advantage of this method is that down- and upscaling within one size of milling chamber does not require additional efforts in terms of milling parameter finding (e.g. rpm, processing time). A FF suspension (25%, 5% DOSS) was used as model at 800 rpm applying 0.2-0.3 mm zirconia beads. A recommended bead fill level of 40 % (volume milling beads/ volume milling vessel) and a mass of 600 mg slurry (corresponding to 150 mg API) were used as starting point for downsizing. Then the bead filling volume and the amount of slurry were reduced linearily to 30, 20, 10 and 5 % and 450, 300, 150 and 75 mg, respectively, in order to reduce the necessary API amount in each milling experiment. In Figure 3.4.5 the results are depicted. Although particle size is varying with changes in the composition particle sizes and PSD stays within given borders even when applying extremely small amounts of milling beads and formulation. This is unexpected as one would consider a more intense wear with a more dense packing of milling beads in the milling chamber. Obviously the chosen ratio between slurry mass and bead filling volume is suitable for downscaling the batch sizes within the presented setup.

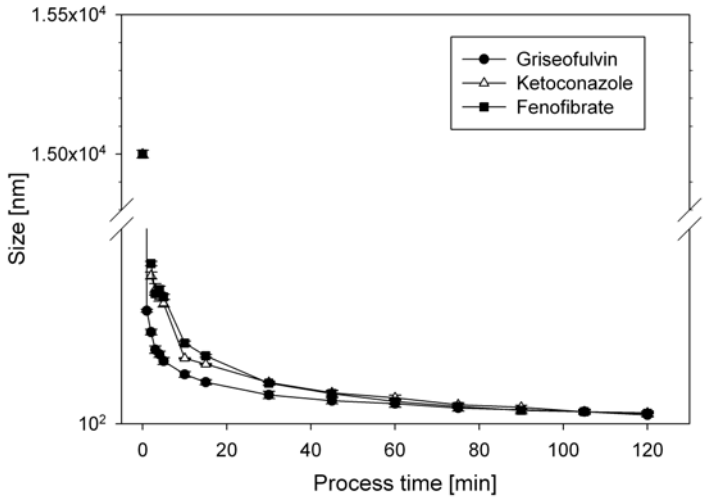

Figure 3.4.6: Influence of processing time on comminution of drug suspensions, 20% (w/w) aqueous API suspensions were stabilized via 2% (w/w) DOSS, 70 % of the milling chamber volume were filled with milling beads (0.15 - 0.25 mm polystyrene beads), mean±sd, n=3

3.4.2 Process development on agitator ball mills

It is understood that scale-up on planetary ball mills is critical. First, only batch mode can be applied in this type of mills, i.e. no continuous processing is possible. Second, batch size is limited to the size of milling chamber which does usually not exceed volumes of one to few litres. In contrast, scalability is given for agitator ball mills [10, 17]. Depending on the industrial application batch sizes in the ton scale are possible. The following section is dealing with the investigation of relevant processing parameters on a lab scale agitator ball mill type WAB Dynomill RL.

3.4.2.1 Processing time

Figure 3.4.6 gives an overview over the grinding behavior of the three different model compounds in an agitator ball milling setup. As for the milling process in the planetary ball mill comminution of large particles occurs rapidly within the first 5 min of milling. The results indicate that comminution of primary large particles is achieved in a short time scale while further grinding occurs much more slowly. It is further evident that all substances show a similar comminution behavior. GF is exhibiting the best grindability. Comminution for KC anf FF is slightly slower, but follows a similar kinetics.

3.4.2.2 Rotational speed

Similar to planetary ball mills the rotational speed of the agitating unit is directly affecting the energy input in agitator ball mills. As a practical approach the influence was directly

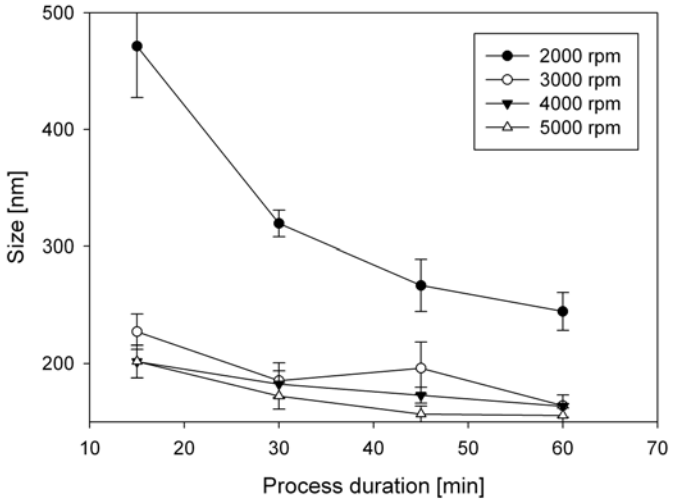

Figure 3.4.7: Influence of rotational speed on comminution of FF suspension, 10% (w/w) aqueous API suspensions were stabilized via 1% (w/w) DOSS, 70 % of the milling chamber volume were filled with milling beads (0.2 mm polystyrene beads), mean±sd, n=3

assessed within this work via testing three different drug substances (FF, GF and KC) that were formulated as slurries of equal quantitative composition. In Figure 3.4.9 the influence of the energy input on FF suspensions is depicted. It can be clearly seen that a power input threshold for comminution exists between 2000 and 3000 rpm. Above this threshold only marginal effects on particle size can be observed. In comparison to that higher energies are required for the comminution of ketoconazole drug crystals (see Figure 3.4.9). Optimum comminution conditions are set between 3000 and 4000 rpm. A further increase in grinding energy as displayed in the 5000 rpm curve does not result in enhanced or accelerated milling efficiency. A milling speed of 5000 rpm was not tested due to high temperatures of $>40°C$ occuring. An interesting behavior is revealed for GF (Figure 3.4.8). There particle sizes tend to decrease in a further step between 4000 and 5000 rpm. In this case also runs at 6000 rpm were performed. The results indicate that a further increase in energy input helps to accelerate particle comminution. It has to be pointed out that the energy transfer is relatively high in the latter case what might have implications on different drug substances that are sensitive to heat. It might be therefore preferable to control the number of wears via varying the process duration instead of working with potentially detrimental wear intensities.

3.4.2.3 Bead filling level

In this section the influence of the bead filling level of poylstyrene beads is investigated. For the influence of the bead filling level of zirconia beads see 3.4.2.7. According to the specification of the manufacturer the Dynomill RL should be run with a maximum bead fill

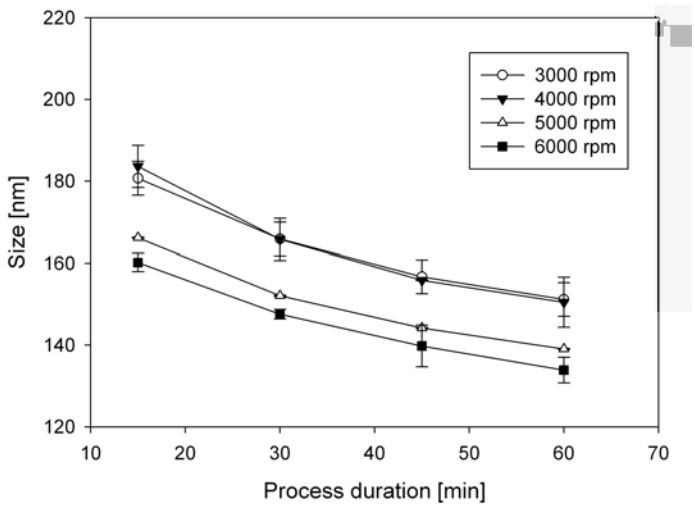

Figure 3.4.8: Influence of rotational speed on comminution of GF suspension, 10% (w/w) aqueous API suspensions were stabilized via 1% (w/w) DOSS, 70 % of the milling chamber volume were filled with milling beads (0.2 mm polystyrene beads), mean±sd, n=3

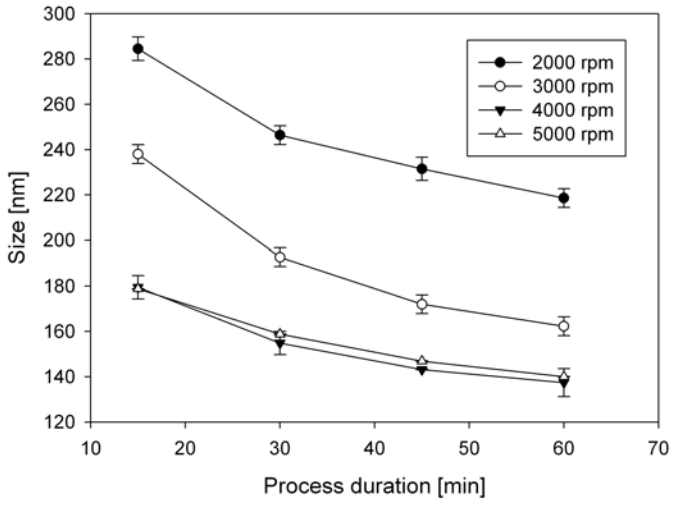

Figure 3.4.9: Influence of rotational speed on comminution of KC suspension, 10% (w/w) aqueous API suspensions were stabilized via 1% (w/w) DOSS, 70 % of the milling chamber volume were filled with milling beads (0.2 mm polystyrene beads), mean±sd, n=3

level of 70% [107]. Regular agitator mills equipped with agitating discs instead of a Dyno® Accelerator can be filled up to 90 % with milling media and are described to have maximal performance with high filling level. Due to the geometry of the Accelerator no fill levels >70% with hard grinding media can be applied because excessive bead wear and agitator blocking would be the consequence. For applying soft grinding media such as polystyrene beads no data were available so the influence of high bead filling level of polystyrene beads was investigated exemplarily on a FF suspension (see Fig. 3.4.10). The results illustrate that between 60% (v/v) and 70% (v/v) particle size reduction is significantly enhanced. Furthermore comminution does in this setup not benefit from a further increase in the amount of grinding media. Due to time reasons this panel of trials was only performed for one model compound. As it was already seen that each drug substance requires different treatment in terms of the intensity of wear (see 3.4.2.2) further substances should be tested for assessing the general grindability at high bead fill levels.

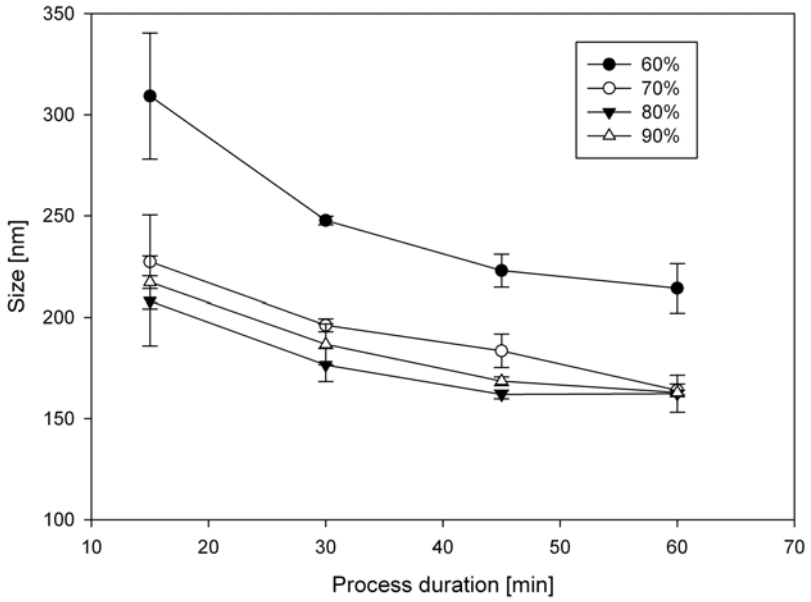

Figure 3.4.10: Influence of bead fill level on comminution of FF suspension, 10% (w/w) aqueous API suspensions were stabilized via 1% (w/w) DOSS, 70 % of the milling chamber volume were filled with milling beads (0.15-0.25 mm polystyrene beads), milling was performed at 3000 rpm, mean±sd, n=3

3.4.2.4 Influence of API concentration

In addition to the evaluation of different bead fill levels the relationship between the API concentration and the bead fill volume was investigated. In the previous section it was demonstrated that a higher number of bead/particle contacts, i.e. a high number of collisions is able to enhance the milling performance per time. In this study it should be

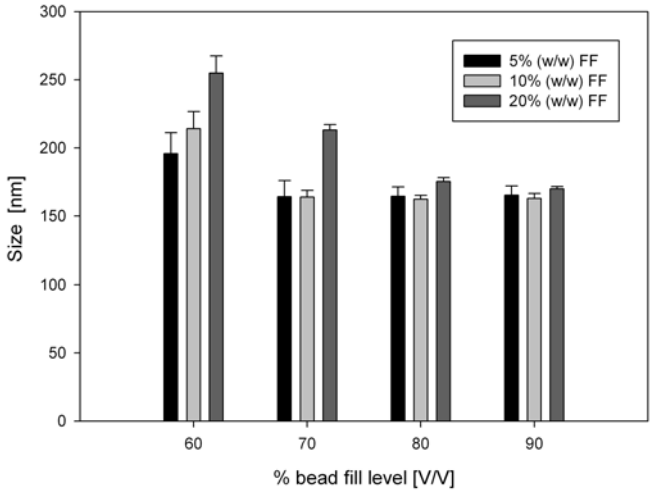

Figure 3.4.11: Correlation between FF concentration and bead filling level (volume beads/volume milling chamber), 5, 10, 20 % (w/w) aqueous API suspensions were stabilized via 0.5, 1, 2 % (w/w) DOSS, 70 % of the milling chamber volume were filled with milling beads (0.15-0.25 mm polystyrene beads), milling was performed at 3000 rpm, mean±sd, n=3

investigated if a higher/lower number of drug particles (= API conentration) is affecting the milling performance. Figure 3.4.11 is depicting milling trials over 60 min at different bead fill levels and three different API concentrations (5, 10, 20 % w/w). A clear trend towards smaller particle sizes can be seen for all API concentrations when shifting from 60 % to 70 % bead fill volume. Also particle comminution is slower the higher the API concentration in the slurry. This is consistent with the theory of number of collisions. The same number of collisions per time unit is leading to a smaller PSD in samples with a lower amount of particles to be comminuted. In congruency to that highly concentrated API suspensions (20 %) require a higher bead filling level (80 %) if all other conditions (rpm, processing time) are kept constant.

3.4.2.5 Type milling beads

Within this study the milling performance of polystyrene (Norstone® Nor08150) and zirconia (SiLi® ZYP 0.1-02 mm) were compared in terms of their comminution efficiency. The mill was loaded with grinding media at 70% (volume/volume milling chamber) and run at 4000 rpm for 120 min, suspensions of 10% (w/w) API stabilized with 1% (w/w) DOSS were applied. The resulting particle sizes and PDI are listed in Table 3.8. Particle sizes are significantly smaller after treatment with polystyrene beads in comparison to zirconia milling media. For griseofulvin results also indicate a more narrow size distribution when

Table 3.8: Average sizes and PDI of three different model compounds ground with polystyrene (Nor08150) or zirconia (SiLi ZYP) milling beads, mean±sd, n=3

API	Nor08150	SiLi ZYP 0.1-0.2
FF	115.8±1.3	147.8±2.5
	0.168±0.04	0.185±0.06
GF	113.7±0.7	145.3±2.8
	0.09±0.02	0.186±0.05
KC	116.7±3.2	138.2±2.9
	0.156±0.09	0.173±0.005

applying polystyrene. As pointed out the two types of milling beads remarkably differ in physicochemical characteristics, such as density and elastic modulus (see also 2.9). For example, density is around 6x for zirconia beads. They therefore generate approximately 6 times the kinetic energy in comparison to polystyrene. As grinding performance is nevertheless better for polystyrene it may be speculated that the lower rigidity of the plastic beads enables a larger contact interface between drug particles and grinding medium due to the deformation the elastic polystyrne. In order to elucidate possible differences in the grinding mechanism, TEM measurements were performed on KC and GF nanosupensions. Unfortunately, it was not possible to obtain pictures from FF nanosuspensions. Due to the susceptibility of FF to the electron beam samples were molten and destroyed already during focussing. For KC the micrographs reveal irregular shaped particles of similar morphology for both grinding media tested (Fig. 3.4.12). In accordance with DLS measurements larger particles can be seen in the zirconia treated samples, esp. coarse particles of about 400 nm are detectable. For GF particles with cubic morphology are obtained. In accordance with DLS data the particles are highly monodisperse in the polystyrene samples (Fig. 3.4.13, left side). Similar to KC samples single large drug crystals can be observed in zirconia-treated suspensions that can be directly translated into larger particle sizes and especially a larger PDI.

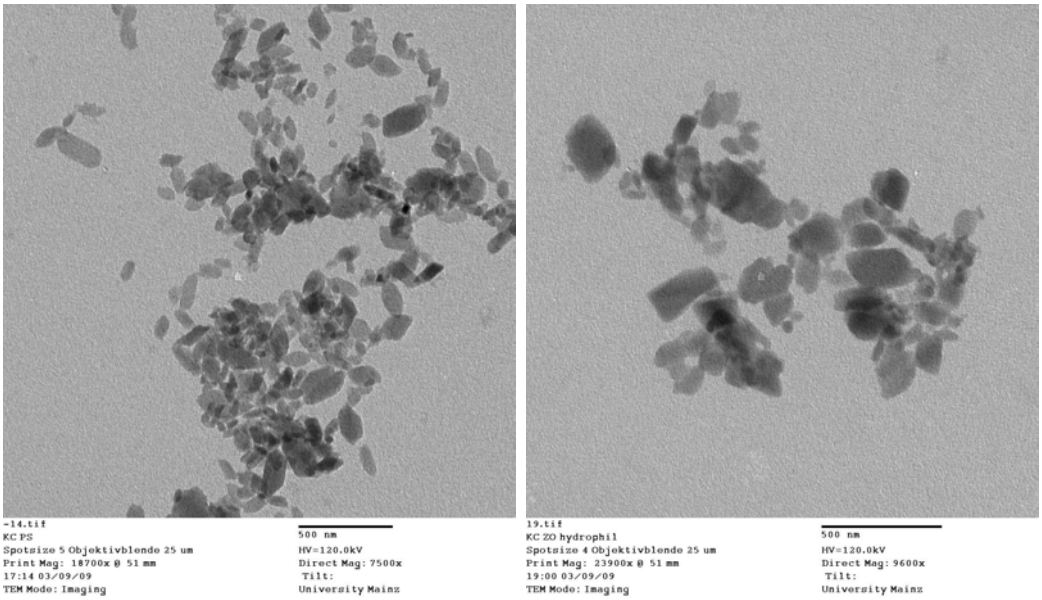

Figure 3.4.12: TEM micrographs of KC nanosupension processed with polystyrene (left) and zirconia (right) beads, 10% (w/w) aqueous API suspensions were stabilized via 1% (w/w) DOSS, 70 % of the milling chamber volume were filled with milling beads , milling was performed at 4000 rpm for 120 min, bar: 500nm

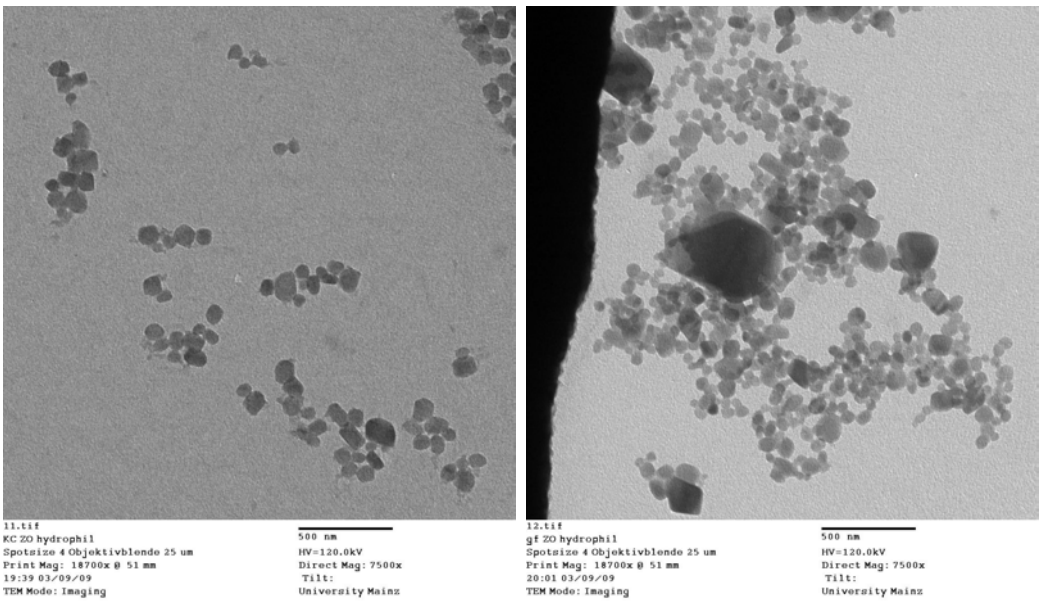

Figure 3.4.13: TEM micrographs of GF nanosupensions processed with polystyrene (left) and zirconia (right) beads, 10% (w/w) aqueous API suspensions were stabilized via 1% (w/w) DOSS, 70 % of the milling chamber volume were filled with milling beads , milling was performed at 4000 rpm for 120 min, bar: 500 nm

3.4.2.6 Process and product temperature

During the last years ball milling processes were modified by performing the milling at cryogenic temperature (i.e. cryomilling). It has been demonstrated for inorganic materials that cryomilling is much more effective than milling at room temperature with a similar energy level [108]. The effectiveness of the cryomilling is due to the low temperature, which slows down recovery or activation of thermally driven processes. For example while the milling of aluminum at ambient temperature took over 100 h to produce a particle size of 25 nm, essentially the same particle size was obtained in 8 h by cryomilling the metal [109]. To assess the influence of the process temperature on the milling performance in our aqueous wetmilling process grinding was performed at two different temperatures of the cooling circuit. In this study 2°C and 20°C were chosen as a standard setting resulting in product temperatures of 15-17°C and 28-30°C, respectively. Trials were performed for the three model compounds fenofibrate, griseofulvin and ketoconazole. All suspensions (20 % w/w) were stabilized with 2 % (w/w) DOSS in the aqueous slurries. It could be seen in pivotal tests that product temperature was generally lower when applying polysytrene instead of zirconia beads what can be easily explained via the low density of polystyrene beads and therefore a lowered net wear intensity [25]. Therefore, to obtain a closer correlation between product and cooling temperature 0.15 - 0.25 mm polystyrol beads (Glenn Mills, USA) were applied in these trials at a rotational speed of 4000 rpm ($= 10.5\,m/s$).

Figures 3.4.14 and 3.4.16 are depicting the respective data for FF and KC. No significant difference can be seen for the two different cooling temperatures. The results suggest that - within the temperature range tested - product temperature does not play a role for comminution. On the contrary, temperature seems to be relevant for GF suspensions (Figure 3.4.15). Particle sizes are significantly reduced when applying low processing temperatures. Interestingly, comminution seems to follow the same kinetics as with 20°C but is shifted towards lower particle sizes. The results presume a strong dependence of the grinding efficiency on specific characteristics of the API.

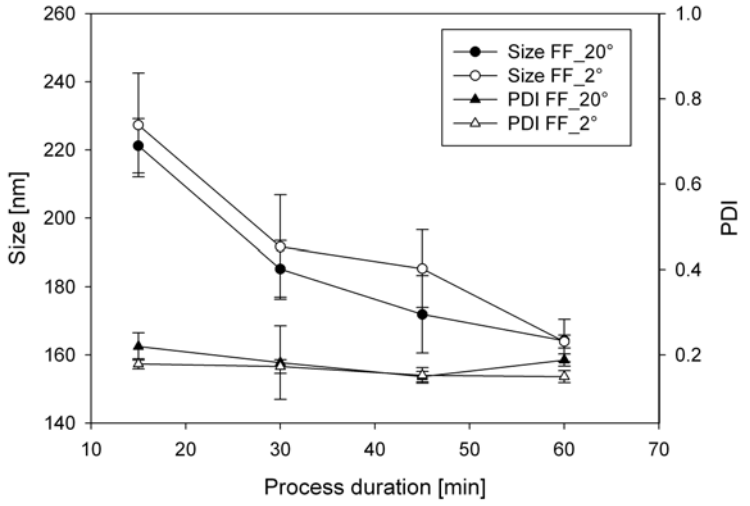

Figure 3.4.14: Influence of process temperature on comminution of FF suspension, 20% (w/w) aqueous API suspensions were stabilized via 2% (w/w) DOSS, 70 % of the milling chamber volume were filled with milling beads (0.15 - 0.25 mm polystyrene beads), milling was performed at 4000 rpm for 60 min, mean±sd, n=3

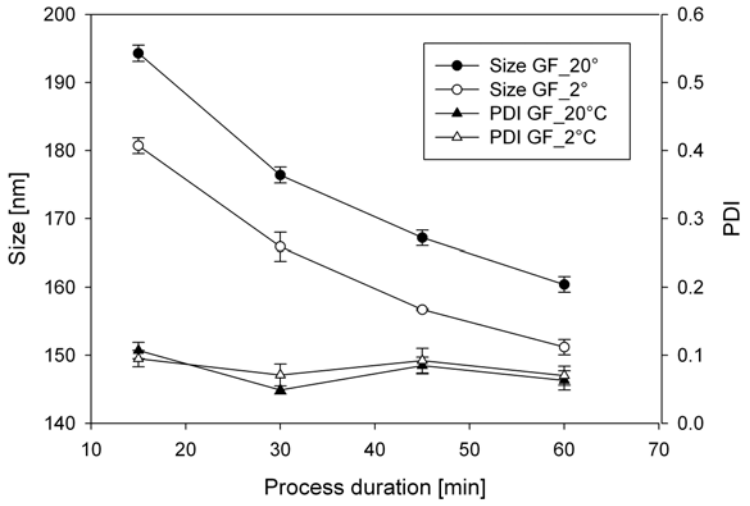

Figure 3.4.15: Influence of process on comminution of GF suspension, 20% (w/w) aqueous API suspensions were stabilized via 2% (w/w) DOSS, 70 % of the milling chamber volume were filled with milling beads (0.15 - 0.25 mm polystyrene beads), milling was performed at 4000 rpm for 60 min, mean±sd, n=3

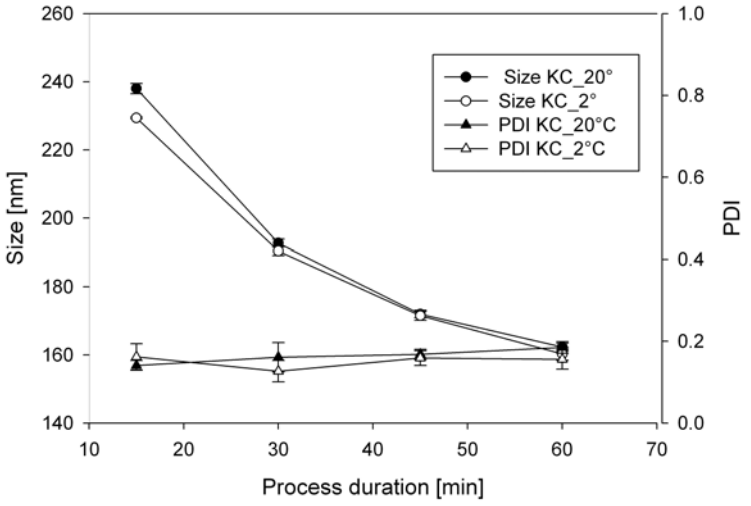

Figure 3.4.16: Influence of rotational speed on comminution of KC suspension, 20% (w/w) aqueous API suspensions were stabilized via 2% (w/w) DOSS, 70 % of the milling chamber volume were filled with milling beads (0.15 - 0.25 mm polystyrene beads), milling was performed at 4000 rpm for 60 min, mean±sd, n=3

3.4.2.7 DoE on parameter optimisation on a FF model suspension

DoE was perfomed on Cornerstone® statistical software. D-optimum design was chosen for determining suitable measurement points within the predefined design space (see Table 3.9). For data treatment only parameters with $p<0.1$ were taken into consideration. Quadratic models as well as power transformation (reciprocal root model) were chosen for computational fitting of raw data. Due to changes in equipment (availability of a more versatile and powerful cryostat) and the availability of a software for statistical design of experiments it was possible to set up a DoE for process optimisation for a FF nanosuspension. 20 % FF stabilized with 0.1 % DOSS and 2.5 % HPMC was used as model suspension. Particle size, melting enthalpy and final product temperature were used as output parameters. Goal of this study was to 1) minimize the particle size, maximize the crystallinity of the API (high enthalpy) and minimize the product temperature. Other than in section 3.4.2.6 milling was performed applying zirconia milling media as these were considered of higher relevance in Merck development projects.

In total 34 experiments were performed, the conditions are listed in Table 3.10. Each experiment was performed twice to improve the robustness of the prediction. In Figure 3.4.17 the predicted reponses are listed for the optimisation of particle size.

The software suggested the following parameters:

Table 3.9: Input and output parameters for DoE on nanomilling process (values and results in brackets)

Factors	Responses
Processing time (5 -120 min)	Particle size (39 µm – 93 nm, SLS)
Rotational speed (1500 - 6000 rpm)	Enthalpy (36 – 82 J/g, DSC)
Bead fill level (30 - 70 %)	Final temperature (0.4 – 75 °C)
Bead size (0.1 - 0.2 and 0.2 - 0.3 mm, SiLi ZYP)	
Temperature cryostat (-20 – 20 °C)	
Batch size (60 - 250 ml)	

- Processing time: 90 min
- Rotational speed: 3640 rpm
- Bead fill level: 61 %
- 0.2 – 0.3 mm milling beads
- Temperature cryostat: -13°C
- Bach size: 80 ml

Interestingly, a minor influence of the bead sizes was evident from the statistical analysis. In tendency smaller bead sizes are preferable. This is consistent with published data [23, 32]. In contrast no clear trend is visible for the applied bead volume. Nevertheless a high value of 61 % bead filling volume is recommended for low particle size and PSD. In accordance with the data presented in 3.4.2.2 the optimum rotational speed for comminution of FF crystals is between 3000 and 4000 rpm. Similar to the trials performed with polystyrene beads a high bead volume of 70 % seems to be optimum. In extension to the data generated for the two different temperatures 2° and 20°C, the optimum cooling temperature for FF seems to be under very cold conditions (-13°C). Generally it must be taken into consideration that the high confidence intervalls for some of the parameters limit the reliability of the prediction despite the preferable results for the goodness of fit listed in Table 3.11. To verify the reliability of the DoE-based optimisation the proposed conditions were run three times on the model suspension. The results in comparison to the predicted values are listed in Table 3.12. Consistent data are obtained for the response parameters particle size and melting enthalpy while the forecast for final product temperature is incorrect. It can further be seen that standard deviations for enthalpy and temperature are relativley high what might explain the large confidence intervals for the parameter prediction and hamper further improvement of the forecast.

Table 3.10: Experimental conditions proposed by Cornerstone software according to D-optimal design, responses are optimized regarding minimum particle size and maximum crystallinity of the API, six different influence factors were included in the experimental design

Time [min]	Bead volume (%)	rpm	Bead size [mm]	Temp cryostat [°C]	Batch size [ml]
91	70	6000	0.2-0.3	20	60
120	70	1500	0.2-0.3	-20	60
5	70	1500	0.1-0.2	-20	60
120	30	1500	0.2-0.3	20	250
91	70	3750	0.1-0.2	0	155
63	70	6000	0.2-0.3	0	155
120	30	6000	0.2-0.3	-20	250
120	30	6000	0.2-0.3	20	60
120	70	6000	0.1-0.2	-20	250
91	30	1500	0.1-0.2	20	60
5	30	3750	0.1-0.2	20	60
5	30	6000	0.1-0.2	-20	250
5	70	6000	0.2-0.3	-20	60
120	30	6000	0.1-0.2	20	250
5	30	1500	0.1-0.2	20	250
34	70	1500	0.2-0.3	20	60
5	70	1500	0.2-0.3	-20	250
5	70	3750	0.2-0.3	20	250
63	70	6000	0.1-0.2	20	60
34	50	1500	0.1-0.2	0	250
120	70	6000	0.2-0.3	20	250
5	30	6000	0.1-0.2	0	60
91	50	1500	0.2-0.3	-20	250
34	30	6000	0.2-0.3	20	250
34	50	3750	0.1-0.2	-20	155
63	70	1500	0.1-0.2	20	250
5	50	6000	0.2-0.3	20	155
120	30	1500	0.1-0.2	-20	250
120	70	1500	0.1-0.2	20	155
120	30	6000	0.1-0.2	-20	60
5	30	1500	0.2-0.3	-20	60
120	50	3750	0.1-0.2	0	60
63	50	1500	0.2-0.3	20	60

Table 3.11: Fitting parameters DoE

Response	R-square	Adj. R-square	RMS error
Reciprocal square root end size [nm]	0.9884	0.9832	0.1136
Reciprocal square root size distribution width [nm]	0.7015	0.6740	0.6397
Enthalpy [J/g]	1.000	0.9998	0.9121
Product temperature [°C]	0.9862	0.9832	2.3571

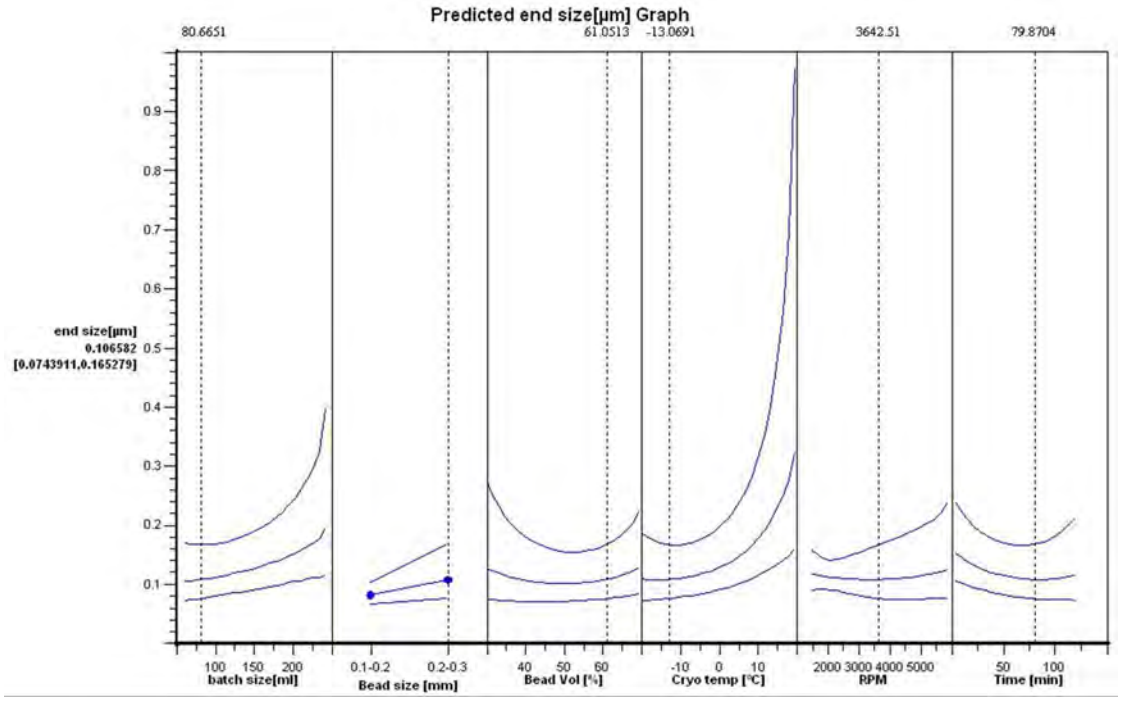

Figure 3.4.17: Response graph for particle size dependence on different parameter inputs (batch size, bead size, bead filling volume, process temperature, revolutions per minute (rpm), processing time). The middle line in all segements displays the impact on product particle size while the upper and lower lines visualize the confidence intervals for each factor

Table 3.12: Comparison of predicted responses versus measured results, 80 ml of 20 % (w/w) FF aqueous suspensions stabilized with 0.1 % (w/w) DOSS and 2.5 % (w/w) HPMC were milled at 3640 rpm for 90 min. 0.2-0.3 mm zirconia milling beads were used at a filling level of 61 % (volume beads/volume milling chamber), cryostat temperature was set to -13°C, mean±sd, n=3

Response	Prediction	Measured
Particle Size [nm]	106.54	104.7± 2.47
Enthalpy [J/g]	70.62	64.64 ± 7.35
Temperature [°C]	18.58	26.23 ± 5.83

3.4.2.8 Comparability milling processes planetary ball mill versus agitator ball mil

To assess whether milling processes are comparable between the planetary ball mill and the agitator ball mill investigated within this work, 6 formulations per each model drug were tested for their transferability from a planetary ball mill to an agitator ball mill setup. Per compound poor and well performing formulations were tested. The milling parameters on the Dynomill agitator ball mill were as follows: 70 % bead fill, 0.2-0.3 mm zirconia beads 3600 rpm, 30 min process time, cooling temperature 2°C. Figure 3.4.18 is presenting graphical overviews for all three substances.

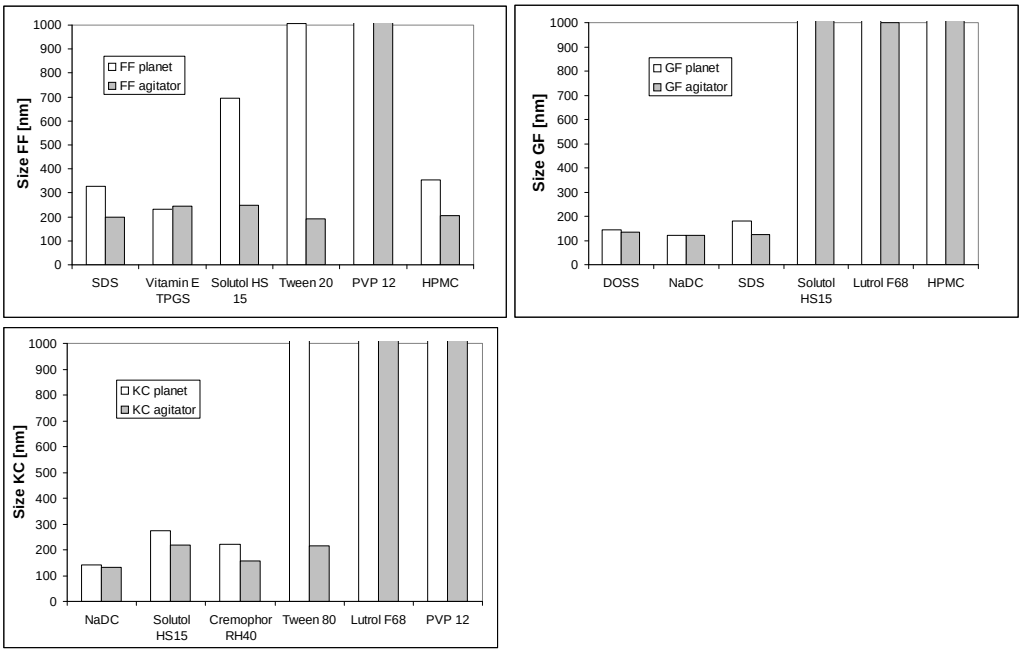

Figure 3.4.18: Comparison of grindability between planetary and agitator ball mill, selected formulations, milling conditions planetary ball mill: 40 % bead fill, 0.2-0.3 mm zirconia beads, 30 min processing time (30 s run+ 30 s pause), 1.0 g slurry weight, milling conditions agitator ball mill: 70 % (volume/volume milling chamber) bead fill, 0.2-0.3 mm zirconia beads 3600 rpm, 30 min process time, cooling temperature 2°C, 60 g slurry weight, n=2

Transferabilty of milling processes is given for all tested formulations in the case of GF. In contrast, FF and KC showed unexpected results for the surfactants Tween® 20/80 and Solutol® HS15. In the case of FF/Solutol particle sizes were almost a factor of 2.5 larger in the planetary ball mill process when compared to the agitator ball mill. For both Tween types size reduction completely failed in the planetary ball mill setup. This phenomenon will be further investigated in 3.4.5.2. The behavior is critical in terms of process transfers from larger mills to smaller planetary type ball mills as there is the risk that formulations are not processable. Regarding particle sizes it can be concluded that for transferable formulations similar particle sizes can be obtained at equal processing times. Particle sizes

are in tendency smaller in the agitator mill setup. It has to be noted that the experimental setup there ran under optimum conditions whereas the planetary mill was not run under optimum conditions for FF (only 40% bead fill volume).

3.4.3 Stabilisation of nanosuspensions

Many authors describe the necessity of proper suspension stabilisation [17, 23, 10, 22]. Other than for inorganic material interface stabilisation via amphiphilic compounds is necessary already at reaching the submicron particle range. A couple of stabilizers are described as being used in the stabilisation of nanosuspensions, such as anionic stabilizers (SDS, DOSS, NaDC), nonionic stabilizers (e.g. Cremophor®, Tween®), block copolymers (poloxamers) and macromolecules from synthetic (PVP) and semisynthetic source (HPMC, HEC etc.) [10, 17]. Often there is only a limited data set of stabilizers and few model compounds investigated within one study. Within this work three model compounds are subjected to stability studies applying a full package of 14 stabilizers from all pharmaceutically acceptable substance classes.

3.4.3.1 Influence of stabilizers on milling efficiency

For testing the influence of different stabilizers on the processability of drug suspensions the following conditions were applied: the planetary ball mill Fritsch Pulverisette P7 was applied that was equipped with 12 mL zirconia beakers. Zirconia beads (SiLi ZYP 0.2-0.3 mm) were used with a bead fill level of 40 % (v/v). 800 rpm were chosen as rotational speed with a total milling time of 30 min. Milling was performed so that 30 s of processing were interrupted by 30 s of pause. Per beaker one mL of slurry was processed. The results are depicted in Figures 3.4.19,3.4.20,3.4.21. Results larger than 1000 nm are cut in the graphics as DLS is an unreliable measurement method in the micron size range.

Fenofibrate Good processability is obtained when applying anionic surfactants (DOSS, NaDC, SDS) and the nonionic surfactant TPGS. Best processability is given with NaDC. Other nonionics such as Solutol® or Lutrol® specialities show some potential in surface stabilisation but perform poorer than anionic surfactants and HPMC. Hydroxypropylmethylcellulose (HPMC) is similarily efficient as SDS in suspension stabilisation. This is remarkable because the molecular characteristics of both molecules extremely differ: SDS is a highly ionic and amphiphilic small molecule while HPMC posseses comparatively high molecular weight and stabilizes suspensions rather by steric hindrance.. When evaluating these data it has to be noted that results may be distorted via the agglomeration or aggregation of drug crystals after the processing what is described to occur after nanonisation of hydrophobic

drug particles. DLS might therefore not always provide the complete picture. On the other hand undesired particle aggregation effects are covered within the measurements.

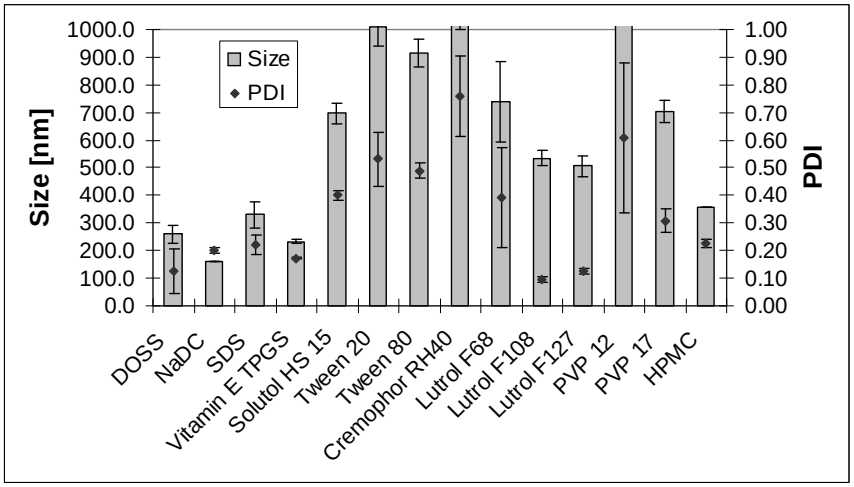

Figure 3.4.19: Influence of different stabilizers on particle size distribution of FF suspensions, zirconia beads (SiLi ZYP 0.2-0.3 mm) were used with a bead fill level of 40 % (v/v). 800 rpm were chosen as rotational speed with a total milling time of 30 min, milling was performed so that 30 s of processing were interrupted by 30 s of pause, mean±sd, n=3, columns cut at 1000 nm depict particles sizes $>>$ 1µm

Griseofulvin Best particle breakage is achieved via anionic surfactants (DOSS, NaDC, SDS) with best results obtained for NaDC. In contrast to this, all other tested stabilizers lead to insufficient comminution within the 30 min milling protocol. Van Eerdenbrugh reported on a stabilizeer screen with 13 stabilizers tested on 9 model compounds, among them also griseofulvin [106]. He found that surface stabilisation was very often possible with high concentrations of TPGS (>25% (w/w) relative to API). For GF finding suitable stabilizers was described as critical. This is in accordance with our findings where only anionic stabilizers lead to sufficient PSD.

Ketoconazole As Figure 3.4.21 indicates KC is more easily amenable to surface stabilisation than the other two model compounds. Adequate stabilisation is given for anionic as well as nonionic stabilizers except for Tween specialities. Also PVPs do not render surface stabilisation, results were extremely poor with Kollidon®K17. This is also indicated by a monolithic block consisting of suspension and milling beads formed after the milling process. As already seen for FF the results were slightly better when applying HPMC as stabilizer. Also in analogy to FF results block copolymers are suitable with Lutrol® F108 exhibiting the best and Lutrol® F68 exhibiting the worst performance. When comparing KC with the structurally similar itraconazole a good correlation between published stabilizers for nanosuspension development and internal findings can be observed. Also for itraconazole,

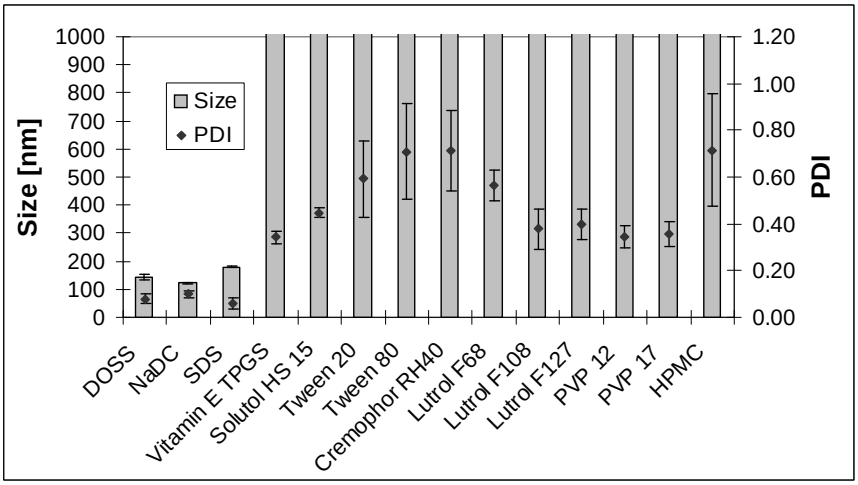

Figure 3.4.20: Influence of different stabilizers on particle size distribution of GF suspensions, for grinding of one mL suspension zirconia beads (SiLi ZYP 0.2-0.3 mm) were used with a bead fill level of 40 % (v/v). 800 rpm were chosen as rotational speed with a total milling time of 30 min, milling was performed so that 30 s of processing were interrupted by 30 s of pause, mean±sd, n=3, columns cut at 1000 nm depict particles sizes >> 1µm, as these particles are not correctly captured via DLS the values are not considered in the graphs

poloxamers [110] and poloxamer-sodium cholic acid mixtures [111] are described as suitable stabilizers.

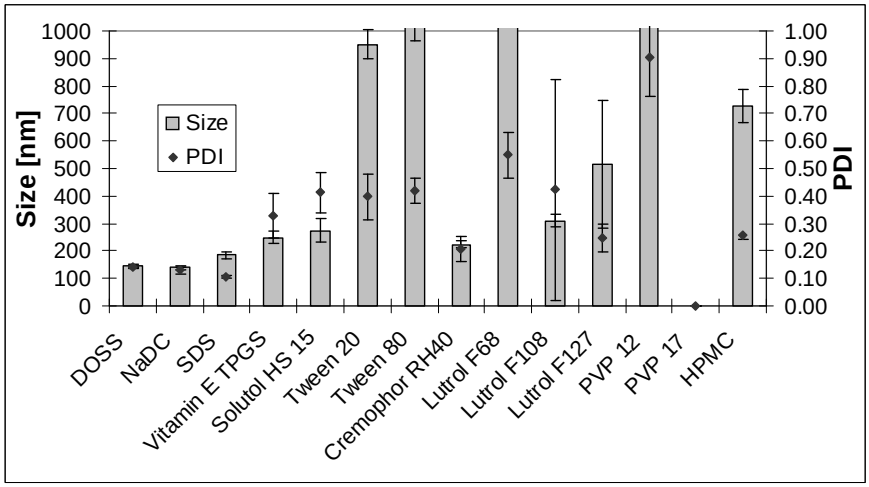

Figure 3.4.21: Influence of different stabilizers on particle size distribution of KC suspensions, for grinding of one mL suspension zirconia beads (SiLi ZYP 0.2-0.3 mm) were used with a bead fill level of 40 % (v/v). 800 rpm were chosen as rotational speed with a total milling time of 30 min, milling was performed so that 30 s of processing were interrupted by 30 s of pause, mean±sd, n=3, columns cut at 1000 nm depict particles sizes >> 1µm, as these particles are not correctly captured via DLS the values are not considered in the graphs

3.4.3.2 Physical stability of nanosuspensions

The physical stability of the nanosuspensions with initial particle sizes of <1000nm at t0 obtained in 3.4.3.1 was assessed at different storage conditions. The formulations were incubated in sealed brown glass vials at 5°C, 25°C and 40°C. Particle sizes were measured after 1 week, 4, 8 and 12 weeks. Within the following figures only 1 week and 12 week graphs are depicted. Nanosuspensions that showed sedimentation together with a clear supernatant were artificially set to 1000nm as larger particle sizes are not reliably measured via DLS. Preferable particle sizes and PDIs are defined to be in range of 100 - 300 nm for average particle sizes and < 0.25 for PDI.

Fenofibrate Regarding Figure 3.4.22 it becomes evident that storage stability is not necessaily correlated with milling efficiency. None of the investigated stabilizers is able to fully preserve particle size even within short time frames of one week. Best results however are obtained with HPMC where particle sizes increase by about a factor of 1.5 after 12 weeks at 40°C. TPGS is at least able to maintain particle size at cooled conditions. All other samples show size increases of >2fold or sediment after 12 weeks. Notably, a storage time of 1 week at elevated temperature seems to be predictive for the situation at 12 weeks. If large size increases occur at 40°C within one week, the stability of the suspensions is severly constricted even at lower storage temperatures after 12 weeks. Results for DOSS are not listed because samples showed complete sedimentation after 1 day.

Griseofulvin Figure 3.4.23 is providing a completely different picture for GF suspensions in comparison to FF. All three stabilizers provide good size preservation with size increases of only approx. 10% even at elevated temperatures. Solely DOSS is not able to maintain particle size at 40°C/12w. Here, a size increase of more than 100% can be detected.

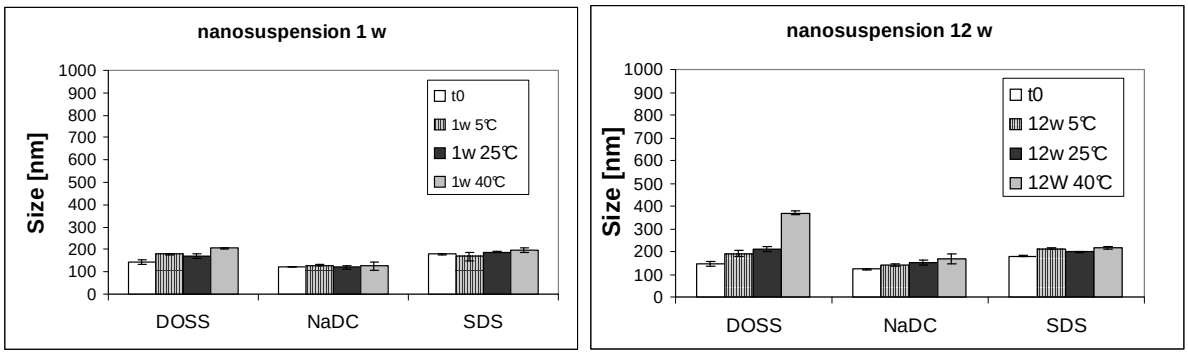

Figure 3.4.23: Storage stability of GF nanosuspensions at different temperatures manufactured via wet-milling, 1 week (left) and 12 weeks (right), mean±sd, n=3

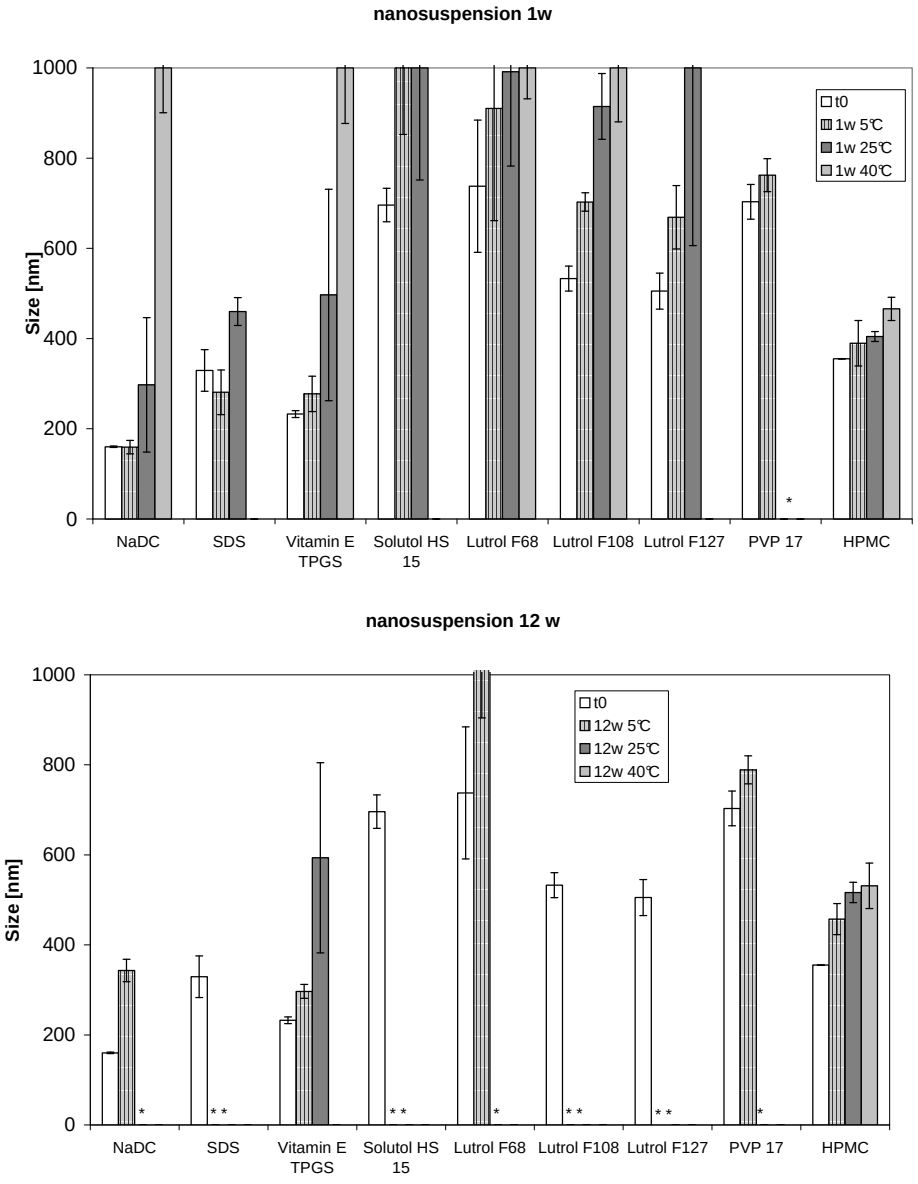

Figure 3.4.22: Storage stability of FF nanosuspensions at different temperatures manufactured via wet-milling, 1 week (upper graph) and 12 weeks (lower graph), mean±sd, n=3, * complete sedimentation, data not measurable via DLS

Ketoconazole Size preservation is preferable for all anionic surfactants (Figure 3.4.24). Even after 12 weeks storage at 40°C no significant deterioration in PSD can be detected. Size is also maintained when applying TPGS and Cremophor® RH40, especially when storing at 5°C. For elevated temperatures a 2-fold increase in particle size can be observed for TPGS, whereas Solutol suspensions are sedimented after 12 weeks at 40°C. Despite poor performance during the milling procedure HPMC is a preferable excipient for enhancing the storage stability of KC nanosuspensions. No significant size increase can be observed after 12 weeks, in contrary PSD is even decreasing. This is a typical behavior for suspension systems that show agglomeration of primary particles due to high surface energies. With increasing storage time a relaxation of the high surface energies occur and particles deglomerate again. Also Tween® 80 is after 1 week storage exhibiting this phenomenon, after 12 weeks particle ripening processes counter this effect and the suspension is completely sedimented. With the exception of KC stabilized by TPGS particle size increases after 1 week are able to forecast the suspension stability after 12 weeks.

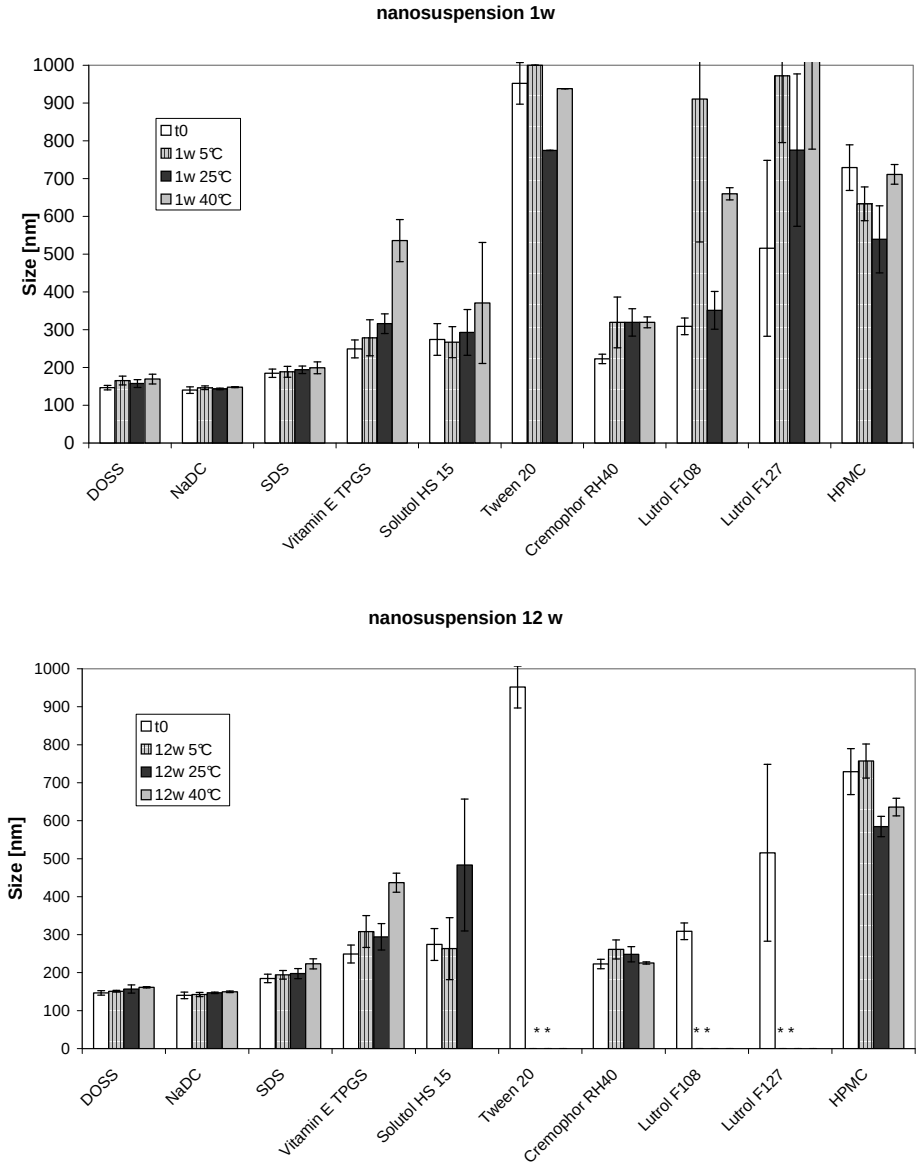

Figure 3.4.24: Storage stability of KC nanosuspensions manufactured via wetmilling at different temperatures, 1 week (left) and 12 weeks (right), mean±sd, n=3

In conclusion it can be stated that - for the three substances tested - no clear correlation can shown for the relationship between milling performance and storage stabilisation for the excipients tested. Both parameters need to be investigated separately. Furthermore, there seems, with some restrictions, to exist a predictability of storage data at 40°C per one week. If large size increases are observed already after one week at this temperature long term stability is in most cases not given for the respective formulation. Generally, anionic surfactants seem to be more preferable in comparison to nonionics given the high success rate within this experimental setup. It has to be conceded that the high concentrations of stabilizers used here (4 % w/w) are not always applicable when an animal or human for-

mulation has to be developed. Furthermore, most anionic stabilizers are restricted to oral use and cannot be applied for parenteral formulations. One strategy would be to limit the use of anionics to a minimum level and replace the lacking stabilizer with stabilizers from other classes that showed preferable properties in the storage stability testing. This was exemplarily performed for a combination of GF with SDS as stabilizing surfactant. There the surfactant concentration was reduced to 0.1 % (1:100 Excipient/API ratio). Two phenomena can be observed. First, grindability seems to be best at a low SDS concentration of 0.5 % without negative impact on 4 weeks storage stability. In addition it can be seen that down to extremely low concentrations of stabilizing agents sufficient stability is maintained even at elevated temperatures (Fig. 3.4.25). The results emphasize the necessity of investigating not only the types of stabilizers but also the most suitable concentration as a compromise between sufficient stability and preferable toxicological profile.

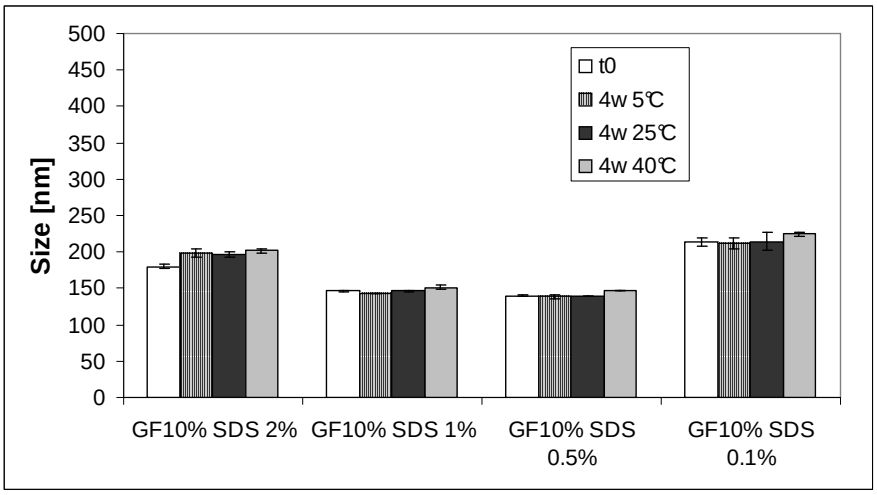

Figure 3.4.25: Particle sizes and storage stability of GF nanosuspensions stabilized with SDS at different concentrations, mean±sd, n=3

3.4.4 Drug-stabilizer interaction

Within this section different approaches for assessment and prediction of drug stabilizer interactions are presented. They cover physicochemical parameters such as zeta potential or melting enthalpy and melting point shifts as well as computational approaches in form of solubility parameters.

3.4.4.1 Correlation between storage stability and zeta potential

According to the DLVO theory net surface charge of particles is highly affecting the stability in a suspension or emulsion. As a rule of thumb suspensions with a zeta potential of ± 30mV should be stable in aqueous media if not other interactions (e.g. flocculation

due to bivalent ions) are affecting stability. It is understood that the theory only holds true when electrostatic stabilizers are used, as in the case of anionic surfactants. Aim of this study is to test whether the principles of DLVO are applicable for the stabilisation of pharmaceutical nanosuspensions. In Figure 3.4.26 the particle sizes after 12 weeks storage are plotted in comparison to the measured zeta potential. It can be seen that in the case of SDS the theory is not valid. Despite highly negative zeta potentials a tremendous particle size growth can be observed. Ion or pH effects can be excluded as suspensions were manufactured via bidistilled water and the pH did not change significantly during the storage period (data not shown). Due to their chemical composition suspensions stabilized via polymers and nonionic surfactants exhibited zeta potential in slight negative range or close to zero. Again, no trend is observable when comparing suspension stability and zeta potential. Regarding GF suspensions highly negative values are obtained for stabilisation with anionic surfactants (Fig. 3.4.27). Here, negative surface charge is correlating with enhanced suspension stability. Due to the fact that solely ionic stabilizers are able to preserve particle size and enable processability of the suspension the results are biased. Better comparability is given for ketoconazole (Fig. 3.4.28). Here, NaDC is leading to zeta potentials of about -20 mV and still the respective suspensions show extremely high stability after 12 weeks storage. As expected no clear trend is visible for suspensions stabilised via anionic stabilizers.

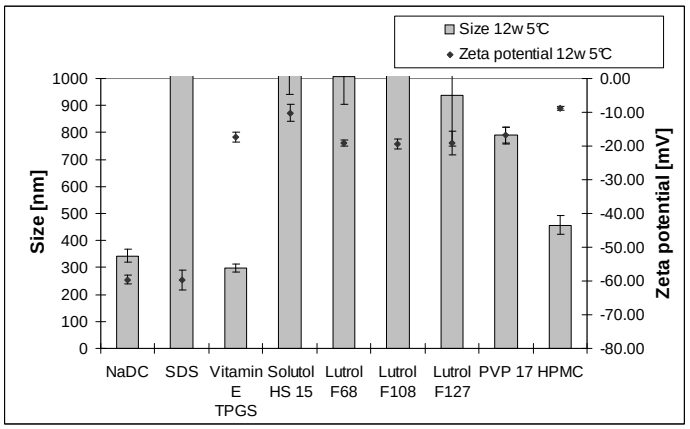

Figure 3.4.26: Zeta potential and particle size of FF nanosuspensions after 12 weeks storage at 5°C, mean±sd, n=3, columns cut at 1000 nm depict particles sizes >> 1µm, as these particles are not correctly captured via DLS the values are not considered in the graphs

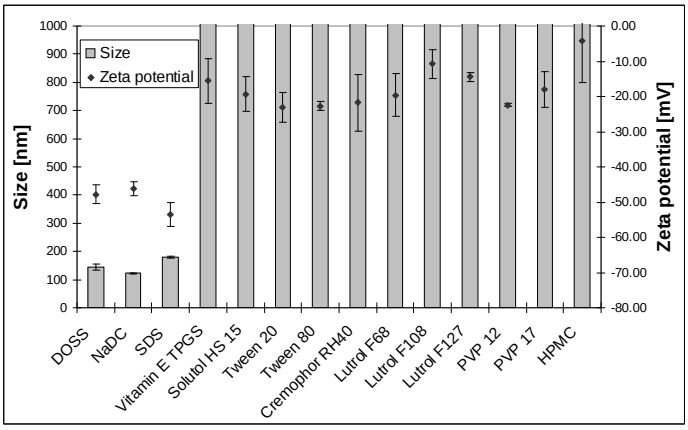

Figure 3.4.27: Zeta potential and particle size of GF nanosuspensions after 12 weeks storage at 40°C, mean±sd, n=3, columns cut at 1000 nm depict particles sizes >> 1µm, as these particles are not correctly captured via DLS the values are not considered in the graphs

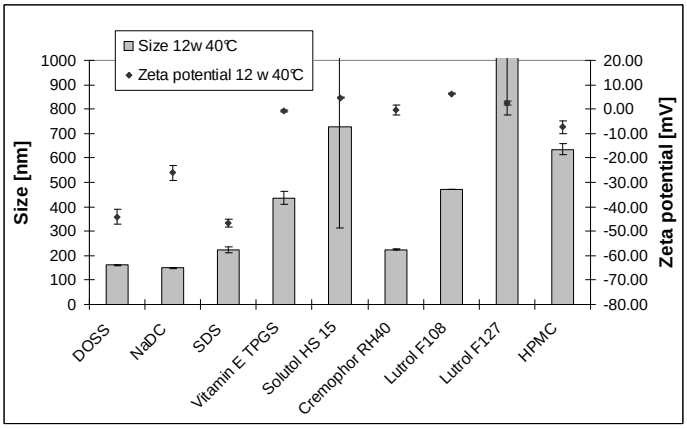

Figure 3.4.28: Zeta potential and particle size of KC nanosuspensions after 12 weeks storage at 40°C, mean±sd, n=3

3.4.4.2 Relationships between thermal parameters and suspension stability

The influence of polymorphic conversion of an API on its physical stability in aqueous solutions is evident. In most cases the transition from a metastable to a thermodynamically more stable solid state is associated with physicochemical changes relevant for particle stability. For example, when amorphous drug content is transferring into a more stable crystalline form this is very often associated with the appearance of larger particles due to solubility differences between the crystalline and the amorphous form. With crystallisation solubility drops dramatically which leads 1) to the precipitation of crystalline particles 2) to the growth of crystalline particles already present in the formulation (Ostwaldt ripening). In the following study DSC thermograms were evaluated regarding changes in the physical state after the milling process. The melting point and melting enthalpy values of samples

after milling were subtracted from the values from physical mixtures of the APIs with the respective stabilizers. It shall be investigated whether physical changes leading to suspension instability could be monitored via DSC.

Fenofibrate Fig. 3.4.29 is depicting the changes in particle sizes together with changes in melting point and melting enthalpy after milling. One week at 25°C was chosen as storage condition to obtain maximum discriminating power between formulations with low, medium and high stability. Only minor changes were detected in melting point in comparison to the respective physical mixtures. Values for enthalpy and size exhibit high standard deviations for a number of stabilizers. Several reasons can be discussed for this phenomenon: First, the measured values tend to scatter for suspensions with larger particle sizes. Considering the volumetric sample preparation deviations might be fostered by a potential imhomogeneity of the samples. These might be especially pronounced given the low sample volumes of approximately 50µL. As a second reason polymorphic changes during the the sample drying step can be discussed. In order to evaporate water the open alumina pans are stored at ambient temperature for 24 hours. During that time frame amorphous fractions of API are likely to recrystallize to different extents. As a result high deviations in the melting enthalpy of crystallline API suspensions can be observed. Decreases in melting point that theoretically could be attributed to changes in the drug polymorph due to the high energy milling process could not be associated with changes in suspension stability. Also extremely low changes either lead to stability or instability of the suspensions depending on the stabilizer applied and therefore do not lead to a consistent trend. Only decreases of more than -7% in all cases lead to severe suspension destabilisation. For FF looking at melting enthalpy to predict physical stability seems to be more promising. In half of all combinations a decrease in enthalpy of more than 30% indicating partial amorphisation of the samples lead to more than 100% size increase after 1 week storage. On the other hand also minor or no changes in enthalpy lead to instability (DOSS, NaDC), Lutrol F68 rendered the suspension relatively stable despite a large postulated amorphous fraction in the sample. The findings suggest that melting enthalpy as measured in the described experimental setting plays a minor role in defining suspension storage stability.

Griseofulvin As already described only DOSS, NaDC and SDS were able to stabilize GF nanosuspensions over a three month timeframe. Fig. 3.4.30 is displaying the respective changes for nanosuspension sizes in relation to changes in melting point and enthalpy. Whereas DOSS and SDS show slight increase in particle size, almost no change (-1.1 %) could be observed for NaDC. Here, changes in enthalpy and melting point showed only minor effects on PSD. In contrast to that a high extent of amorphisation was detected in

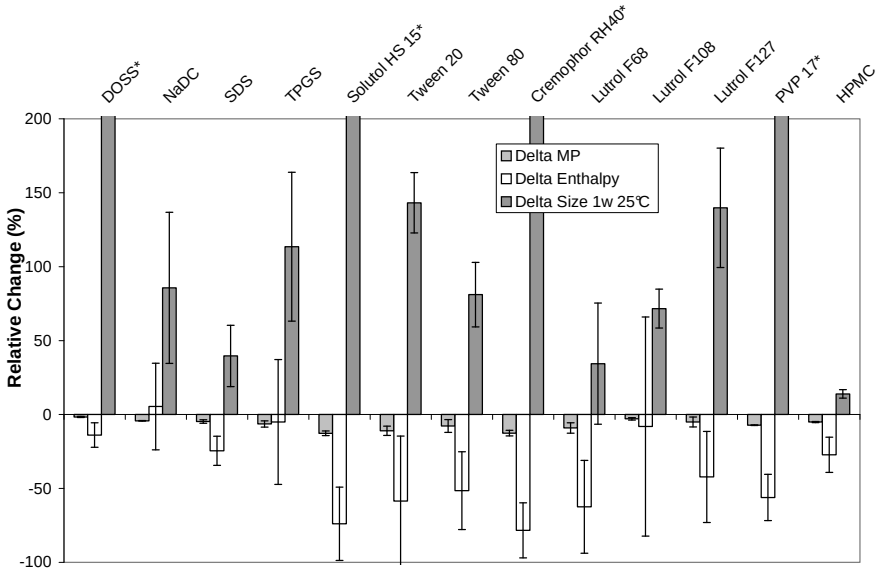

Figure 3.4.29: Changes in melting point MP, melting enthalpy and physical stability (Delta Size 1w 25°C) of FF nanosuspensions, mean±sd, n=3, ' indicate results >> larger than threshold corressponding to results >> larger the typical DLS measurement range

all other formulations. Tween® 20, 80 and Lutrol® F68 rendered the suspension completely amorphous in DSC readout. Interestingly, this lead to poor results in comminution, but showed less deteriorating effects on particle stability. Lutrol® F68 leads to in tendency decreased particle sizes, but the observation cannot be considered significant. Generally, it can be observed that all formulations with poor comminution results showed partial or complete amorphisation during the milling process. For some of these formulations further increases in particle size can be measured, for Cremophor® RH 40 PSD is out of measurement range after one week and the sample could not be resuspended.

Ketoconazole As discussed in 3.4.3.2 the following stabilizers were able to preserve KC suspension stability: DOSS, NaDC, SDS, TPGS, Solutol® HS15, Cremophor® RH40 and HPMC. The trend is basically also detectable for the 1-week data. Interestingly enough, remarkable depressions in melting point and enthalpy are observable in all tested systems (Fig. 3.4.31). Again, as for the other model compounds these physical changes could not be translated in the prediction of stable or unstable formulations. Again, as for the other APIs standard deviations are higher when large particles are measured. In DLS as well as DSC these particles present high variability. Notably, three samples (Tween® 20, Tween® 80, Lutrol®F 68) could not be redispersed. HPMC showed a tendency towards smaller particles after one week.

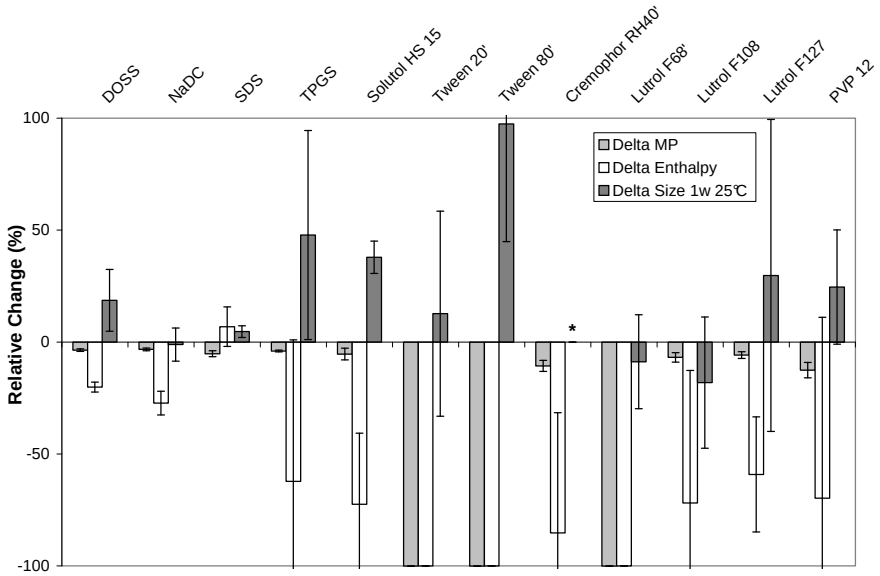

Figure 3.4.30: Changes in melting point MP, melting enthalpy and physical stability (Delta Size 1w 25°C) of GF nanosuspensions, mean±sd, n=3, ' indicate results >> larger than threshold ,* indicates that the sample could not be measured because resuspension of samples was not possible

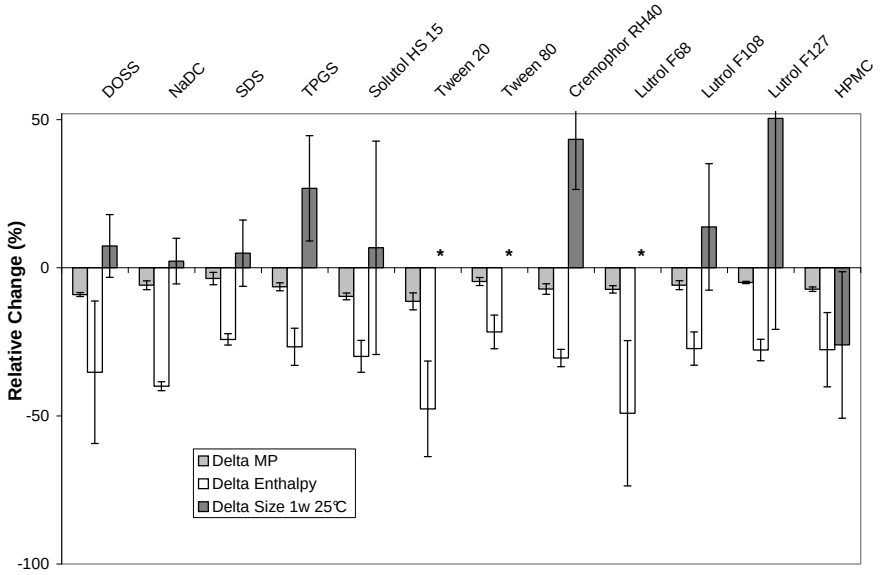

Figure 3.4.31: Changes in melting point MP, melting enthalpy and physical stability (Delta Size 1w 25°C) of KC nanosuspensions, mean±sd, n=3, * indicates that the sample could not be measured because resuspension of samples was not possible

3.4.4.3 Comparison DSC versus X-ray diffraction (XRD)

As another suitable analytical tool to characterize the physical state of drug nanocrystals x-ray diffraction is described [46, 17, 12]. Although access to XRD equipment was limited within this work some examples could be investigated in more depth to elucidate data comparability between thermal analysis and x-ray diffraction. Exemplarily, Figure 3.4.32 shows two different examples of KC nanosuspensions. In DSC both samples insinuate an increase in amorphous fraction (20-30 %) and a shift in melting temperature of -4.6% (Tween® 80) and -7.2% (Cremophor® RH40). XRD of the Tween® 80 containing samples show no signs of amorphisation and a preservation of the polymorphic form of the API. On the contrary, RH40 leads to a change in the polymorphic form. This can be seen in distinct pattern changes at 7° and around 20°. Again there is no halo detectable that would give hints to an amorphisation of the sample. Consequently, changes in the melting enthalpy of the API are likely to be due to the large fraction of solubilizer in the sample. The API is partly dissolved in the excipient, the already dissolved fraction consequently does not contribute to the melting enthalpy value. The question is to be raised why the effects of API dissolution during the heating could not be detected in the physical mixtures during DSC measurements. One reason might be that the dissolution kinetics is much quicker if the API is submicron-sized and intensively mixed with the surfactant. Remarkably, X-ray signal intensity is much lower for the Tween® 80 containing suspension. This is very often the case when extremely small crystallites are measured via DSC and has been described by other authors. Interestingly, in this case the x-ray diffraction signals do not correlate with the particle size measured via DLS (1242±279nm, PDI: 0.42±0.05). A potential reason may be that small primary particles aggregated after processing and led to the large particle sizes in DLS. Another example of small roentgen signals is given in Figure 3.4.33. In contrast to the other examples the suspension shows small and nearly monodisperse PSD in DLS (185±11nm, PDI: 0.11) and good physical stability over several weeks storage.

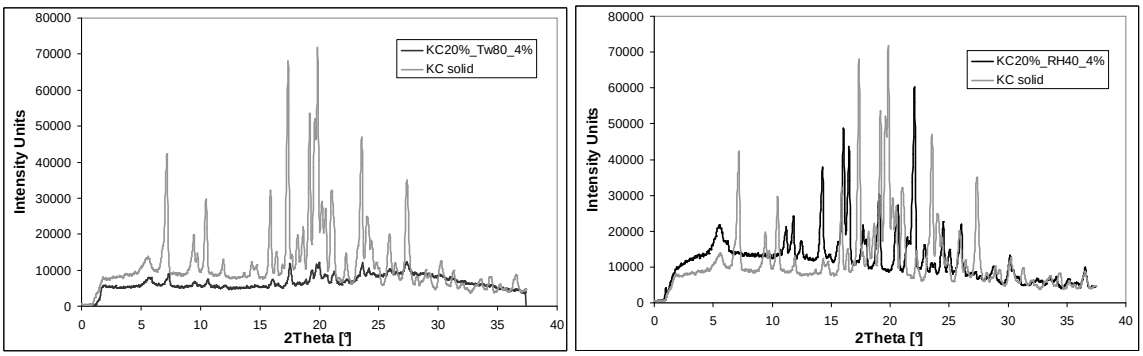

Figure 3.4.32: Diffractograms of different KC nanosuspensions (black line) and the respective API batches (grey line)

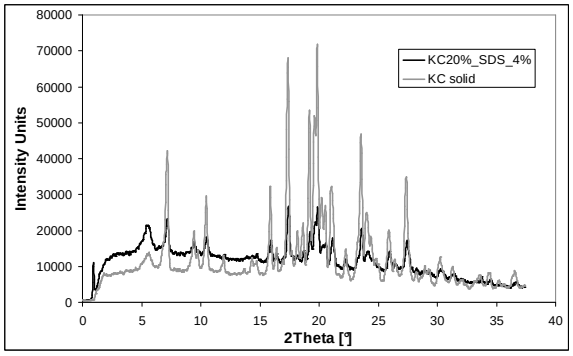

Figure 3.4.33: XRD of a KC nanosuspension stabilized with SDS (black line) in comparison to unprocessed KC (grey line)

3.4.4.4 Solubility parameters as prediction tool for drug-stabilizer interaction

The concept of solubility parameters was established by Hildebrand [112] and Charles Hansen [113] in the mid of the 20th century in order to mathematically describe the solubility behavior of binary mixtures of substances. It is widely applied in chemical industry and gained growing interest in the mathematical prediction of phase solubilities for pharmaceutical excipient/API mixtures [114] and solid dispersions [115]. The basic concept of solubility parameters is based on the calculation of the cohesive energy density CED, i.e. the sum of the attractive forces between molecules. The solubility parameter δ is calculated from CED by

$$\delta = (CED)^{1/2} = (\Delta E_v / V_m)^{1/2} \tag{3.4.1}$$

where $\Delta E_v$is the enthalpy of vaporization and $V_m$the molar volume.

Different methods to calculate the group contributions are applied, most commonly the approaches by Hoftyzer/Van Krevelen [116], Hoy [117] and Fedors [118]. For the following considerations the method proposed by Van Krevelen will be applied. The single contributions are based on the assumption that the total solubility parameter $\delta_t$is the sum of the individual parameters for dispersion (d), polar (p)and H-bonding (h) forces.

$$\delta_t^2 = \delta_d^2 + \delta_p^2 + \delta_h^2 \tag{3.4.2}$$

Figure 3.4.34 gives an example for the calculation of $\delta_t$for the molecule fenofibrate.

Group	n	F_{di}	n x F_{di}	F_{pi}	n x F^2_{pi}	E_{hi}	n x E_{hi}	V_m	n x V_m
$-CH_3$	4	420	1680	0	0	0	0	33,5	134,0
-CH<	1	80	80	0	0	0	0	-1	-1,0
>C<	1	-70	-70	0	0	0	0	-19,2	-19,2
C_6H_4 (o,m,p)	2	1270	2540	110	24200	0	0	52,4	104,8
-COO-	1	390	390	490	240100	7000	7000	18	18,0
>C=O	1	290	290	770	592900	2000	2000	10,8	10,8
-O-	1	100	100	400	160000	3000	3000	3,8	3,8
-Cl (aromat)	1	450	450	550	302500	400	400	28	28,0
sum			5460		1319700		12400		279,2

$$\delta_d = \frac{\sum F_{di}}{V} = 19.56 \qquad \delta_p = \frac{\sqrt{\sum F^2_{pi}}}{V} = 4.11 \qquad \delta_h = \sqrt{\frac{\sum E_{hi}}{V}} = 6.66$$

$$\delta_t = \sqrt{\delta_d^{\,2} + \delta_p^{\,2} + \delta_h^{\,2}} = \mathbf{21.07}$$

Figure 3.4.34: Example for solubility parameter calculation for FF, Van Krevelen/Hoftyzer method [116], F_{di}group contribution of dispersion component, F_{pi}group contribution of polar component, E_{hi} hydrogen bonding component

Respective calculations were performed for the model compounds and all stabilizers performed in the milling trials. The respective values are listed in Table 3.13. In an aqueous environment preferably the hydrophobic contributions should be responsible for particle/stabilizer interactions. Therefore the respective contribution for dispersion and H-bonding is listed.

Table 3.13: Solubility parameters and group contributions for APIs and excipients used in milling experiments, calculated according to Van Krevelen/Hoftyzer method

Compound	δ_t	δ_h	δ_d	Excipient	δ_t	δ_h	δ_d
FF	21.07	6.66	19.56	DOSS	19.83	6.06	16.54
GF	20.3	7.54	18.15	SDS	19.49	7.43	16.13
KC	20.07	6.37	18.43	NaDC	34.07	7.93	31.32
				Solutol	21.75	8.66	19.8
				RH40	21.75	8.66	19.8
				TPGS	20.08	8.56	18.07
				Tween 80	22.49	9.09	20.44
				Tween 20	21.29	9.60	20.91
				Lutrol F68	19.78	8.88	17.66
				Lutrol F127	19.75	8.89	17.63
				HPMC	25.25	17.65	19.55
				PVP	26.85	5.55	20.44

The correlation of similarity of different contributions is compared to physical stability results of nanosuspensions described under 3.4.3.1. For GF the anionic surfactants NaDC, DOSS and SDS were defined as potent stabilizers. All other substances failed to stabilize the suspensions. Given a similarity range of $\pm$0.5 - 1.0 the data do not unravel a clear

relationship for d_t or single group contributions. The same applies for FF where NaDC, HPMC and SDS were identified as hits. Finally, ketoconazole leads to stable suspensions with a variety of hits. A comparison of solubility parameters and contributions between APIs and surfactants can be found in table 3.13.

3.4.5 Material properties and grindability

Especially in the field of alloy research and grinding of anorganic materials the correlation of grinding to intrinisic material properties has been extensively studied [119, 24, 19]. Correlations have been found between minimum obtainable crystallite size and melting temperature, activation energy and normalized hardness [119].

3.4.5.1 Nanoindentation

Taylor et al. recently proposed a system to predict the grindability of pharmaceutical API via nanoindentation and calculation of the brittleness index (BI) [120]:

$$BI = \frac{H}{K_c} \tag{3.4.3}$$

H is the hardness [GPa] measured via nanoindentation, $K_c$is the fracture toughness [MPa $m^{1/2}$] introduced by Dukino et al. [121]. Fracture toughness measurements imply the measurement of a crack length after indentation via SEM. The authors found a direct correlation between grindability of the dry powder and the brittleness of the 5 compounds. No such correlation could be found by just comparing elastic modulus or hardness of the substances.

For the three test compounds hardness and young's modulus were determined under the conditions described in 2.2.12. Generation of drug crystals suitable for indentation was critical as the necessary particle size of more than 1mm side length could hardly be obtained by using the organic solvents that were applied by the manufacturer in the purification process. Application of the correct solvent is crucial as it determines among other factors type and number of crystal lattice dislocations. These in turn determine the breaking behavior of the drug crystal. Especially KC was hard to crystallize in sufficiently large crystals. Apart from that the API seemed to form amorphous domains or regions with high numbers of dislocations what had tremendous impact on the reproducibility of indents. Results of the indentation trials are displayed in Figure 3.4.35. Whereas standard deviations for FF are high but in acceptable ranges, data for KC show high scattering. Generally, results are in accordance with published data for pharmaceutical compounds [120]. Surprisingly, results for E and H are closely correlating. It must be noted that E and H are not necessarily dependent on each other. Further it can be seen that FF displays the highhest values for

hardness and tensile strenghts. GF is showing lowest values for both parameters whereas KC seems to be in the mid range. Unfortunately, the comparison between KC and FF/GF is beyond acceptable levels of significance and can at best serve to define a general trend. The test protocol for KC would have to be modified for further experiments.

Despite these drawbacks the results can be correlated to inherent properties of the drug substances (Fig. 3.4.36). Material hardness can - for the 3 drug substances - be correlated to their melting points. For inorganic compounds a relationship between melting point and material hardness was shown [119]. Interestingly, for the compounds tested here, an inverse relationship seems to exist. This might not be easy to explain because stronger bonds in a crystal lattice normally correlate with high melting temperatures and high material hardness. Probably due to the brittleness of KC and GF an inconsistent picture via the nanoindentation setup is given what might be partly expressed by the high standard deviation of the measurements. Meanwhile the determined values for H are very consistent when comparing them with the „milling efficiency“ of the three substances. Therefore milling data for an optimum 120 min process were compared for the three drug compounds (see Figure 3.4.6). It can there be seen that even after breaking of aggregates and large particles within the first one to five minutes the kinetics of comminution are different for the three drug compounds. Furthermore it is apparent that particle size levels off at app. 115 nm after 120 min for all three compounds, i.e. all compounds are reaching the same particle size, but with different kinetics. Therefore a simple measure for the Relative Size Decrease (RSD) is introduced. It takes into account that 1) starting particle sizes of the three compounds are slightly differing in the beginning and 2) that the three compounds may exhibit different kinetics for deaggregation or deagglomeration what can distort results in the DLS readout. It considers the particle sizes in a timeframe of 15 min to 120 min. The respective formula is

$$RSD[\%] = \frac{Size(15min) - Size(120min)}{Size(15min)} x100 \tag{3.4.4}$$

It is understood that the proposed parameter can only be a tool for relative comparison for formulations where exactly the same experimental conditions have been applied. The RSD is high for substances that require long processing times for particle comminution, it is low for highly grindable substances that show effective particle comminution already in the first minutes of processing. It can be seen that the relative size decrease directly correlates with values for the hardness of the test substances. It must be noted that all data generated within this section depict a very limited data set. Therefore the author is reluctant to draw general conclusions. In addition, hardness measurements did show a high variability, especialy for KC. The relevance and validity of the obtained values must therefore be discussed with caution. Unfortunately, it was not possible to determine the brittleness

index for the tested compounds as no SEM microscope was available when performing indentation runs. No cracks could be observed via light microscopy in the tested samples.

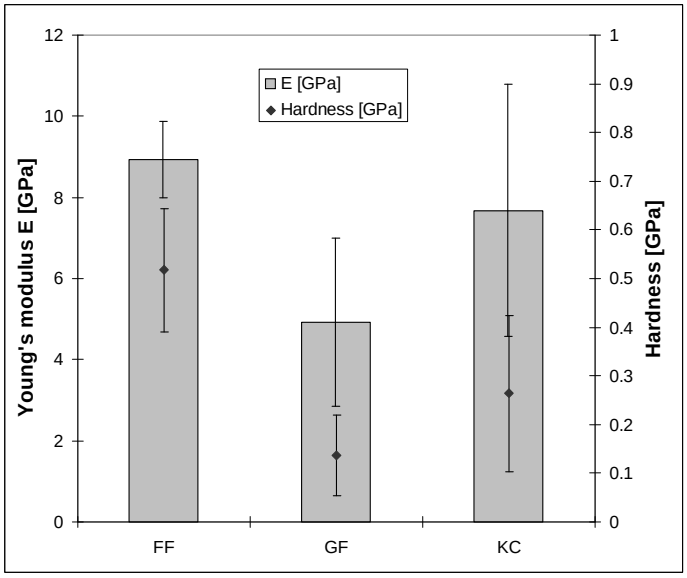

Figure 3.4.35: Young's modulus E and hardness H of three model compounds, mean±sd, n=25

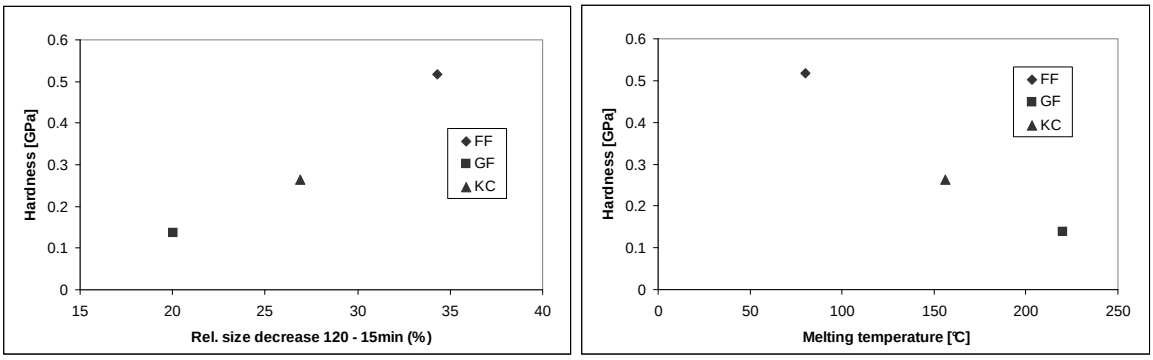

Figure 3.4.36: Correlations between hardness and a) relative size and b) melting temperature

3.4.5.2 Rheological properties

Rheological properties of several model suspensions were investigated as described under section 2.2.3. As indicated in 3.4.2.8 effects such as shear thickening will be more intensively investigated. One example was a suspension of KC applying Tween® 80 as stabilizer. When comparing milling processes on agitator and planetary ball mills two differences might come into play regarding differences in the milling results: One might be that the applied shear stress is significantly higher in one of the processes. This can be ruled out as agitator and planetary ball mill processes end up in similar particle sizes with a tendency towards lower particle sizes for agitator ball mill processes. What could be taken into consideration is the energy input per time unit that may cause extensive heating and physical changes in the

sample. Therefore the process on the planetary ball mill is interrupted by pauses to prevent strong heating of the product. In fact the milling processes are designed such that process temperatures never exceed +40°C in the process in agitator as well as planetary ball mills. The big advantage in agitator ball mills is the possibility to constantly cool the system and therefore run the process without pauses. In the example mentioned it can be seen that on the planetary ball mill the milling trial completely fails and the liquid bed plus milling beads has a paste like appearance. In contrast to that milling on a planetary ball mill in a constant process is feasible. To elucidate this observation different types of shear stress via a cone plate rheometer were applied (Figure 3.4.37). Although not being able to completely simulate the conditions in a ball mill the applied shear should at least give some hints on possible explanations. In a first set of experiments viscosities were tested within increasing and decreasing shear rate (left figure). The suspension can be identified as non-newtonian fluid and shows thixotropic behavior with no perceptible hysteresis. This correlates well to the uncritical milling process on an agitator ball mill. In contrast Figure 3.4.37 (right figure) is giving clear evidence of increasing viscosity after about 8 cycles of shear stress à 30 s followed by 30 s pause. Although only a low increase in viscosity is detected, a clear trend towards thickening can be detected. The reason for this phenomenon is unclear. The data suggest that thickening might be fostered by relaxation phases after intense mechanical stress.

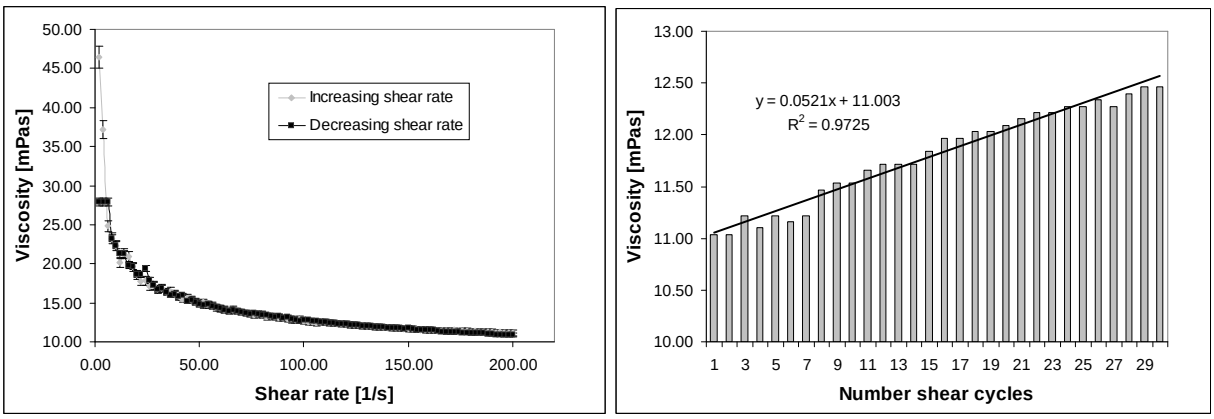

Figure 3.4.37: Rheological investigations on suspensions 20 % KC and 4 % Tween 80. Left: Shear gradient Right: Intermittent shear stress at 300 s^{-1}.

3.5 In vitro-permeation of nanoscopic drug delivery systems

Caco-2 permeation tests are well established for assessing drug permeability over mucosal barriers. Apart from that they show some potential in predicting the in vivo performance

of drug delivery systems. Within the scope of this work it shall be assessed if size reduction in suspensions and lipidic carrier systems lead to an enhanced permeation of the drug substance. In the following data the size effect was investigated for three test compounds in suspension systems. Due to the poor oil solubility of griseofulvine and ketoconazole, solely fenofibrate was applied in the lipidic carrier systems.

To assess the influence of bile salts and lecithine in the media of the donor compartment on drug permeation, FaSSIF and FaSSIFblank (i.e. buffer medium without the respective amount of surface active substances) are tested in parallel. FeSSIF was not included as transport medium because it was shown that standard FeSSIF is toxic to Caco-2 cells and therefore not suitable for transport experiments [122]. Modified versions of FaSSIF and FeSSIF for the use in in-vitro permeation experiments have been proposed [123][124], but were not included within these investigations as the primary goal was to assess pure presence versus absence of solubilizing components in the transport medium.

3.5.1 Suspension versus nanosuspension

3.5.1.1 Fenofibrate

Table 3.14 is depicting the size characteristics of the test coarse suspension and nanosuspension. The coarse suspension and nanosuspension are equally composed and consisted of 10% (w/w) API and 0.5% SDS dispersed in bidistilled water. The nanosuspension was processed on a Fritsch P7 CL planetary ball mill before usage (see 2.3.3). It can be seen that FF particles are efficiently comminuted to particle sizes $<$ 200nm whereas the unprocessed suspension is showing median values of around 15 µm. Both coarse and nanosuspensions were tested in FaSSIFblank and FaSSIF to assess the influence of solubilizers on the permeation behavior. Prior to administration to the apical part of the transwell chamber suspensions or nanosuspensions were diluted in the respective medium to a drug concentration of 0.5mM. FF and fenofibric acid concentrations were measured via RP-HPLC (see section 2.2.14 for experimental details). Figure 3.5.1 shows the permeated amount of drug over a time period of 120 minutes. It can be seen that by applying FaSSIF as apical medium a higher mass transfer (3.2 % versus 2.4 %) after 2 hours can be achieved. Slight solubility or permeability enhancing effects can also be seen when comparing the permeation of a FF nanosuspension (5.6 % versus 5.0 %) but these are less pronounced.

Table 3.14: Fenofibrate coarse suspension and nanosuspension, SLS data, nanosuspensions were produced via wetmilling, mean±sd, n=3

Fenofibrate	coarse suspension [µm]	nanosuspension [nm]
Mean	19.2±2.3	163.1±11.2
particle size distribution described as sdv	8.26±2.2	130.3±17.2
Median	19.3±1.9	122.1±13.1
Stabilizers	SDS 0.5% (w/w)	SDS 0.5% (w/w)

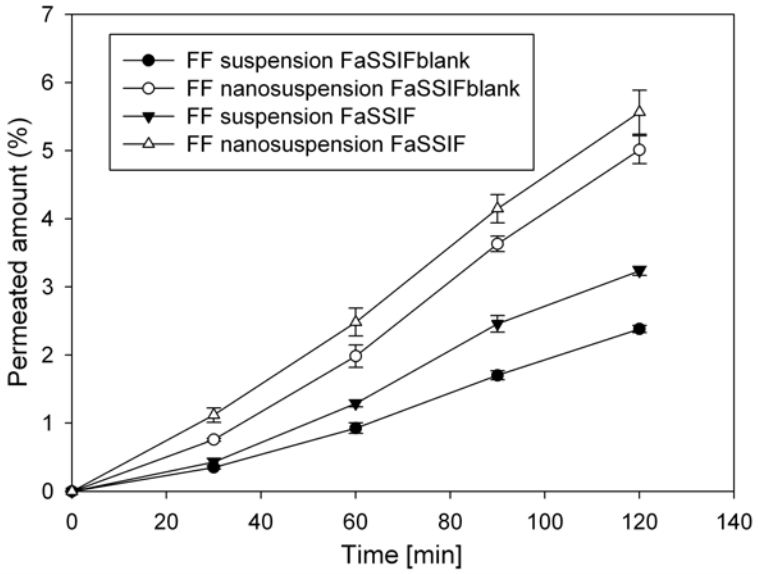

Figure 3.5.1: Caco-2 permeation data of fenofibric acid from micro-and nanosuspensions in different apical media, mean±sd, n=4-6

3.5.1.2 Griseofulvin

Physical parameters of GF nanosuspensions are listed in Table 3.15. As discussed in the nanomilling section GF particles show preferable properties for size reduction what is seen in the low median size value of the nanosuspenion. Figure 3.5.2 is displaying the corresponding permeability data in FaSSIFblank and FaSSIF. Two observations can be made: First, permeability enhancement by nanonisation is occuring to a lesser extent than for FF where a more than 2fold increase in permeated mass was detected in FaSSIFblank (see Figure 3.5.1). Second, permeability is hardly affected by the presence of solubilizing micelles in the transport medium (FaSSIF). Enhancement of dissolution speed via comminution shows approximately 60 % improvement in permeation. Enhancement of absolute solubility due to surface active substances is not significantly affecting drug permeation in comparison to the transport medium FaSSIFblank.

Table 3.15: Griseofulvin coarse suspension and nanosuspension, SLS, mean±sd, n=3

Griseofulvin	Coarse suspension [µm]	Nanosuspension [nm]
Mean	17.3±0.1	123.1±4.6
particle size distribution described as sdv	10.0±0.1	83.3±11.6
Median	13.6±0.2	100.2±5.2
Stabilizers	SDS 0.5% (w/w)	SDS 0.5% (w/w)

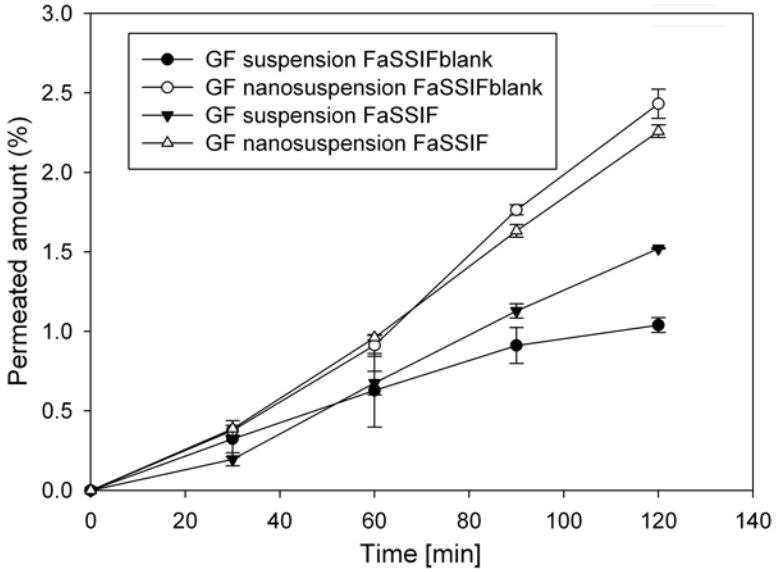

Figure 3.5.2: Caco-2 permeation data for GF micro-and nanosuspensions in different apical media, mean±sd, n=4-6

3.5.1.3 Ketoconazole

Permeation data for KC suspensions are depicted in Figure 3.5.3. In contrast to FF suspensions, a low permeation enhancement in FaSSIF compared to FaSSIFblank between suspensions and nanosuspensions of only factor 1.4 at 120 min is observed. The value is obtained by calculating the ratio of the permeated mass of KC nanosuspension/ KC suspension. As for GF there is no clear difference observable between the two apical media.

Table 3.16: Ketoconazole coarse suspension and nanosuspension, SLS, mean±sd, n=3

Ketoconazole	Coarse suspension [µm]	Nanosuspension [nm]
Mean	11.3±0.3	138.2±2.9
Size distribution width described as sdv	8.8±0.2	95.5±11.6
Median	13.6±0.2	111.23±7.1
Stabilizers	SDS 0.5% (w/w)	SDS 0.5% (w/w)

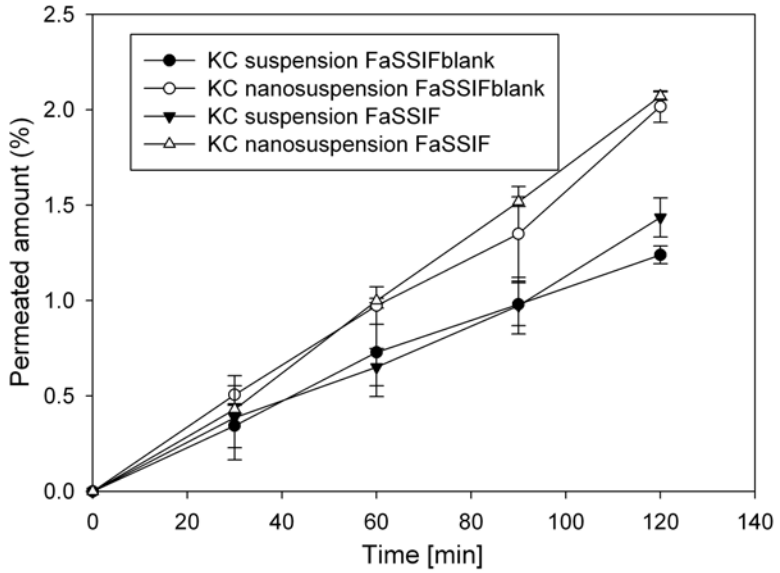

Figure 3.5.3: Caco-2 permeation data for KC micro-and nanosuspensions in different apical media, mean±sd, n=4-6

3.5.2 Emulsion versus nanoemulsion

Two different emulsion systems were chosen exemplarily for permeability testing. In both cases 20 % (w/w) Miglyol was chosen as the lipid carrier. Solutol® HS15 and the sucrose ester Ryoto® L1695 were used as surfactants. Emulsions were prepared according to the procedure described in 2.3.1. Particles sizes of the formulations tested are listed in Table 3.17. Figure 3.5.4 displays remarkable differences between emulsions stabilized by Solutol and the sucrose ester L1695. Generally, for both emulsions as well as nanoemulsions permeation is higher when applying the sucrose ester type surfactant. In addition, nanoemulsions containing L1695 exhibit far higher absolute permeation after 120 min (5.1 versus 3.3 %).

Table 3.17: Particle sizes of emulsions and nanoemulsions applied in Caco-2 experiments, SLS, mean±sd, n=3

Fenofibrate	Solutol emulsion [µm]	Solutol nanoemulsion [nm]	L1695 emulsion [µm]	L1695 nanoemulsion [nm]
Mean	15.3±0.3	135.1± 8.3	12.5±2.3	92.4±10.1
Size distribution width described as sdv	3.4±0.2	23.6±5.3	4.4±0.5	33.4±11.0
Median	14.1±0.1	116.3±6.8	13.3±1.1	8.3±4.3
Stabilizers	Solutol HS15 2 % (w/w)	Solutol HS15 2 % (w/w)	L1695 2 % (w/w)	L1695 2 % (w/w)

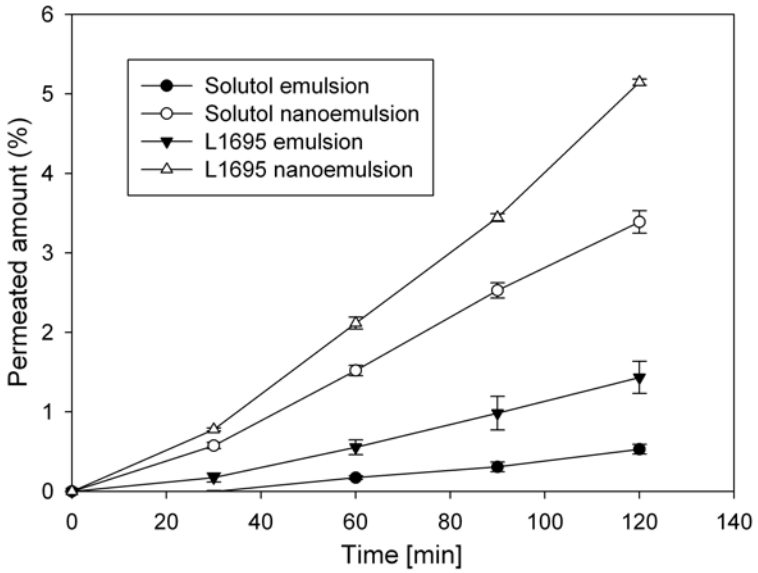

Figure 3.5.4: Permeation amount of FFA of emulsions and nanoemulsions containing FF, apical medium: FaSSIF, mean±sd, n=3-4

3.5.3 Microemulsion

The SMEDDS formulation described in section 3.2 was tested with a drug load of 25 mg/g, 50 mg/g and 100 mg/g fenofibrate to assess whether the surfactant - API ratio is affecting the permeation kinetics of FF across the mucosal barrier. Respective amounts of preconcentrate were added to the transport media directly before exchanging the culture medium versus transport medium and mixed gently several times with a pipette to allow rapid emulsification. Again FaSSIF and FaSSIFblank were applied as media in the apical compartment. Assessing the permeability of drug substances in the presence of large amount of surfactants is always critical as the cell layer integrity may be severly compromised. Fig. 3.5.5 displays transepithelial resistance values of a 100 mg/g formulation in FaSSIF or FaSSIFblank. Two observations can be made. First, the TEER values drop as soon as the culture medium is changed from DMEM to FaSSIF/FaSSIFblank. Second, TEER values decrease to values of app. 200 Ωcm^2 after 2 h incubation in the FaSSIF medium. Hydrophilic markers such as Fluorescein-sodium can be used to further assess cell layer density. In this particular case the ester cleavage reaction of FF into FFA was applied to assess harsh impacts on cell layer integrity.

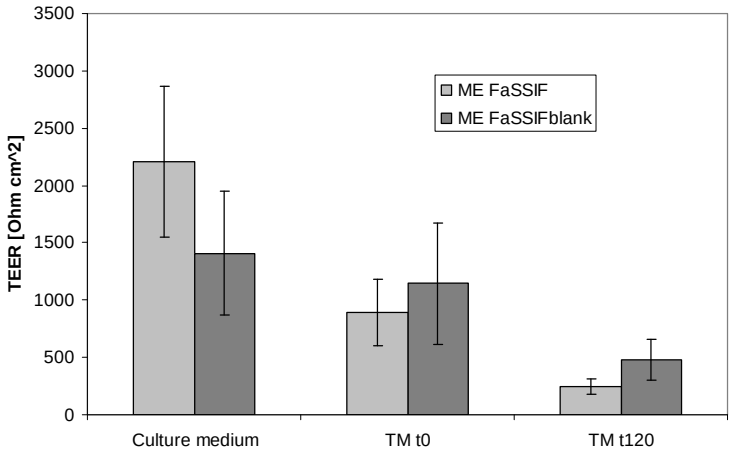

Figure 3.5.5: TEER values of Caco-2 cells incubated with 100 mg/g FF microemulsion formulation at different time points, mean±sd, n=4-6

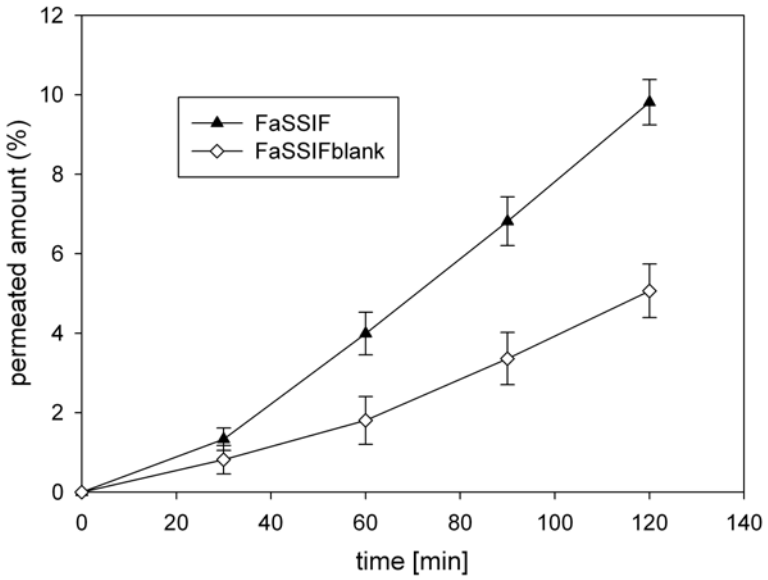

Figure 3.5.6: Permeation of FF in Caco-2 cells in microemulsion carrier, 100 mg/g, mean±sd, n=4-6

The assumption is that as soon as tight junctions are broken up microemulsion droplets containing FF are supposed to pass the filter membrane. The presence of FF in the basolateral medium therefore indicates dysfunction of the mucosal barrier. FF and FFA were measured via HPLC in the basolateral medium at all sample points. It was shown that no FF was detectable on the basolateral side in experiments applying FaSSIFblank as apical medium. In contrast, FF could be detected in concentrations $> 0.3\,\mu g/mL$ already after

60 min in the basolateral side when FaSSIF was applied. When comparing the the influence of different excipient/API ratios on the permeation behavior of fenofibrate (Fig. 3.5.7) it can be seen that permeation is highest in the formulation applying the highest drug load of 100 mg/g. A simple experiment helps to understand the phenomenon. Microemulsion preconcentrates at 25, 50 and 100 mg/g FF drug load were dispersed in FaSSIF at the same concentration that was applied in Caco-2 experiments and incubated in glass vials at 25°C for 5 d. Afterwards the emulsions were assessed via optical light microscopy, DSC and HPLC. It can be seen in Figure 3.5.8 that recrystallisation of FF crystals from the model microemulsion is more pronounced with increasing drug load of the preconcentrate. Whereas at 25 mg/g no visible precipitation can be detected even after 5 days emulsions at 50 mg/g showed some drug crystals. At 100 mg/g a large number of crystals can be seen. Via DSC the existence of FF crystals could be confirmed, HPLC analysis proved the absence of large amounts of hydrolized drug (FFA $< 2\%$ in relation to FF). Although in-vivo and in cell culture different time windows are of relevance the results indicate that physical instability might foster the redistribution of the lipophilic API into other lipophilic compartments (such as cell membranes) and therefore explain the higher permeated amount for the high concentration preconcentrates. Further experiments at elevated temperatures in biorelevant media should be executed to prove this hypothesis.

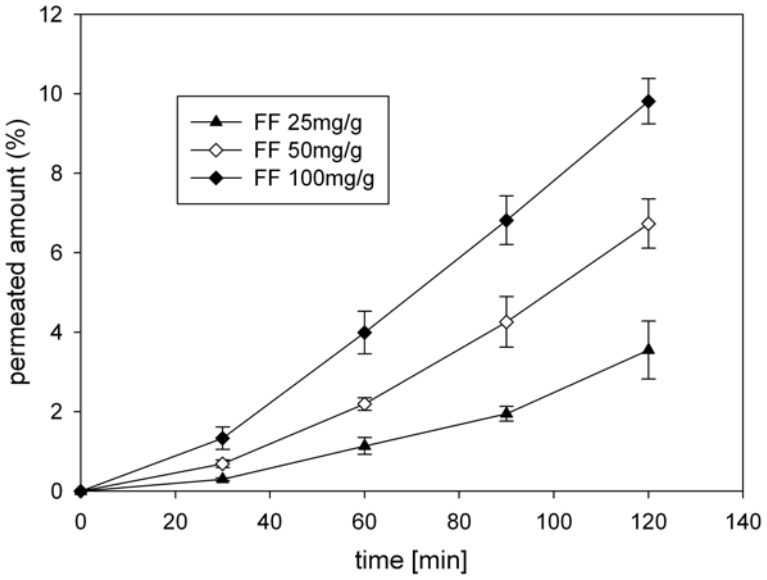

Figure 3.5.7: Caco-2 permeation of microemulsion formulation in FaSSIF comparing different drug loads of FF, mean±sd, n=4-6

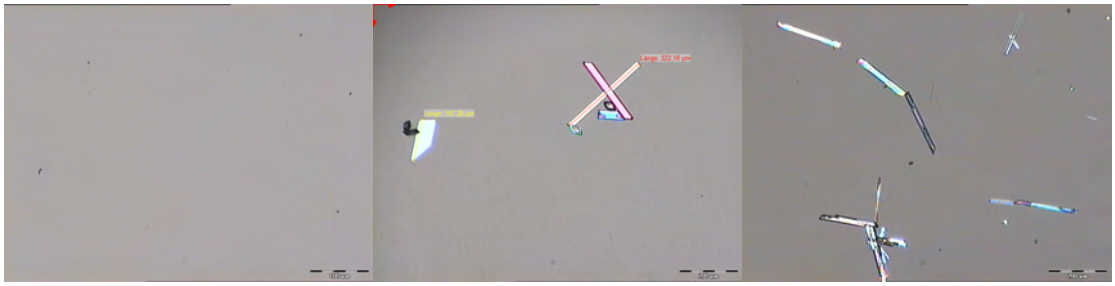

Figure 3.5.8: Incubation of FF microemulsion formulations (25, 50, 100 mg/g from left to right) in FaSSIF, 500x magnification, scale bar: 200 µm

3.6 In vivo study

Five formulations assessed in the in vitro permeation test were investigated in an in-vivo study on male wistar rats. Because being able to be formulated within a wide range of drug delivery systems fenofibrate was chosen as model compound. The formulations were as follows (all concentrations in w/w):

1. Pure drug substance dispersed in an aqueous slurry containing 0.5 % Methocel K4M and 0.055 % Tween® 20
    - Particle size: 19.2 µm, sdv 7.2 µm
2. Microemulsion preconcentrate consisting of 60% Solutol® HS15, 20% Capryol® 90 and 20% Miglyol® 812, containing 100 mg/g fenofibrate, dispersed in bidistilled water
    - Particle size: 35.5 nm PDI: 0.05
3. Nanoemulsion consisting of 2% Solutol® and 20% Miglyol® , containing 20 mg/g fenofibrate
    - Particle size: 208.0 nm PDI: 0.072
4. Nanoemulsion consisting of 2% L1695 and 20% Miglyol® , containing 20 mg/g fenofibrate
    - Particle size: 114.3 nm PDI: 0.152
5. Coarse suspension consisting of 2.5% HPMC (Pharmacoat 603) and 0.1% docusate sodium and 200 mg/g fenofibrate
    - Particle size: 20.1 µm sdv 3.4µm
6. Nanosuspension consisting of 2.5% HPMC (Pharmacoat 603) and 0.1% docusate sodium, containing 200 mg/g fenofibrate

- Particle size: 138.5nm PDI: 0.17

Plasma profiles of the formulations are displayed in Figure 3.6.1.

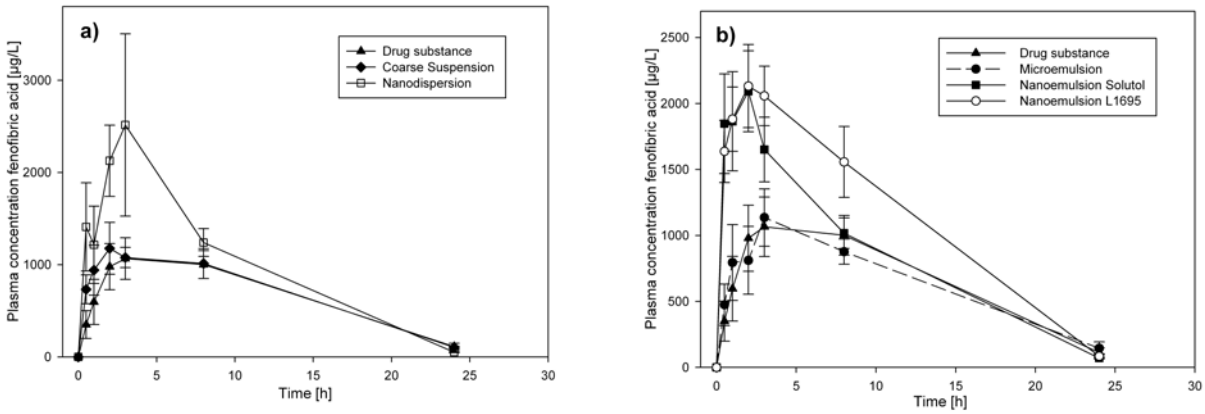

Figure 3.6.1: Plasma concentrations of fenofibric acid after administration of different oral fenofibrate formulations to wistar rats, n=3-4, mean±SEM, a) displays the micronized API (drug substance) and the API in an aqueous dispersion containing the same stabilizer as in the nanosuspension formulation, b) comprises the drug substance in comparison to the lipidic formulations (microemulsion + two nanoemulsions)

Table 3.18: PK parameter of different oral fenofibrate formulations administered in rats at 2.1 mg/kg, n=2-4, mean±sd, * only two values (values given in parentheses)

Sample	AUC [µg*h/L]	t_{max}[h]	C_{max} [µg/L]	$t_{1/2}$ [h]
Pure drug substance	13800±4910	2.67±0.58	1070±433	5.06±1.30
Microemulsion preconcentrate	13700±4330	4.67±2.89	1140±498	6.57±2.92
Nanoemulsion Solutol	17500±4750	1.25±0.87	2090±756	4.32±0.83
Nanoemulsion L1695	20200* (17500/22900)	4.33±3.21	2130±551	3.98* (4.08/3.88)
Coarse suspension	14400±3860	1.67±0.58	1180±486	4.93±0.46
Nanosuspension	20000±8740	1.50±1.22	2520±1980	3.51±0.43

Despite high individual variations in the different test groups a clear trend towards the performance enhancement of nanoscale formulations can be detected. Results for the nanosuspensions are significantly higher ($p<0.05$) in comparison to the microemulsion and non nanosized formulations. The following roughly patterned rank order can be implemented:

Nanosuspension > Nanemulsion Sucrose ester = Nanoemulsion Solutol HS15 > Microemulsion = Coarse suspension = Drug substance.

AUC and C_{max} for the nanoemulsions containing Solutol or L1695 are not significantly different (Tab. 3.18). Data for L1695 suggest a trend towards a broader window of absorption for FF as the plasma concentrations are significantly higher at 8 h. When attempting to set up an in-vitro in-vivo relationship between Caco-2 and in-vivo data a correlation can be

found between the relative increase in permeation and the relative increase in AUC (Figure 3.6.2). The relative enhancement was calculated in relation to the respective values obtained for the FF drug substance. The microemulsion was excluded in these considerations because a lack of correlation is most likely caused by disintegration of the Caco-2 cell layer in the in-vitro test setup. Potential reasons for the in-vivo failure of this formulation will be discussed within the following section. For the other formulation approaches it can be seen that permeation and permeability enhancement can be correlated. Nevertheless a strong linear relationship could not be found.

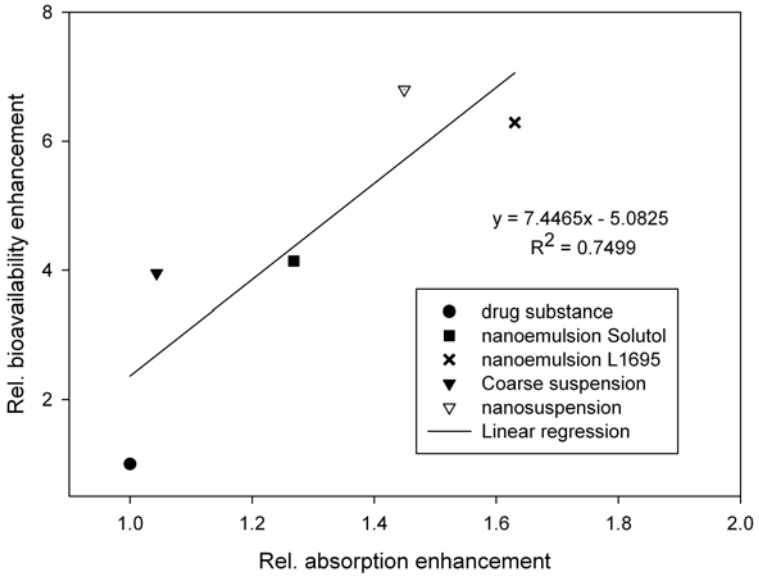

Figure 3.6.2: Correlation between relative permeation enhancement and relative bioavailability enhancement, permeation enhancement was calculated as permeated amount after 120 min in comparison to solid drug substance in the Caco-2 model applying FaSSIF as donor medium, bioavailability enhancement is defined as the relative AUC increase in comparison to micronized drug substance. Values for drug substance were set to 1

4 Discussion

4.1 Cyclodextrins

Complexation studies in the two cyclodextrin variants revealed that the influence of the surfactant Polysorbate 20 is limited when formulating the three model compounds under standard liquid conditions in buffer as performed within preclinical formulation development. The question was worth following as numerous examples in literature describe interactions between cyclodextrins and surfactants, alcohols, acids and other chemicals [125]. Yang et al. for example demonstrated that solubilisation of a poorly soluble compound was heavily compromised when applying SDS and a sulfobutyl-beta-cylodextrin in combination at different ratios [126]. Other authors describe similar effects for HP-β-CDs [127, 128]. In our study only low Polysorbate 20 concentrations around the CMC of the surfactant (app. 0.01 % w/v) were tested. Up to concentrations of 0.03 % w/v no influence of the surfactant was detected except for a trend towards higher solubility for KC+Kleptose mixtures. Notably high standard deviations were observed in all tests as soon as the tenside was added so it must be stated that the relevance of the test is limited. It was seen that the addition of the surfactant disturbed the ability to centrifugate the samples properly what is the most likely cause for the high deviations. The results nevertheless foster the opinion that the combination of cyclodextrins and surfactants should be done with caution. Interactions are likely and cannot be foreseen. Biosimulating as well as physiological media also contain surface active compounds. The interaction of these substances with cyclodextrins, i.e. lecithins and bile salts were topic of investigation [129, 130, 131]. In the present study the question needed to be answered if the addition of surfactants present in common biosimulating media FaSSIF and FeSSIF affect the binding behavior of the three model compounds. The phase solubility studies revealed that at the low concentrations the complexation efficiencies were affected by the media. A comparison between FeSSIFblank and FeSSIF displayed that these effects were not solely due to changes in ionic strength and pH, but also directly related to the addition of bile salt and lecithin. The relevance for in-vivo as well as for formulation development must be discussed. Despite the limited set of substances tested it can be concluded that for polar substances such as ketoconazole it is of benefit to test the addtion of solubilizers such as lecithins and bile salts as these significantly enhanced

total solubility at 50 mM cyclodextrin concentration. For griseofulvin the binding behavior was negatively affected by the addition of buffer and surfactant. With the substances and settings tested it can also be stated that investigating phase solubility behavior did not result in findings that might be of interest in early formulation finding. Solubility testing at one given concentration of CD $\pm$ additional solubilizers might be sufficient. In preclinical development rather high CD concentrations (up to 400 mM) are applied. The relevance of interfering effects occuring at low concentrations should therefore be investigated at higher concentration ranges.

4.2 Investigation of a model microemulsion

Solubility of fenofibrate in different lipidic matrices was assessed by several authors. [132, 133, 134, 135, 136]. The results found there are in most cases in good agreement with the data generated within this work although the measurement protocols differed between the different authors. Other authors also describe important formulation aspects such as stability of microemulsions upon dispersion and maximum loading capacities in different biorelevant media. The focus of this work was not set on these formulation aspects as relevance and methodology are described in numerous publications. In terms of drug loading of the carrier it is to be highlighted that for the model compound fenofibrate solubility is higher in the mixture of the components (Solutol®, Capryol®, Miglyol®) in comparison to the solubility in the single components. This observation is often made in complex solvent or excipient mixtures. Although being adressed in computational approaches such as molecular modeling of API/excipient interactions no reliable tools to predict the solubility have been found yet. It emphasizes the necessity of excipient screening also for optimisation of drug payloads in microemulsion systems.

Considering physical characteristics of microemulsion droplets and the influence of dispersion media only a minor influence of different salt and pH conditions could be found (Fig. 3.4, 3.5). Slightly lower particle sizes were determined in SIFsp, whereas in acidic medium the preconcentrate dispersed in larger vesicles with a remarkably broadened size distribution. Generally, PDIs were found higher in disperion media other than water. While for FaSSIF and FeSSIF this can be attributed to the presence of other particle species, namely mixed micelles, an influence of salt and pH must be discussed for SGF and SIF. CryoTEM micrographs in Figure 3.2.3 reveal a highly polydisperse distribution in SGF with a large fraction of non-sperical shapes. In SIF, a large fraction of small droplets is accompanied by single large spheres that introduce a higher degree of polydispersity into the system. It was not within the scope of the work what would be the implication for drug loading of these particles. Furthermore, it would be of interest to see how droplets change upon changing

the dispersion medium from acidic to more neutral media. Thi et al. performed release studies for different compounds in a dialysis setup and could detect differences upon pH change [135]. The authors mainly attributed this to the pH dependent solubility of the model compounds. For neutral compounds (e.g. danazol, fenofibrate) no changes could be seen despite the droplet sizes of the microemulsion also there differed between different dispersion media. In fact, changes in the size of particles always lead to differences in the number of particles when keeping the volume of preconcentrate constant. In theory, this should lead to increased or decreased interfaces to the dispersion media and most likely to changes in the stability of the microemulsion systems. The aspect should be further investigated in in-vitro and in-vivo studies. Within this work the SMEDDS formulation containing fenofibrate was part of an animal study in rats (see section 3.6). There the formulation failed to increase bioavailability after peroral administration. Reformation of droplets and therefore destabilisation of the microemulsion may be discussed as one of the potential reasons for the failure.

In section 3.2.3.1 the dispersion process of the microemulsion preconcentrate was described. It could be shown that the emulsification process is slow and occurs within a timeframe of several minutes. To elucidate the processes involved in this slow droplet formation time resolved SANS studies were performed over a time window of up to 20 minutes. The results demonstrated that SANS is able to detect differences between the different measurement time points although an interpretation of the data is intricate. In both models applied data indicate the presence of smaller spheres at the beginning of the emulsification process which increase in size over a time frame of around 200 s. Data interpretation is hindered by an higher polydispersity of the system at the first measurement points. This is mainly due to the presence of larger fractions of undissolved and partly hydrated preconcentrate concomitantly with the microemulsion droplet. This also might explain the higher apparent volume fraction f_p modeled for the SPHERE+Chain algorithm. This more simplified model insinuates an increase only in the total radius RHS of the particles while core radii, meaning the core composition, stay relatively constant. Notably, the radii of the hydrophilic shell is in good agreement with the reported chain length of short chain PEGs, such as the ones in Brij® 700 [61]. The gyration radii in this study R_g were found to be a range from 2.20±2.28 to 4.06±0.12 nm, depending on concentrations and models applied. The values are by a factor of 2-3 lower than those found for PEG solutions in D_2O reported by Lancz et al. [137]. The authors also described an expected Gaussian coils structure. In Figure 4.2.1 the dimensions of Solutol were calculated via Chemsketch®. Although being a rather rough estimate for a stretched PEG chain, the dimensions found for the length of the hydrophilic part correlate well with the radius of the hydrophilic shell that is obtained via RHS - R_{core}: At equilibrium state shell radii of 5.0 -5.5 nm are calculated in

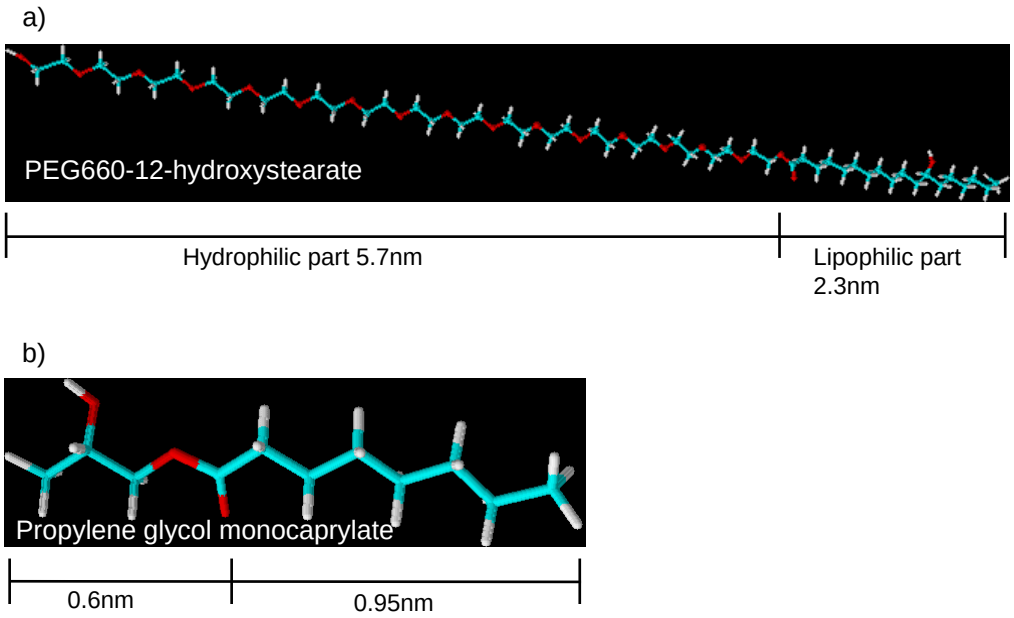

Figure 4.2.1: Structure and dimensions of hydrophilic and lipophilic parts of a) Solutol® HS15 and b) Capryol® 90, dimensions were calculated via ChemSketch® software by summing up bond lengths

both models corresponding well to the calculated value of 5.7 nm.The results insinuate that the PEG chains exist in a hydrated and fully stretched conformation after a time frame of approx. 200-300 s.

Another finding needs to be discussed regarding the relative composition of the droplets. Comparing core and shell volumina of a spherical particle of 12 nm radius, 42% of the volume must theoretically equal a radius of app. 9 nm. In contrast core diameters of 6nm are found that corresponds to 12.5% of the particle volume. In other words, a far higher fraction of the volume is occupied via the hydrophilic shell than it is expected by the composition of the preconcentrate. It must be hypothesized that hydration with D_2O dramatically increases the hydrophilic fraction of the droplets and therefore influences the distribution between lipophilic (i.e. core) and hydrophilic parts of the spheres. The presented data therefore suggest sufficient validity and probability of the data interpretation. Summarizing the findings it was found that spherical particles are detaching from the preconcentrate bulk during droplet formation concomitant with a slight increase of the outer droplet diameter over time. Two aspects are important: 1) the composition is at all time points different from pure Solutol micelles meaning that even at t= 0-30 s the oily phase is encapsulated into the core of the forming droplets 2) droplet size and composition seems to change during

the hydration process, with an increase in total droplet diameter detectable during the first 200-300 s. After that time window the fraction of large droplets is too high to detect further small vesicles. Figure 4.2.2 is representing schematically the formation process.

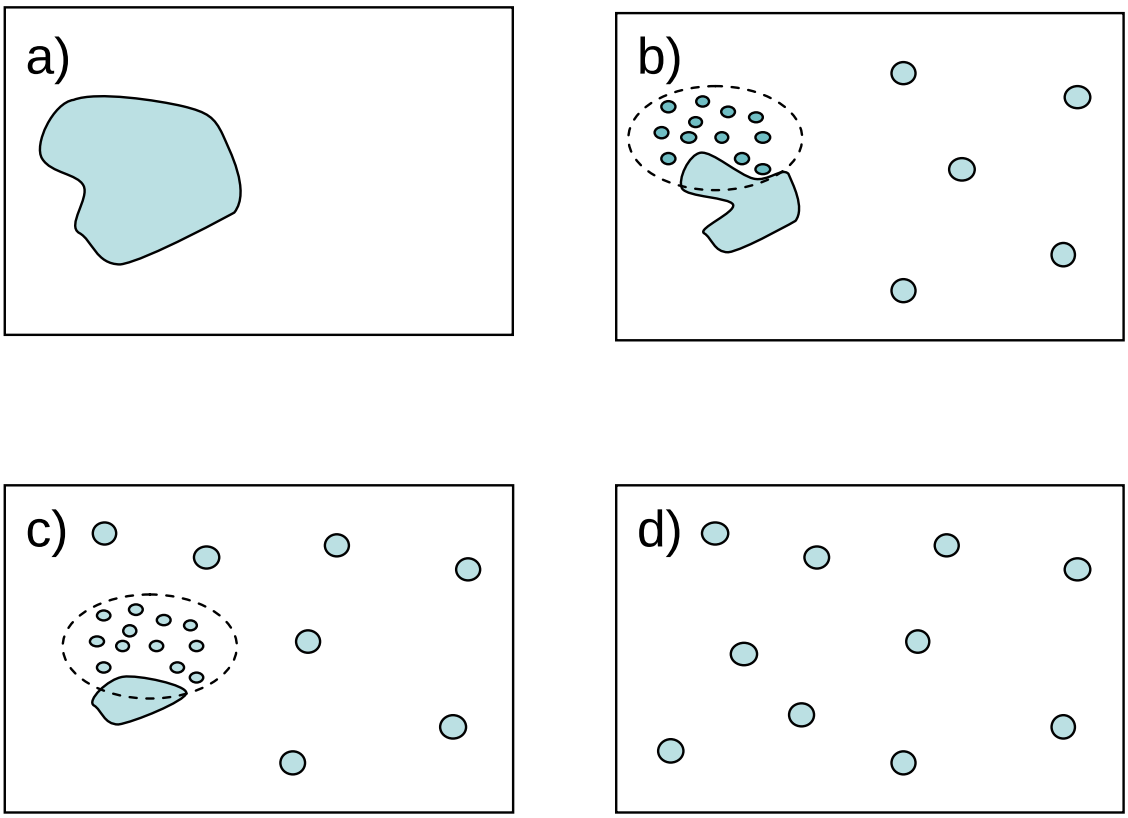

Figure 4.2.2: Scheme of particle formation during hydration of ME preconcentrate at a) 0 s b) 30-60 s c) 60-200 s d) 600 s

4.3 Nanoemulsions

Fig. 3.3.1 and 3.3.2 reveal that smaller particle sizes are obtained for sucrose esters in comparison to lecithins and pegylated nonionic surfactants. Two aspects can help to explain the differences in particle size. First, the kinetics of covering new water-oil interfaces by the surfactant is highly dependent on the properties of the tenside and might be slower for lecithins than for PEG glycerol esters. Another aspect is size and molecular weight of the surfactants. The experiments within this work were performed at constant weight ratios. While this approach is reasonable for handling heterogeneous substances it also means that for a small molecule such as sucrose laurate (Mw = 524g/mol) a higher number

of molecules is available for interface stabilisation than for the comparatively large PEG-15-hyroxystearate (Solutol® HS 15, average molecular weight $\sim$ 960g/mol [138]). The resulting higher molar ratio between surfactant and oil is influencing particle sizes after high pressure homogenization. Buttle demonstrated a decrease in the amount of surfactant at constant oil concentrations lead to an increase in particle size [139]. Another important aspect is that sucrose esters are compact molecules that lack of voluminous PEG-chains for steric hindrance. This again might contribute to the formation of smaller droplets in this case. In addition sucrose esters do not possess permanent charges as e.g. lecithins. The high net surface charge of lecithin emulsions leads to a less dense packing of molecules and therefore to a less efficient energy transfer during homogenisation. Zeta potential values are determined as -60 mV to -100 mV for lecithin emulsions and values of -6 mV to -25 mV for nonionic surfactants. In good agreement with the theory of steric hindrance the low surface charge emulsions containing nonionic surfactants show good physical stability which indicates that stabilization is achieved via steric effects of the large hydophilic PEG chains of the surfactants. Korner et al. have shown that the presence of phosphatidic acid and phosphatidyl inositol in emulsions containing soy lipids is responsible for the high negative surface charge of the droplets [140]. Egg based lecithins (e.g. Lipoid® E80) in contrast contain phosphatidylethanolamines which are neutral in charge and therefore result in a lower net surface charge [62, 141]. It can be concluded that sufficent size preservation is maintained with all surfactant systems. Stability was comparable in systems with steric as well as electrostatic repulsion as driving mechansim for interfacial stabilisation. With regard to zeta potential values there is a significant decrease visible for Cremophor® RH40 within the 3 months time frame. This should be further investigated with focus on lipid oxidation and hydrolysis. Due to strategic reasons the investigation of degradation pathways was not within the scope of this work and should be addressed in future studies. Phosphilipid stabilisation in pharmaceutical products is characterised for decades and therefore well investigated [142]. Chemical stability of sucrose esters is addressed for different applications [143, 144] but deserves special interest in pharmaceutical compositions.

Subsection 3.3.3 dealt with the incorporation of fenofibrate in nanoemulsions containing MCT. Whereas emulsions with standard compositions showed a pronounced size increase when FF was loaded into the oil droplets PSDs of sucroes ester emulsions were less affected by the addition of the lipophilic small molecule. Similar effects were seen in the chapter dealing with microemulsions where the addition of FF lead to a significant size increase of microemulsion vesicles containing Solutol and MCT. It can be hypothesized that depending on the solubility and interaction characteristics of the API with the surfactant applied the drug rather distributes at the oil surfactant interface (lecithins, Solutol) or is solubilized in the oily core. The localisation of the API in the emulsion droplets should be further inves-

tigated in future studies. The influence of drug loading on physicochemical characteristics should be further evaluated in extended stability studies. Remarkably data again exhibit no significant differences in zeta potential after 12 weeks storage. Nevertheless and regarding the limited set of data it can be hypothesized that no extended redistribution of the drug substance or its products between oily and aqueous phase occurs over the storage time.

Lyophilized drug delivery systems offer several advantages in comparison to liquid drug delivery systems. Generally, physical and chemical stability is enhanced over the shelf life. Also, by adjusting the reconstitution volume the operator is more free to choose a suitable concentration for administration. Due to their fluid and fragile structure lipidic systems such as liposomes and nanoemulsions are not directly amenable to lyophilisation but require certain amounts of lyoprotectants in order to preserve the structure of the droplets and to prevent agglomeration or coalescence [62]. Most commonly sugars and sugar alcohols are applied, but also esters of sucrose and fatty acids were described to act as cryo- and lyoprotectants for lipid vesicles [145]. A novel aspect in this work structure-preserving effects of hydrophilic sucrose esters were exploited to deliver both interfacial stabilisation and cryoprotection. Pronounced size preserving effects were observed especially for sucrose laurate (L1695) when applied in excess within formulations. A couple of questions are still to be addressed for this application. Despite showing good reconstitution after freeze drying storage stability of dry formulations must be critically investigated, especially with regard to the hygroscopicity of sucrose esters that we observed after storage of the raw materials at ambient conditions . Further areas of interest are the influence of drug incorporation on stability and morphology when transformed from the liquid to the freeze-dried state and the general structure of sucrose ester lyo cakes in comparison to sugars.

4.4 Nanosuspensions

4.4.1 Comparison milling processes

As outlined in the introductory part of this work nanosupensions are a versatile tool in formulation development of poorly soluble NCEs. Especially in early preclinical stages the development of a liquid formulation that is able to deliver high concentrations of API ($>$100 mg/mL) for high dose PK and toxicology studies is often necessary. In this work an API concentration range of 20 - 200 mg/mL was covered.

Taking a look at considerations such as energy input and the impact on grinding performance, one is prone to insinuate differences between milling beads of different matter. Indeed, Scherliess found significant differences in grinding media made of different polymers (polystyrene, polycarbonate) and stabilized zirconia [23]. When comparing similar size frac-

tions of different bead materials he observed an enhanced size reduction in an intraconazole nanosuspension for polystyrene grinding media. Apart from zirconia beads polystyrene is the most commonly used but not yet established material for pharma grinding applications, also drug delivery suppliers rely on special types of crosslinked polystyrene [146]. Nevertheless zirconia milling media are still a gold standard as the toxicological assessment of polystyrene (esp. leacheables) is still under discussion. In the present studies the grinding performance of zirconia versus polystyrene beads was compared in two different high energy ball mills. To our knowledge this was the first study that elucidated the milling performance of pharmaceutical APIs with both planetary and agitator ball mills under usage of polystrene beads. Especially the applicability of low density beads in planetary ball mills needs to be questioned as the respective energy impact to be achieved is highly dependent on bead density and consequently weight. Polystyrene exhibits only approximately one sixth of the specific weight of zirconium oxide (Tab. 2.9), therefore the specific energy input is only around 17% in comparison to the high density media.

Process parameter optimisation on the planetary ball mill was solely performed on zirconia beads because poylstyrene beads were not available in sufficient quality at that stage of the work. The size of milling beads proved to have a significant impact on the final size of the comminuted particles. When comparing 0.2-0.3 mm versus 1 mm beads the influence of the energy input of larger beads gets evident: Large beads enable sufficient comminution at rotational speeds of around 500 rpm whereas comminution of FF requires high rotational speeds for the smaller grinding medium. On the other hand the particles are ground to a more uniform particle size distribution when applying the small medium. This is due to the the more dense packing of smaller spheres with less free volume in the interspace what enables more efficient grinding of fine particles. In addition the higher number of smaller beads leads to a higher number of collisions per time unit. When investigating the influence of API concentration in the suspensions on grindability it can be seen that grinding of FF is most efficient at a solid concentration of 20-30 % (w/w). Low API concentrations of $<$15% lead to insufficient comminution. High concentrations of $>$40% can be processed but show significant broadening of the size distributions with heavily increased PDI values. This is most likely due to an increased amount in coarse particles leading to broadened size distributions. While large fractions of API enhance the total viscosity of the suspension and therefore impede kinetic energy transfer, the drop in processability at low FF concentrations is not easily explained. One reason might be that FF is heavily sticking to bead surfaces and therefore only low amounts of FF are amenable to grinding between milling beads and drug particles. The effect of bead filling level was investigated on the three model compounds. FF showed poor processability at low bead fill levels of 40%, whereas the other compounds were effectively comminuted at this bead volume. In this case the suspension volume and

mass was kept constant what resulted in different ratios between API and milling beads. As this ratio determines the number of collisions per time the investigation of the optimum ratio would most probably improve the grinding results for FF. As a practical approach working with a volume ratio of >1:5 (API/Beads) is likely to provide sufficient grinding in most cases.

It is understood that processing time is directly correlated to the energy input and therefore exerts a predominant influence on comminution. When looking at a milling processes at high energies - in our case at 800 rpm - adequate particle comminution can easily be achieved in a 60 min process. In fact, despite avoiding heating of the sample the PSD is prone to deteriorate when aplying milling durations >120min (Fig. 3.4.3).The effect is described for milling processes where an excess in energy input is fostering particle aggregation again. It can be concluded that for the two substances tested processing times of less than 2 hours are favorable. Another important point to note is that breaking of primary particles occurs within short time frames of few minutes. Afterwards particle size reduction occurs more slowly and tends asymptotically to a size minimum. The same observation can be made for the respective processes on an agitator ball mill (Fig. 3.4.6). Given a sufficient energy input milling towards a „limit size“ of particles can be achieved within short time periods of less than two hours. This milling behavior is observed by various authors (e.g. [32]) and can be attributed to the breaking mechanisms occuring at different stages in the milling process [32, 147].

Eerdenbrugh reported on small scale trials (down to 10 mg API per trial) in planetary ball mills and in 96 well plates stired on a shaking plate [21]. He found that comminution was possible in both settings, although the ball mill gave more robust results. The study relied on milling in small glass containers (minimum vial size 0.3 mL) within an insert for a milling beaker of a commercial planetary ball mill. Especially for the use of 96w plates the author reported on high wear of the walls of the plates which is not surprising as zirconia milling beads were used in all cases. Attrition in glass vials was unfortunately not discussed but is expected to be an issue due to low hardness of glass in comparison to zirconia. Therefore, within this work milling fully relied on low abrasive equipment made of zirconia. The question was if small scale milling trials could also be performed in comparatively large milling beakers of 12 mL. Therefore a constant API/milling beads volume ratio was chosen for milling trials. Fig. 3.4.5 is demonstrating that the API amount per milling trials can easily be lowered to 15 mg. Whereas Eerdenbrugh et al.[21] relied on different vessel sizes for obtaining compariable milling results this is not compulsory. The data generated in FF rather suggest that the ratio between milling beads and API are the predominant factor for grinding. The settings were tested for several Merck Serono test compounds and the resulting particle sizes were in all cases comparable for 5% bead fill (15 mg API) and 40%

bead fill (data not shown).

When comparing grinding via zirconia versus polystyrene milling media data suggest that polystyrene grinding media enable a more thorough and uniform comminution of drug crystals. Particles milled with styrenene did not contain fractions of >500 nm wherase these crystals could be observed in zirconia samples. Nevertheless the TEM micrographs have to be evaluated with caution as they only convey a limited, non-statistical view on the samples. Within this study 10 pictures per sample were recorded and representative pictures included in the document. Interestingly, the micrographs also suggest that there are no visible differences between the breaking mechanisms. The morphology seems rather be dependent on the inherent properties of the API and not on the grinding media applied. As a practical implication it can be concluded that milling processes set up with zirconia milling beads are transferable to polystyrene grinding media.

As already indicated for milling processes on planetary ball mills differences in grindability could be observed depending on the drug substance and the rotational speed applied. On the Dynomill® RL accelerator speeds of 1500 - 6000 rpm can be applied. In the experiments distinct differences could be seen between 2000 and 3000 rpm. When further increasing rotational speed differences between the substances get obvious. Whereas FF does not further decrease in particle size upon enhancing power input, GF and KC crystals comminute towards smaller PSDs. KC is reaching a maximum comminution level at 5000 rpm, whereas GF shows significant size decrease when further enhancing the power input. GF was the only substance that was processed at 6000 rpm because the sample temperature reached 30°C and more. It is worth discussing if these observations correlate to the physchem properties of the substances. One aspect is that substance brittleness and hardness is determining or influencing the grindability [119, 120]. Hardness testing via nanoindentation in this study (see Fig. 3.4.36) suggested that FF built the hardest crystals or structures, whereas GF showed the smallest resistance upon cracking. While this relationship might explain the rank order for particle grain size (GF<KC<FF) to a certain extent it is not obvious why a KC and FF show no response on further increase of power input. Here suspension viscosity might be discussed as a parameter of relevance. Lower dispersion viscosity leads to an higher kinetic energy of milling balls and hence to an higher energy transfer to the product. No measurable differences between suspension viscosities could be found via the cone-plate rheometer applied. Restrictively it must be mentioned that all obtained values were near the lower limit of quantification of the instrument in a range of 1 - 2 mPas. API specific differences can also be detected when varying the process temperatures: GF is showing pronounced decrease in grain size when decreasing the temperature of the cooling circuit from 20 - 2°C. The other two compounds presented themselves unaffected by product temperature. In another experimental setup the influence was investigated for FF over a wider temperature range

(Tab. 3.9). Results clearly demonstrate that also for FF decreasing product temperatures foster the comminution of the nanoparticles. If this effect is also driven by the stabilizer used in these trials was not investigated within this work and should be part of future studies. For FF the influence of bead filling level and the interactions with suspension concentration were investigated. For zirconia as well as polystyrene grinding media an optimum filling level could be detected. Notably, these levels were found to differ - app. 60% (v/v) are sufficient for zirconia beads (Fig. 3.4.17) whereas 70 - 80 % (v/v) can be defined as optimum range for polystyrene beads (Fig. 3.4.10). In addition, Fig. 3.4.11 reveals that for low API concentrations at a constant processing time higher media filling levels are beneficial. This can be explained by the fact that a larger number of beads can convey a higher number of collisions per time unit and particles undergo processing at a higher probability. At high API concentrations additionally the effect of self comminution [148] plays an important role. It means the grinding of smaller API particles via API particles via friction and collision. Whereas at high particle concentrations self-comminution contributes to grain size a higher number of milling bead/API particle contacts is required for efficient milling. Stenger et al. additionaly highlight that a minimum concentation of product must be present to be effectively entrapped between milling beads for grinding [18]. The influence of API concentration was recently described for miconazole [22]. Also here a decreased PSD could be observed after enhancing the API concentration from 5 % to 12.5 % and 20 %. Unfortunately the autor did not investigate if this effect could be leveled by adaption of the amount of milling beads. The influence of the type of stabilizer on the milling performance was intensely investigated within 3.4.3.2. It became evident that each API requires specific determination of the most suitable stabilizer. A trend is seen towards the applicability of anionic stabilizers (SDS, DOSS, NaDC): at least one of these substances proved to be efficacious for each model compound. Titration of the optimum concentration of each stabilizer was not wihin the scope of this work but is described by other authors [23, 22, 10]. All authors confirm the relevance of finding the suitable stabilizing agent and the relevance of a mimimum stabilizer concentration to effectively comminute the product. Interestingly, stabilizer concentrations higher than needed for processing to not impede grindability but negatively affect the stability of suspensions [22]. Another approach was followed by Van Eerdenbrugh and colleagues [106]. They compared the processability of nanosuspensions on different compounds with different polymers and the nonionic surfanctants Tween 80 and TPGS. No correlation to physicochemical parameters such as melting point and logP was found. Instead surface hydrophobicity and resulting tendency to stabilizer adsorption and aggregation were postulated to be of relevance. Results were contradictory for the compound griseofulvin which was also used in this study. The authors claim efficient comminution for a 1:4 ratio of API and TPGS which could not be confirmed by the internal

data. As different milling protocol was applied in these studies (250 rpm, 24 h, no pause) a potential reason might be found in the phenomenon discussed in the next paragraph. As a second contradiction it was found for the three model compounds in this work that hardness determined via nanoindentation indeed correlated with grindability and the melting point of the drug substances. A correlation with the melting point of the substances (Fig. 3.4.36) might be coincidence given the limited number of test substances. Nevertheless a high melting point was also found of relevance by another study on other drug substances [40]. Moreover the experimental setup of the stuy by Van Eerdenbrugh must be questioned. It would have been beneficial to put a stronger focus on optimum processing conditions instead of stabilizer selection for correlating to physchem properties as it became evident in the publication that aggregation heavily influenced the obtained data. Summarizing the discussion it can be concluded that rotational speed, processing temperature, bead fill level and API concentrations in suspension and the type of stabilizer are parameters to be considered in wetmilling process development.

Unfortunately, a direct comparison of milling efficiency in planetary and agitator ball mills is intricate. Different parameters for measuring and comparing the energy input into mills have been defined and some of them have been presented in the introductory section. Applied energy input in a milling process is an appropriate and helpful parameter for both types of mills. It is regularily applied when transferring milling processes to different scales within a milling method [149]. Whereas it is easily computable for agitator ball mills the energetic description within a planetary ball mill requires simulation of the collision and movement of the milling beads. Access to the respective computational methods is limited so 30 min processes on both mills were compared applying different surfactants (Fig. 3.4.18). Processes are transferable with good comparability of poor and well performing stabilizers. Exceptions are seen for the use of Polysorbate 20 and Solutol® HS15. Rheological measurements reveal that shear is inducing changes in viscosity. Although the effect is not unexpected for suspension systems the observation surprises that in case of KC and Tween 80® viscosity was only increased after intermittent shear stress (Fig. 3.4.37) whereas constant processing does not induce shear thickening. Although effects are far less pronounced as in 30 cycles of milling on a planetary ball mill, the trend fosters the hypothesis that intermittent shear stress is causing shear thickening in this example. Stenger and Peukert summarized attempts to describe particle-particle interactions and the respective effects such as shear thinning, shear thickening and thixotropy [150]. They also mathematically described viscosity-modifying parameters for a wetmilling process on alumina suspensions. Viscosity was affected via decrasing particle size and particle-particle interactions. The authors were able to reduce viscosity via maximizing the zeta potential (pH adjustment). A good accordance with these findings on alumina can be found for griseofulvine ground

in presence of Lutrol® F68. Here in both milling processes (agitator and planetary) shear thickening could be observed. The viscosity increase occured in the agitator ball mill after a processing time of >30 min. Temperature can be excluded as an influence factor in this case as the temperature of the sample did not change more than ±0.5°C during the process. Interestingly, shear thickening was only observed for nonionic surfactants and PVP in the experiments within this work that sterically stabilize the suspensions. As ionic surfactants do not exhibit this phenomenon the addition of electrostatic stabilizers might be a tool to suppress shear thickening effects.

In conclusion it can be stated that given the limited data set within this study processes seem to be transferable from planetary to ball mills. In contrast to this, caution has to be taken when transfering formulations to the smaller scale. Depending on the milling protocol applied (constant processing versus milling with pauses) viscosity effects are prone to alter the milling performance.

4.4.2 Stabilisation of suspensions

Formulation scientists all over the world strive for computational systems to predict formulability of substances and excipients as these approaches could help to dramatically speed up the formulation feasibility process and save huge amounts of manpower and material resources. In the case of nanosuspensions only few attempts have been made so far to correlate material parameters with relevant physchem properties of surfactants. Konkel et al. performed molecular modeling on different BCS II class compounds and their interaction with Tween 80 [151]. They could indeed demonstrate the computability of drug stabilisation. Nevertheless the approach was rather empirical because no knowledge could be gathered on general rules of the conformation of stabilizer attachement. Basically all possible conformations were modeled and compared to the experimental data. Verma et al. reported on the investigations of surfactant/API interactions via atomic force microscopy [152]. They could demonstrate valid stabilizer selection via testing surface interactions on a drug particle with stabilizers. Both methods suffer from being extremely time consuming and not applicable to a large number of formulations. The atomic force methodoloy in addition requires high operational skills and significant amounts of API for method validation and statistically valid experimental data.

Therefore this work relied on more straightforward readout parameters. An important finding is that efficiency of grinding for a stabilizer does not necessarily correlate with the ability to physically stabilize the resulting suspensions. Results are biased as such that only one concentration of stabilizer (4% w/w stabilizer, corresponding to a drug/stab. ratio of 5:1) was applied. The relevance of the concentration of the excipient was shown by others [22]. It could be shown that physical stability is compromised due to enhanced drug

solubility and resulting Ostwald ripening of drug crystals. Nevertheless in the combined screening and stability study a max. excipient concentration of 4% was chosen in order to achieve optimimum stabilisation of small particles during milling. Other authors applied API/excipient ratios that are far higher (up to 1:1 ratio) and reported on preferable results at higher excipient concentrations [106]. This must be critically discussed as high excipient concentrations are prone to lead to increased excipient-related side effects in-vivo. An API/excipient ratio of 1:4 was therefore set as the tolerable maximum within Merck discovery projects. Considering the results in 3.4.3.2 the general and expected observation is that physical stability is increased at storage at 2-8°C. This is most likely due to the lower drug solubility and the lower mobility of API crystals at this temperature. Drug solubility in relation to the excipients applied were not measured within this set of experiments. The aspect is worth following and should be topic of future investigation. That stabilizer concentration can be reduced significantly without compromising processability and stability is shown in one example (Fig. 3.4.25). The SDS concentration can be reduced to 0.1% (w/w), an optimum regarding stability and PSD is obtained at 0.5% stabilizer.

Particle stability was correlated with zeta potential and changes in physical state of the APIs detected via DSC and XRD. It is commonly accepted that zeta potential values of more than +30mV and less than -30mV are indicaive for efficient electrostatic stabilisation. While in the tested substances this held true for GF and KC, FF particles showed pronounced growth upon storage (Fig. 3.4.26) also for anionic surfactants that enabled highly negative surface. No polymorph change or amorphisation could be detected, so solubility related effects or aggregation of particles can be discussed as reasons for the instability. As expected for steric stabilizers no correlation between surface charge and particle stability can be detected. DSC results were plotted versus stability of suspensions after 1w at 25°C. The results indicate that DSC is not the most suitable tool to allow reliable detection of suspension stability. Depending on the drug substance useful information may be provided for pronounced effects such as complete amorphisation. On the contrary, common effects such as melting point depression might rather be attributed to the decrease in crystal size than to polymorphic changes. Similarily, a decrease in melting enthalpy very often cannot be attributed to decreased suspension stability. To summarize the findings for the three drug substances DSC is not sufficient to replace stability data of nanosuspensions in a feasibility study. The examples presented in 3.4.4.3 demonstrate that also XRD data are not necessarily related to physical stability of nanosuspension systems. Changes in the polymorphic form, also to a metastable modifiation as in the case of KC stabilized with Cremophor RH40, do not render the suspension unstable as long as the metastable state is preserved. The results further suggest that changes in melting point and melting enthalpy do not mandatorily correlate with physical changes of the API in nanosuspensions and might in

some cases be due to the size decrease of the crystallites. In conclusion DSC and XRD provide useful information on effects such as amorphisation or polymorphic change but they are not able to replace stability studies for nanosuspensions.

As a simple computational approach the suitability of solubility parameters for predicting grindability and stability was assessed in 3.4.4.4. While some similarities between the parameters of excipients and APIs can be detected a reliable prediction of the processability or suspension stability fails. One drawback might be that the solubility parameter per se is not able to depict large differences between the model compounds, a phenomenon also observed for the prediciton of phase solubility in solid solutions. A correlation to the single contributions or combinations, namely dispersion or the H-bond contribution, might be worth of a follow up but still require the introduction of factors that are able to describe the API-surfactant-water interaction more accurately. Originally, solubility parameters were designed to describe binary mixtures and interactions solely originating from the substances of interest. In a drug nanosuspension the situation is more complex. The conformation of the stabilizers in the aqueous medium as well as the characteristics of the particle surface upon grinding need to be considered. By nature this compromizes the applicability of such basic models as the solubiliy parameter concept. In conclusion performing milling trials in small scale proved to be reliable approach of choice for assessment of processability and stability of nanosuspensions. Computational as well as analytical methods to predict nanosuspension stability were not able to substitute feasibility trials in the chosen settings.

4.5 In-vitro and in-vivo experiments

Nanosuspensions

The permeability enhancement seen in Fig. 3.5.1 can at one hand be attributed to increased solubility of FF in FaSIFF in comparison to FaSSIFblank. Vogt [80] compared FF solubility in FaSSIF and FaSSIFblank and obtained values of 13.7±0.5 µg/mL and 0.2±0.0 µg/mL respectively. The values are in good agreement with the ones measured internally at 37°C (14.1±0.3 and 0.3±0.0 µg/mL). In addition the results show a similar trend as reported by Buch et al. [153]. The authors observed an app. 10fold increase in permeation of TriCor® in comparison to bulk fenofibrate in a vertical dissolution/permeation system. The discrepancy in the relative amounts of permeated FF might be attributed to higher API concentrations in the donor compartment (50mM) and additional surface active excipients present in the marketed formulations applied (e.g SDS in the case of TriCor®). In comparison with FF permeability enhancement for GF and KC is only moderate. Here, the influence of dissolution speed can be discussed: Other than for FF, dissolution and therefore permeability might not be controlled via the dissolution kinetics of the drug substance,

meaning that an increase in dissolution speed only poorly enhances total mass transfer. Ingels et al. [154] reported for KC a decreased apparent permeability P_{app} when applying FaSSIF instead of buffered saline as transport medium. This phenomenon might be explained via decreased solubility or a strong retention of KC in the micelles of the medium thereby impeding the cell transport. This hypothesis is confirmed by the fact that KC is showing an app. 5x enhancement of solubility when comparing FaSSIFblank and FaSSIF [155]. Theoretically the increased fraction of dissolved API should transfer in an respective increased permeation. Fig. 3.5.3 is giving an opposing picture suggesting that increased solubility only partly increases drug permeation. Also GF suspension and nanosuspension did only show minor differences when applying FaSSIF instead of FaSSIFblank as apical medium. For GF this can be explained via the fact that introducing taurocholate and lecithin into the transport medium only leads to a minor increase in solubility of factor 1.5 [156]. Correspondingly, only minor differences in permeation can be detected between FaSSIF and FaSSIFblank in Fig. 3.5.2.

The question arises if the increase of permeation in nanosuspensions originates from altered solubility characteristics of nanocrystals. Eerdenbrugh [20] discussed this aspect in more detail with reference to the underlying principle, the Ostwald-Freundlich equation. Considering solubility measurements as well as the computational basis he concluded that for nanosuspensions in a particle size range of 100-200 nm only a minor increase in solubility of $+5$ - $+10$ % can be expected. Within this work it was tried to measure the solubility of FF, GF and KC nanosuspensions in FaSSIF. Depending on the method of particle separation (filtration, centrifugation) resulting solubilities were overestimated due to measurement of nanoparticles or could not be acurately determined due to phase separation of the micellar medium. Crisp et al. [110] and Lindfors et al. [157] proposed methods for in situ measurement of solubility and dissolution of drug nanosuspension. Both found the complete dissolution to take place within a time frame of less than 60 s for small particles in the range of 100 - 200 nm. In contrast the dissolution of microparticles usually takes place wtihin a minute to hour time window. This clearly indicates that enhanced dissolution speed is responsible for the increased apparent permeability found for the nanosuspensions of all model compounds in comparison to the microparticulate suspensions. Another aspect described in literature is that comminution of a drug substance to the nanoparticle size range helps to suppress food effects [1, 8, 17]. It means that the bioavailability after oral administration is less different and variable when comparing fasted and fed state in the intestine. A similar trend can be seen in the in-vitro setup: Differences between nanosuspensions in permeation when comparing with and wihout surfactant addition are less pronounced (FF) or not detectable (GF) in contrast to the permeation seen for microparticles. For KC no tendencies can be detected. Nevertheless, it must be stated that bile salt/lecithin concentrations differ

from in-vivo conditions in this setting and FaSSIF is usually supposed to mimic the fasted state.

In conclusion, nanosupensions of all three test compounds show permeability enhancement in comparison to their unprocessed suspensions. The extent of permeability increase apparently depends on the intrinisic properties of the test compounds (e.g. solubility increase in biorelevant media) and the dissolution kinetics upon nano-sizing. For KC and GF it can be hypothesized that permeation through the cell layer is less limited by dissolution speed of the drug particles than for FF. Correspondingly, one can detect pronounced effects in permeability enhancement for FF up to a factor 2 (nano/micro) whereas only 40-60% enhancement are observed for the other two compounds. Due to the strong increase of solubility in surfactant-containing medium FF was the only compound that showed additional mass tranfer over the cell barrier whereas for KC and GF no additional effect due to bile salts could be shown. Unfortunately it is out of the scope of this work how the in-vitro permeability enhancement correlates with in-vivo bioavailability enhancement of the three formulations. Solely FF could be tested in an in-vivo setting. Here the increase in AUC for nanosuspensions versus microsuspensions correlated with the relative permeability enhancement (see 3.6) .

Nanoemulsions/Microemulsion

Nanoemulsions and emulsions containing L1695 exhibit remarkably higher measured permeation in the Caco-2 model compared to emulsions stabilized by Solutol® HS15. Whereas a size effect may be discussed for the nanoemulsions (average droplet size app. 50 nm smaller) only minor differences were observed for the coarse emulsions. A permeability enhancing effect by the surfactant seems more likely and is worth to be discussed within the experimental setup tested. Sucrose esters are described to increase permation over biological barriers. Many publications and patents relate to skin delivery (e.g.[158, 159]), but also an increase of absorption via the mucosal route has been described, especially for polar molecules [160] and larger peptides such as insulin [161]. In both cases sucrose monolaurate was identified as the most potent absorption enhancing component. Another study descibes the use of sucrose monostearate (S1670) as surfactant for an oil emulsion for the oral delivery of quercetin [162]. Here no significant permeation enhancement could be detected for the long chain (C18) stearic acid ester. However contrary effects were observed in a study by Nakada [163]. There longer chain length promoted absorption of human calcitonin in rat mucosa. It must be stated that molecular mechanisms are still unclear and available data inconsistent. Due to the limited time the molecular mechanism of permeation enhancement properties is not investigated in detail within this work. No differences were observed in transepithelial resistance (to app. 500 Ωcm^2) that could po-

tentially explain the differences in permeation between the surfactants L1695 and Solutol HS15. Cytotoxicity studies (e.g. MTT), degradation of surfactants and profiling of potential transporters should be performed to elucidate the molecular mechanisms for permeation enhancement.

FF-loaded microemulsions show the highest permeation values within the conducted set of experiments. Moreover pronounced differences can be seen between FaSSIF and FaSSIFblank. Especially TEER is affected to a higher extent in the lecithin/bile salt containing FaSSIF. As TEER values $>$500 Ωcm^2 indicate sufficient cell layer integrity it can be seen that cell layers are not expected to provide sufficient density after two hours of incubation. It can be hypothesized that the enhanced permeation depicted in Fig. 3.5.6 is to a significant extent attributed to membrane disintegration. Herefore, also the increasing slope of the FaSSIF after 30 min incubation time may be indicative. Regarding differences in permeation in relation to the relative drug load of the microemulsion preconcentrate (Fig. 3.5.7), saturation of the lipidic carrier with API might be discussed. A drug load at 100mg/g is closer to saturation solubility. Therefore in aqueous systems, drug redistribution into aqueous phase or hydrophobic interfaces is more likely for formulations with high drug load as small amounts of FF are more efficiently retained within the lipidic core of emulsion droplets than large concentrations. Fig. 3.5.8 underlines this aspect. Although being investigated for a highly prolonged time frame the results suggest that the pressure for drug distribution out of emulsion droplets is higher for formulations with high drug load what eases the diffusion of free drug from lipophilic emulsion droplets to the micelles of the transport medium or to the mucosal membrane.

Permeation ranking of nanoscalic drug carriers

Fig. 4.5.1 is comprising the permeated amounts of fenofibrate in different drug delivery systems tested in FaSSIF medium. Highest permeation rates are determined for the microemulsifying formulation (100 mg/g FF) with app. 10x enhancement of permeated mass after 2 hours. These results are biased by the fact that cell layer integrity was not preserved during the test and most likely microemulsion droplets bypassed the cell layer. All drug delivery systems exhibit measurable permeation enhancement in comparison to pure drug substance. Remarkably, the application of 0.5% SDS in the „coarse suspension“ already seemed to have enhancing effects in comparison to pure drug substance. Drug permeation is enhanced 5x for the nanomilled product. While permeability is increased for the nanoemulsion containing the sucrose ester L1695, the use of Solutol® HS15 as surfactant does only result in values similar to those obtained for micronized fenofibrate suspension. It is hypthesized that drug substance released from drug delivery systems in the $>$100nm size range has to redistribute into aqueous medium or solubilizing substances of the re-

lease medium before it is able to pass biological barriers. Permeation data of Solutol® and L1695 nanoemulsions of similar size show higher values for the L1695 emulsion. This effect is most likely attributed to the higher stability of Solutol® nanoemulsion droplets. DLS data indicated size preservation also after 2 h incubation in FaSSIF media (data not shown) whereas L1695 nanoemulsions showed visible creaming of the MCT phase at the air-liquid interface what could not be measured via DLS. The observation suggests that instability of the oil-water interface fosters redistribution of free drug substance into bile salt micelles or biological membranes what could have led to the higher pemeation values. Another possible reason might be a permeation enhancing effect of the L1695 surfactant by e.g. disturbing the integrity of the mucosal layer. The following rank order for permeation enhancement can be set: Microemulsion preconcentrate>Nanosuspension>Nanoemulsion L1695>Nanoemulsion Solutol>Coarse suspension>Drug substance.

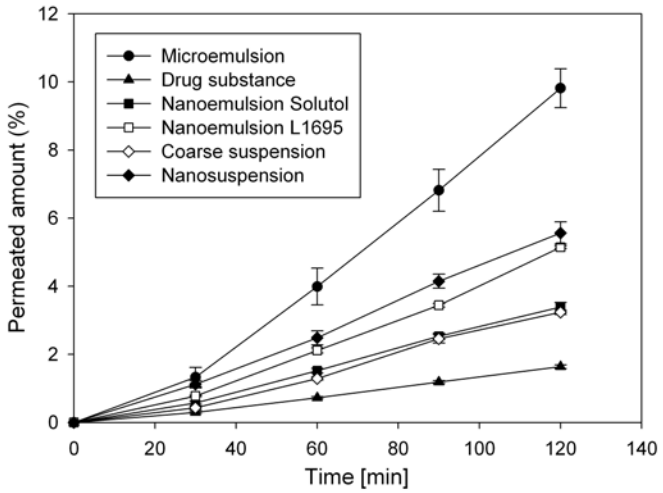

Figure 4.5.1: Caco2 permeation data for different drug delivery systems containing fenofibrate, FaSSIF was applied as apical medium, n=3-6, mean±sd

In-vivo study

The rank order in general confirms the results obtained by the Caco-2 in vitro results (see section 3.6). Noteworthy is the failure of the microemulsion formulation which showed highest permeation values in-vitro. As mentioned the in-vitro results might be distorted via loss of cell layer integrity. Nevertheless this might not explain why bioavailability was as poor as that of pure drug substance despite the use of significant amounts of solubility and penetration-enhancing surfactants (Solutol®HS15, Capryol® 90). Another reason might be the inherent compromised stability upon dispersion of Type III systems. Mohsin et al. reported on low solubility of fenofibrate upon dispersion of different SMEDDS in different media and rapid crystallization of the drug [136]. Although recrystallisation was observed

in our in-vitro experiments this took only place in a hour to day time window. Considering the results shown in 3.5.7 it may nevertheless be hypothesized that the drug recrystallized rapidly in the rat intestine and therefore did not perform better than pure drug substance.

It remains also questionable why the high content of surfactant enhancing drug solubility in the micellar state and affecting permeability of mucosal barriers does not lead to enhanced bioavailability of the model compound. Considering nanoemulsion formulations BA enhancement can be seen despite only low amounts of surfactants. Sucrose ester containing formulations tend to show increased absorption in comparison to the formulation containing Solutol®. If differences in absorption are due to the lower particle size of L1695 nanoemulsions of approx. 50 nm in the Z-Ave or to inherent bioavailability enhancing effects of the sucrose ester needs to be investigated in further studies. Digestion effects that take place for nanoemulsion formulations should be discussed. Bioavailability in the present case is rather influenced by the composition of the lipidic carrier itself and not the particle sizes of the oil droplets. The investigation of coarse emulsions in in-vivo settings should therefore be target of future investigation. Bioavailability enhancement is found to be in agreement with literature data for FF, although absolute values for C_{max}were reported to be higher by twofold [41] or threefold [153]. AUC values differ accordingly whereas t_{max} was found to be in good accordance (1h/1.83 h versus 1.5$\pm$1.22 h). As in the case of Buch et al. the same dose was applied one would have expected similar plasma levels in comparison to this study. One potential reason to explain the differences might be that in the first case a marketed formulation containing further solubilising additives (DOSS, SDS) was applied. These might have further promoted permeation compared to the extremely low surfactant content in our study. When comparing the curves of bulk fenofibrate with the internal data on the coarse FF suspension similar PK values are obtained. Another reason that might have distorted the results in the present study is that the metabolism of the animals was influenced by stress during the blood sampling. This might be fostered by the fact that the measured profiles showed very high variation between the single animals. Overall, despite statistical limitations data clearly demonstrate the superiority of nano-formulations in comparison to coarse suspensions. The nanosuspension proved to be a robust system that exhibits enhanced drug uptake or permeation in-vivo and in-vitro.

5 Conclusion

The work focussed on three preparation techniques for enabling vehicles for poorly soluble compounds. Microemulsion, nanoemulsion and nanosuspension approaches were applied to the model compounds fenofibrate, griseofulvin and ketoconazole. In addition two different modified β-cyclodextrins that are applied in preclinical formulation finding were evaluated regarding their ability to solubilize the model compounds. Suitable formulations were further characterized regarding their ability to enhance permeation of the model compounds in the Caco-2 cell model. Microemulsion, nanoemulsion and nanosuspension formulations of the model drug fenofibrate were tested in-vivo in rats for bioavailability enhancement upon peroral administration.

As expected solubility in cyclodextrins was highly dependent on the physicochemical properties of the API. In good agreement with literature data high inclusion efficiency was found for ketoconazole in both cyclodextrin variants while the approach was less suitable for the other drugs. The influence of Tween® 20 and and the biorelevant media FaSSIF and FeSSIF on solubilisation in cyclodextrin complexes was investigated. Tween® 20 did not alter the solubilisation capacity for the three compounds. In contrast phase solubility tests in FaSSIF and FeSSIF revealed only minor effects on complexation for fenofibrate and griseofulvin, but an almost two fold increase in total solubilisation for ketoconazol in FeSSIF in comparison to pure buffer medium at the respective pH. The observation underlines the complexity of interactions in cyclodextrin inclusion complexes. In addition the findings might open a way for fine tuning formulation development of cyclodextrin/API complexes. Therefore the influence of media changes from gastric fluid to intestinal fluid should be investigated in more depth.

Microemulsion systems or SMEDDS are established as fast and straightforward approach to solubilize APIs in preclinical development. A SMEDDS formulation containing Solutol® HS15, Capryol® 90 and Miglyol® 812 was investigated in more detail. The preconcentrate is characterised via a slow dissolution kinetics in aqueous media. Therefore the dissolution process was further investigated via small angle neutron scattering (SANS). The findings suggest that formation of the microemulsion droplets is not a one step process. Within the first 200s s of the formation process small spherical structures occur which finally grow to the droplet size of the microemulsion. Regarding composition of the droplets modeling suggests

that the spheres consist of all three components at all time points with the ratio differing over time. Unfortunately, SANS is the only technology with sufficient time resolution to monitor the process. Microcalorimetric measurements were not able to resolve different process from an energetic point. The model SMEDDS was loaded with fenofibrate and assessed in in-vitro and in-vivo experiments. While high permeation increase could be observed in the Caco-2 model most likely due to destruction of cell layer integrity, the system failed to increase bioavailability in the rat model. As a potential reason the rapid and quantitative precipitation of the API out of the microemulsion droplets in the rat stomach and/or intestine due to reformation or instability of microemulsion droplets may be hypothesized.

Nanoemulsions were prepared using a commercially available high pressure homogenizer. Emulsions were conveniently processed at 10 mL scale and droplet comminution below 200 nm could be achieved via simple protocol applying 8 homogenization cycles. The primary goal was to investigate the potential of sugar based excipients for the production of nanoemulsions in comparison to standard excipients such as phosphatidylcholines and polyethoxylated glyceroles for parenteral and peroral use. Sucrose ester-based emulsions resulted in smaller particles than the reference surfactants. They showed size dependency depending on the ratio of surfactant to oil and on the fatty acids applied for sugar esterification. Physical stability was comparable to synthetic excipients at 25°C for three months. Sugar esters proved to be highly advantageous in lyophilizing of the nanoemulsions. Whereas reference emulsions showed complete collapse of the system sugar esters were - when added in excess - able to serve as a lyoprotectant. Particle integrity was preserved during the freeze-drying step, the lyophilisates were well redispersible. When using the carrier in-vitro and in-vivo for the delivery of fenofibrate the sugar ester L1695 exhibited superior permeation in the Caco-2 model in comparison to Solutol® HS15. Differences in bioavailability in a rat animal model can not be regarded as significant. Although being described as non-toxic for peroral use in animal models toxicology and potential effects on biological barriers (e.g. intestinal mucosa) require further investigation.

Nanosuspensions were produced by wet-milling in water. Milling processes were optimized regarding particle size on two different types of ball mills - a planetary ball mill for small scale trials in early development and a larger agitator ball mill for batch sizes $\geq$ 60 mL. On both mills optimum results were obtained by applying grinding media in a size range of 0.1 - 0.3 µm. Notably, dependent on the drug substance different rotational speeds, meaning different energy inputs are required to effectively break down the API crystals. On planetary ball mills high rotational speeds together with high filling levels lead to most efficient grinding within a 60 min milling protocol. On agitator ball mills the filling level of grinding media and the rotational speed were detected as the most relevant parame-

ters aside the processing time. It must be pointed out that optimum grinding efficiency is already obtained at rotational speeds of 3000 - 4000 rpm on the chosen milling setup. This power input is preferable due to lower level of heat dissipation that would otherwise compromise the quality of the milled drug product. Interestingly, soft grinding media such as polystyrene spheres exhibit similar grinding efficiency as high-density zirconium oxide media. In addition the processed product exhibits a similar morphology for both media. This leads to the conclusion that 1) the tested APIs are sufficiently brittle to be cleaved via soft and elastic milling beads and 2) the fine grinding via abrasion is not driven via high energy impact but rather by the number of particle collisions and the level of friction. Stabilisation of the liquid-particle interface is the by far most important factor for obtaining physically stable API nanosuspensions. No general guidance for the selection of stabilizers could be detected, screening different stabilizer classes is the method of choice. Care should be taken when correlating changes in the physical state of an API with the storage stability of the suspension. Despite changes in the polymorph or partial amorphisation of the drug physical stability can still be obtained for several weeks or months. Stable nanosuspensions could be obtained for all three model compounds. The formulations exhibited superior permeation in the Caco-2 cell assay in comparison to microparticle suspensions. The fenofibrate nanosuspension outperformed in-vitro and in-vivo all other tested formulation techniques. Moreover, the nanomilling proved to be technically feasible for all model compounds independently from the physicochemical parameters such as logP and melting point that are described as relevant selection criteria for formulation approaches. Apart from that nanosuspensions were able to deliver the highest drug loads in the formulation approaches tested. It is therefore proposed to apply nanomilling as an enabling formulation technology already in early preclinical development as soon as „simple“ vehicles such as surfactant or cyclodextrin solutions fail to enable sufficient solubilisation or high doses of the API are required (e.g. for toxicological studies).

Taking these aspects into consideration it becomes evident that nanosuspensions manufactured by wet-milling provide a powerful drug delivery system for a variety of poorly soluble small molecules. Despite differing significantly in physicochemical parameters such as logP and melting point the nanomilling approach was technically feasible for all model compounds. In addition the nanosuspension provided robust permeation enhancement in a cell-based as well as in an in-vivo model. By closing the loop and taking reference to the introduction of this work the following modified decision tree for early formulation development for NCEs based on the system by Rabinow [1] is proposed:

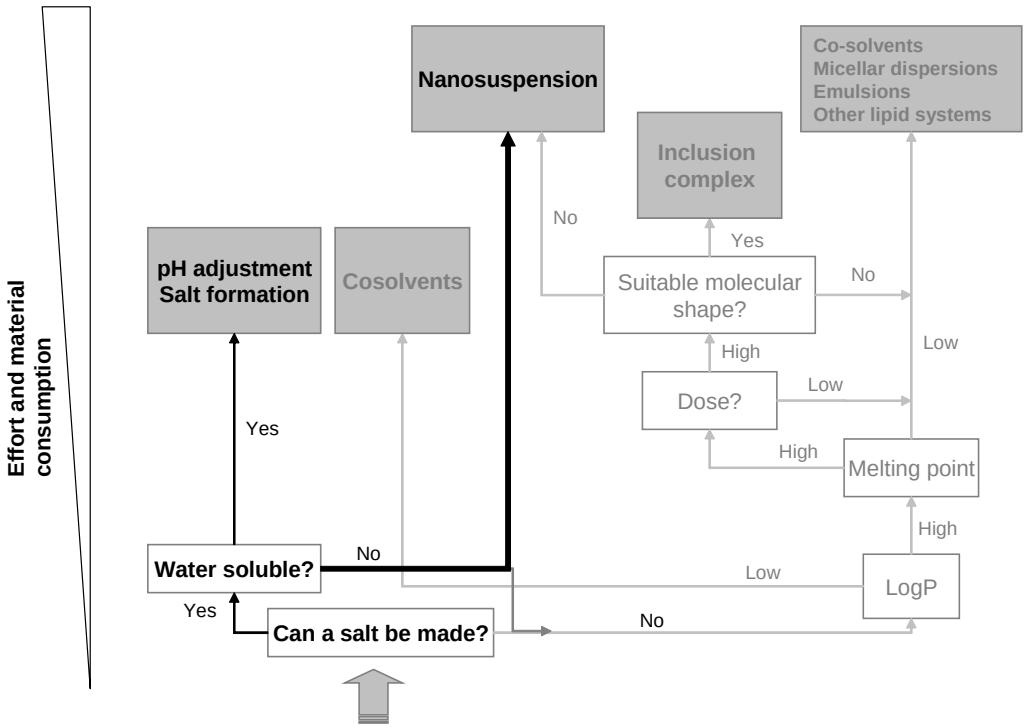

Figure 5.0.1: Decision tree for NCE formulation screening in preclinical development (modified after [1]), the orignal workflow is depicted in grey lines and boxes, the proposed modified workflow is highlighted via black lines and dark grey boxes. In addition the effort for feasibility and manufacturing of preclinical vehicles is ranked by the position of the boxes from bottom to top

6 Summary

Several processing techniques for the bioavailability enhancement of poorly soluble drugs are described in this work. Three model substances (fenofibrate, griseofulvin, ketoconazole) are evaluated for technical feasibility in nanosuspension, nanoemulsion/microemulsion (fenofibrate only) and cyclodextrin formulations. Different preparational and analytical aspects of the technologies were investigated. Small angle neutron scattering (SANS) was utilized to explore the emulsifying mechanism of a microemulsion preconcentrate. Results suggest development of spherical structures in the first 200s of the process with further size increase of the emulsion droplets later on. Only minor changes in chemical composition of the droplets are suggested. Nanoemulsion formulations were manufactured via novel sucrose ester tensides and compared to established surfactants for parenteral use (Solutol® HS15, Cremophor® RH40, Lipoid® E80, Lipoid® S75). Results demonstrate the suitability of hydrophilic lauryl and myristyl esters regarding particle size and stability. In comparison to other tensides sucrose esters allow for production of smaller particle sizes and stabilize the resulting emulsions during freeze-drying and redispersion. Wet milling in different ball mills was evaluated for manufacturing of nanosuspensions. Besides processing time the bead fill level, rotational speed and size of milling beads were identified as relevant parameters. Differences in comminution efficiency were detected dependent on API chemistry and the stabilizers used. The data underline the relevance of selection of stabilizers and optimization of stabilizer concentration for every individual API to achieve optimal comminution efficiency and dispersion stability. Optimized drug delivery systems were investigated in-vitro in Caco-2 transwell systems. Higher permeation of nanoscalic formulations could be measured in comparison to non-processed API. Nano- and microscale formulations of fenofibrate were tested in an in-vivo study in rats. After peroral administration the nanosuspensions and nanoemulsions lead to higher bioavailability of fenofibrate in accordance to increased permeation in the in-vitro tests. A microemulsion failed to demonstrate increased bioavailability in comparison to pure API. The work demonstrates the applicability of nanosuspension technology as platform for different poorly soluble compounds. Wetmilling proved to be a suitable technique for processing even in the low milligram scale for different API chemistries which qualifies the technique as ideal tool for preclinical and clinical development. Building on a published scheme a decision tree for selection of formulation technologies is proposed

that accounts for the technical applicabilities of the different formulation approaches.

7 Zusammenfassung

Die vorliegende Arbeit beleuchtet verschiedene Herstelltechniken zur Bioverfügbarkeitserhöhung von schwer wasserlöslichen Wirkstoffen. Die Modellsubstanzen Fenofibrat, Griseofulvin und Ketoconazol wurden mittels unterschiedlicher Formulierungssysteme (Cyclodextrine, Mikroemulsion, Nanoemulsion, Nanosuspension) verarbeitet. Verschiedene analytische und präparative Aspekte der Technologien wurden untersucht. Beispielsweise wurde das Emulgierverhalten eines Mikroemulsionskonzentrates zeitaufgelöst mittels Kleinwinkelneutronenstreuung (SANS) beobachtet. Die Daten unterstellen einen mehrstufigen Prozess mit dem Entstehen kleiner sphärischer Strukturen in den ersten 200 Sekunden der Emulgierung und anschließendem Anwachsen der Emulsionströpfchen. Die chemische Zusammensetzung scheint dabei nur leichten Veränderungen unterworfen zu sein. Im Rahmen der Formulierungsentwicklung für Nanoemulsionen wurde die Eignung verschiedener Sucroseester im Vergleich zu etablierten Tensiden (Solutol®HS15, Cremophor® RH40, Lipoid® E80, Lipoid® S75) untersucht. Besonders hydrophile Ester der Laurin- und Myristinsäure zeigten positive Formulierungseigenschaften und Stabilität. Im Vergleich zu Standardtensiden weisen die Emulsionen von Sucroseestern kleinere Partikelgrößen auf und sind aufgrund ihrer strukturgebenden Eigenschaften in der Lage, Emulsionen während und nach Lyophilisation zu stabilisieren. Für die Herstellung von Nanosuspensionen wurde die Technologie der Nassvermahlung in Kugelmühlen näher charakterisiert. Als relevante Prozessparameter für die Partikelzerkleinerung wurden bei unveränderter chemischer Komposition neben der Prozesszeit die Mahlkörpergröße, der Mahlkörperfüllgrad und die Umdrehungszahl der Mühle identifiziert. Unterschiede in der Zerkleinerungseffizienz wurden in Abhängigkeit des verwendeten Wirkstoffs und des verwendeten Stabilisators detektiert. Geeignete Stabilisatoren sind für die Zerkleinerung und Lagerstabilität der Nanosuspensionen essentiell und müssen für jeden Wirkstoff individuell ermittelt und in der Konzentration optimiert werden. Geeignete nanoskalige Trägersysteme wurden in Transwell-Transportversuchen am Caco-2 Modell näher untersucht. Es konnte gezeigt werden, dass alle Formulierungsoptionen eine erhöhte Arzneistoffpermeation im Vergleich zu Suspensionen nicht-formulierten Wirkstoffes bewirken. Nanoskalige Formulierungen für die Modellsubstanz Fenofibrat wurden an Ratten nach peroraler Gabe auf Ihre Bioverfügbarkeitserhöhung hin getestet. Dabei zeigten die getesteten Nanoemulsionen und die Nanosuspension in Übereinstimmung mit den Ergeb-

nissen aus den in-vitro Transportversuchen eine erhöhte Aufnahme des Arzneistoffes. Eine ebenfalls getestete Mikroemulsion, welche eine erhöhte Arzneistoffpermeation im Zellmodell zeigte, konnte eine bioverfügbarkeitserhöhende Wirkung im Tiermodell nicht bestätigen. Die gezeigten Resultate unterstreichen die Eignung von Nanosuspensionen als Technologieplattform für unterschiedliche schwerlösliche Substanzen. Die verwendete Technik der Nassvermahlung ist selbst in kleinstem Maßstab nahezu universell auf schwerlösliche Wirkstoffe anwendbar und eignet sich somit als Plattformtechnologie für die präklinische und frühe klinische Entwicklung. In Anlehnung an ein publiziertes Schema für einen Entscheidungsbaum in der Formulierungsfindung wird ein Modell vorgeschlagen, welches der Anwendbarkeit der unterschiedlichen Formulierungssysteme stärker Rechnung zu tragen versucht.

List of Figures

List of Tables

Bibliography

[1] B. Rabinow, Nanosuspensions in drug delivery, Nature Reviews Drug Discovery 3 (9) (2004) 785–796.
URL http://dx.doi.org/10.1038/nrd1494

[2] C. Lipinski, Avoiding investment in doomed drugsand is poor solubility an industry wide problem?, Current Drug Discovery 4 (2001) 17–19.

[3] C. Lipinski, Poor aqueous solubility - an industry wide problem in drug discovery, American Pharmaceutical Review 5 (2002) 82–85.

[4] G. Amidon, H. Lennernäs, V. Shah, J. Crison, A theoretical basis for a biopharmaceutic drug classification: the correlation of in vitro drug product dissolution and in vivo bioavailability, Pharmaceutical Research 12 (1995) 413–420.

[5] A. K. Shah, S. A. Agnihotri, Recent advances and novel strategies in pre-clinical formulation development: An overview, Journal of Controlled Release 156 (2011) 281 – 296.

[6] C. Keck, R. Mueller, Drug nanocrystals of poorly soluble drugs produced by high pressure homogenization, Eur. J. Pharm. Biopharm. 62 (2006) 3 – 16.

[7] J. Hu, K. Johnston, R. Williams, Nanoparticle engineering processes for enhancing the dissolution rates of poorly water soluble drugs, Drug Development and Industrial Pharmacy 30 (3) (2004) 233–245. arXiv:http://informahealthcare.com/doi/pdf/10.1081/DDC-120030422, doi:10.1081/DDC-120030422.
URL http://informahealthcare.com/doi/abs/10.1081/DDC-120030422

[8] E. Merisko-Liversidge, G. Liversidge, E. Cooper, Nanosizing: a formulation approach for poorly-water-soluble compounds, European Journal of Pharmaceutical Sciences 18 (2003) 113–120.

[9] F. Kesisoglou, S. Panmai, Y. Wu, Nanosizing - oral formulation development and biopharmaceutical evaluation, Adv Drug Deliv Rev 59 (2007) 631 –644.

[10] B. V. Eerdenbrugh, G. V. den Mooter, P. Augustijns, Top-down production of drug nanocrystals: Nanosuspension stabilizationand miniaturization and transformation into solid products, International Journal of Pharmaceutics 364 (1) (2008) 64–75. doi:DOI:10.1016/j.ijpharm.2008.07.023.
URL http://www.sciencedirect.com/science/article/pii/S0378517308005280

[11] Pharmacircle Database, www.pharmacircle.com.
URL www.pharmacircle.com

[12] L. P. J. Hirvonen, Pharmaceutical nanocrystals by nanomilling: critical process parametersand particle fracturing and stabilization methods, Journal of Pharmacy and Pharmacology 62 (2010) 1569–1579.

[13] J. Kipp, The role of solid nanoparticle technology in the parenteral delivery of poorly water-soluble drugs, International Journal of Pharmaceutics 284 (2004) 109–122.

[14] T.-H. Hou, C.-H. Su, W.-L. Liu, Parameters optimization of a nano-particle wet milling process using the taguchi methodand response surface method and genetic algorithm, Powder Technology 173 (2007) 153–162.

[15] H. Mio, J. Kano, F. Saito, K. Kaneko, Optimum revolution and rotational directions and their speeds in planetary ball milling, International Journal of Mineral Processing 74 (2004) S85 – S92.

[16] H. Mio, J. Kano, F. Saito, Scale-up method of planetary ball mill, Chemical Engineering Science 59 (2004) 5909–5916.

[17] E. Merisko-Liversidge, G. Liversidge, Nanosizing for oral and parenteral drug delivery: A perspective on formulating poorly-water soluble compounds using wet media milling technology, Advanced Drug Delivery Reviews 63 (6) (2011) 427–440, nanodrug Particles and Nanoformulations for Drug Delivery. doi:DOI:10.1016/j.addr.2010.12.007.
URL http://www.sciencedirect.com/science/article/pii/S0169409X11000044

[18] F. Stenger, S. Mende, J. Schwedes, W. Peukert, Nanomilling in stirred media mills, Chemical Engineering Science 60 (2005) 4557–4565.

[19] W. Peukert, Material properties in fine grinding, International Journal of Mineral Processing 74 (Supplement 1) (2004) S3–S17, special Issue Supplement Comminution 2002. doi:DOI:10.1016/j.minpro.2004.08.006.

URL http://www.sciencedirect.com/science/article/pii/S0301751604000675

[20] B. V. Eerdenbrugh, J. Vermant, J. A. Martens, L. Froyen, J. V. Humbeeck, G. V. den Mooter, P. Augustijns, Solubility increases associated with crystalline drug nanoparticles: methodologies and significance, Mol. Pharmaceutics 7 (2010) 1858 – 1870.

[21] B. V. Eerdenbrugh, B. Stuyven, L. Froyen, J. V. Humbeeck, J. Martens, P. A. sand G. Van den Mooter, Downscaling drug nanosuspension production: Processing aspects and physicochemical characterization, AAPS PharmSciTech 10 (2009) 44–53, 10.1208/s12249-008-9170-5.
URL http://dx.doi.org/10.1208/s12249-008-9170-5

[22] A.M.Cerdeira, M. Mazzotti, B. Gander, Miconazole nanosuspensions: Influence of formulation variables on particlesize reduction and physical stability, International Journal of Pharmaceutics 396 (2010) 210–218.

[23] H. Scherliess, Waessrige nanosuspensionen zur pulmonalen applikation, Ph.D. thesis, University of Kiel (2008).

[24] L. Vogel, W. Peukert, From single particle impact behaviour to modelling of impact mills, Chemical Engineering Science 60 (18) (2005) 5164–5176. doi:DOI:10.1016/j.ces.2005.03.064.
URL http://www.sciencedirect.com/science/article/pii/S0009250905003490

[25] A. Kwade, L. Blecher, J. Schwedes, Beanspruchungsintensitaet und bewegung der mahlkoerper in ruehrwerkmuehlen, Chemie Ingenieur Technik 69 (1997) 836–839.

[26] L. Blecher, A. Kwade, J. Schwedes, Motion and stressintensity of grindingbeads in a stirred media mill. part 1: Energy density distribution and motion of single grindingbeads, Powder Technology 86 (1996) 59–68.

[27] A. Kheifets, I. Lin, Energy transformations in a planetary grinding mill part 2. model verification, International Journal of Mineral Processing 47 (1996) 21–31.

[28] J. Raasch, Trajectories and impact velocities of grinding bodies in planetary ball mills, Chemical Engineering & Technology 15 (4) (1992) 245–253. doi:10.1002/ceat.270150406.
URL http://dx.doi.org/10.1002/ceat.270150406

[29] Y. Feng, K. Han, D. Owen, Discrete element simulation of the dynamics of high energy planetary ball milling processes, Materials Science and Engineering A 375-377 (2004) 815–819.

[30] H. Mio, J. Kano, F. Saito, K. Kaneko, Effects of rotational direction and rotation-to-revolution speed ratio in planetary ball milling, Materials Science and Engineering: A 332 (2002) 75–80.

[31] R. Rajamani, P. Songfack, B. Mishra, Impact energy spectra of tumbling mills, Powder Technology 108 (2000) 116–121.

[32] S. Hennart, W. Wildeboer, P. van Hee, G. Meesters, Identification of the grinding mechanisms and their origin in a stirred ball mill using population balances, Chemical Engineering Science 64 (19) (2009) 4123–4130. doi:DOI:10.1016/j.ces.2009.06.031.
URL http://www.sciencedirect.com/science/article/pii/S0009250909004205

[33] C. Varinot, S.Hiltgun, M.-N. J. Dodds, Identification of the fragmentation mechanisms in wet-phase fine grinding in a stirred bead mill, Chem 52 (1997) 3605 – 3612.

[34] M. Gao, E. Forssberg, Prediction of product size distributions for a stirred ball mill, Powder Technology 84 (1985) 101 – 106.

[35] A. Dolenc, J. Kristl, S. Baumgartner, O. Planinsek, Advantages of celecoxib nanosuspension formulation and transformation into tablets, Int J Pharm 376 (2009) 204 – 212.

[36] P. Langguth, A. Hanafy, D. Frenzel, P. Grenier, A. Nhamias, T. Ohlig, G. Vergnault, H. Spahn-Langguth, Nanosuspension formulations for low-soluble drugs: Pharmacokinetic evaluation using spironolactone as model compound ., Drug Dev Ind Pharm 31 (2005) 319 – 329.

[37] M. Chaubal, C. Popescu, Conversion of nanosuspensions into dry powders by spray drying: a case study, Pharm Res 25 (2008) 2302 – 2308.

[38] S. Moghimi, J. Szebeni, Stealth liposomes and long circulating nanoparticles: critical issues in pharmacokinetics, opsonization and protein-binding properties, Prog Lipid Res 42 (2003) 463 – 478.

[39] J. Y. Choi, C. Park, J. Lee, Effect of polymer molecular weight on nanocomminution of poorly soluble drug, Drug Deliv 15 (2008) 347 – 353.

[40] J. Lee, J. Choi, C. Park, Characteristics of polymers enabling nano-comminution of water-insoluble drugs, International Journal of Pharmaceutics 355 (1-2) (2008) 328 – 336. doi:DOI:10.1016/j.ijpharm.2007.12.032.
URL http://www.sciencedirect.com/science/article/pii/S0378517307010654

[41] X. Li, L. Gu, Y. Xu, Y. Wang, Preparation of fenofibrate nanosuspension and study of its pharmakokinetic behavior in rats, Drug Development and Industrial Pharmacy 35 (2009) 827 – 833.

[42] C. Jacobs, O. Kayser, R. Müller, Nanosuspensions as a new approach for the formulation for the poorly soluble drug tarazepide., Int J Pharm 196 (2000) 161 – 164.

[43] Y. Gao, Z. Li, M. Sun, H. Li, C. Guo, J. Cui, A. Li, F. Cao, Y. Xi, H. Lou, G. Zhai, Preparation, characterization, pharmacokinetics, and tissue distribution of curcumin nanosuspension with tpgs as stabilizer, Drug Dev Ind Pharm 36 (2010) 1225 – 1234.

[44] Y. Zhao, H. Hua, M. Chang, W. Liu, Y. Zhao, H. Liu, Preparation and cytotoxic activity of hydroxycamptothecin nanosuspensions., Int J Pharm 392 (2010) 64 – 71.

[45] I. Ghosh, S. Bose, R. Vippagunta, F. Harmon, Nanosuspension for improving the bioavailability of a poorly soluble drug and screening of stabilizing agents to inhibit crystal growth, Int J Pharm 409 (2011) 260 – 268.

[46] S. Verma, S. Kumar, R. Gokhale, D. Burgess, Physical stability of nanosuspensions: Investigation of the role of stabilizers on ostwald ripening, International Journal of Pharmaceutics 406 (1-2) (2011) 145–152. doi:DOI:10.1016/j.ijpharm.2010.12.027.
URL http://www.sciencedirect.com/science/article/pii/S0378517310009683

[47] D. Everett, Manual of symbols and terminology for physicochemical quantities and units, Vol. 31, PERGAMON PRESS, 1972, Ch. Appendix II: Definitionsand terminology and symbols in colloid and surface chemistryand part I, pp. 577–638.

[48] K. Meleson, S. Graves, T. Mason, Formation of concentrated nanoemulsions by extreme shear, Soft Materials 2 (2004) 109–123.

[49] J. Stevens, P. Mims, N. Coles, Lipid emulsions as drug delivery systems, Pharmatech 2003 - May 2003 (Business Briefing: Pharmatech) (2003) 1 – 4.

[50] C. Pouton, Formulation of poorly water-soluble drugs for oral administration: Physicochemical and physiological issues and the lipid formulation classification system, European Journal of Pharmaceutical Sciences 29 (2006) 278–287.

[51] C. Pouton, Lipid formulations for oral administration of drugs: non-emulsifyingand self emulsifying and self microemulsifying drug delivery systems, European Journal of Pharmaceutical Sciences 11 (2000) S93–S98.

[52] C. Pouton, C. Porter, Formulation of lipid-based delivery systems for oral administration: Materials, methods and strategies, Advanced Drug Delivery Reviews 60 (2008) 625–637.

[53] M. Lawrence, G. Rees, Microemulsion-based media as novel drug delivery systems, Advanced Drug Delivery Reviews 45 (2000) 89–121.

[54] J. Klier, C. Tucker, T. Kalantar, D. Green, Properties and applications of microemulsions, Advanced Materials 12 (2000) 1751–1757.

[55] R. G. S. Benita, Self-emulsifying drug delivery systems (sedds) for improved oral delivery of lipophilic drugs, Biomedicine and Pharmacotherapy 58 (2004) 173–182.

[56] M. A. Moreno, M. P. Ballesteros, P. Frutos, Lecithin-based oil-in-water microemulsions for parenteral use: pseudoternary phase diagramsand characterization and toxicity studies, Journal of Pharmaceutical Sciences 92 (2003) 1428 – 1437.

[57] A. A. Date, M. Nagarsenker, Parenteral microemulsions: An overview, International Journal of Pharmaceutics 355 (2008) 19 – 30.

[58] S. R. Hwang, S.-J. Lim, J.-S. Park, C.-K. Kim, Phospholipid-based microemulsion formulation of all-trans-retinoic acid for parenteral administration, International Journal of Pharmaceutics 276 (2004) 175 – 183.

[59] W. Warisnoicharoen, A. B. Lansley, M. J. Lawrence, Light-scattering investigations on dilute nonionic oil-in-water microemulsions, AAPS Pharmsci 2000; 2(2) article 12 2and article 12 (2000) 1–11.

[60] P. A. Reynolds, E. P. Gilbert, J. W. White, High internal phase water-in-oil emulsions and related microemulsions studied by small angle neutron scattering. 2. the distribution of surfactant, J. Phys. Chem. B 105 (2001) 6925 – 6932.

[61] C. Sommer, G. R. Deen, J. S.Pedersen, P. Strunz, V. M. Garamus, Microemulsion droplets decorated by brij700 block copolymer: Phase behavior and structural investigation by saxs and sans, Langmuir 23 (2007) 6544 – 6553.

[62] J. P. Fast, S. Mecozzi, Nanoemulsions for intravenous drug delivery in: Nanotechnology in Drug Delivery, AAPS Pressand Springer, 2009.

[63] T. Mason, J. Wilking, K. Meleson, C. Chang, S. Graves, Nanoemulsions: formationand structureand and physical properties, Journal of Physics: Condensed Matter 18 (2006) R635–R666.

[64] D. Sarker, Engineering of nanoemulsions for drug delivery, Current Drug Delivery 2 (2005) 297–310.

[65] Rote Liste® Service GmbH, Frankfurt/Main, Germany, Rote Liste (2012).

[66] E. M. M. del Valle, Cyclodextrins and their uses: a review, Process Biochemistry 39 (2004) 1033 – 1046.

[67] M. E. Brewster, T. Loftsson, Cyclodextrins as pharmaceutical solubilizers, Advanced Drug Delivery Reviews 59 (2007) 645 – 666.

[68] L. A. Miller, R. L. Carrier, I. Ahmed, Practical considerations in development of solid dosage forms that contain cyclodextrin, Jounal of Pharmaceutical Sciences 96 (2007) 1691 – 1707.

[69] A. Trapani, A. Lopedota, N. Denora, V. Laquintana, M. Franco, A. Latrofa, G. Trapani, G. Liso, A rapid screening tool for estimating the potential of 2-hydroxypropyl-beta-cyclodextrin complexation for solubilization purposes, International Journal of Pharmaceutics 295 (2005) 163 – 175.

[70] T. Loftsson, D. Hreinsdóttir, M. Másson, Evaluation of cyclodextrin solubilization of drugs, International Journal of Pharmaceutics 302 (1-2) (2005) 18–28. doi:DOI:10.1016/j.ijpharm.2005.05.042.
URL http://www.sciencedirect.com/science/article/pii/S0378517305004400

[71] J. Taraszewska, M. Kozbial, Complexation of ketoconazole by native and modified cyclodextrins, Journal of Inclusion Phenomena and Macrocyclic Chemistry 53 (2005) 155 – 161.

[72] H. S. Lin, C. S. Chean, Y. Y. Ng, S. Y. Chan, P. C. Ho, 2-hydroxypropyl-b-cyclodextrin increases aqueous solubility and photostability of all-trans-retinoic acid, Journal of Clinical Pharmacy and Therapeutics 25 (2000) 265 – 269.

[73] M. Veiga, P. J. Diaz, F. Ahsan, Interactions of griseofulvin with cyclodextrins in solid binary systems, Journal of Pharmaceutical Sciences 87 (1998) 891 – 900.

[74] A. C. Jain, M. C. Adeyeye, Hygroscopicity, phase solubility and dissolution of various substituted sulfobutylether b-cyclodextrins (sbe) and danazol - sbe inclusion complexes, International Journal of Pharmaceutics 212 (2001) 177 – 186.

[75] S. Gould, R. C. Scott, 2-hydroxypropyl-b-cyclodextrin (hp-b-cd): A toxicology review, Food and Chemical Toxicology 43 (2005) 1451 – 1459.

[76] W. Blaschek, S. Ebel, E. Hackenthal, U. Holzgrabe, K. Keller, J. Reichling, V. Schulz, Hagerrom 2002. hagers handbuch der drogen und arzneistoffe, Springer Verlag Heidelberg (2002).

[77] J. D. C. Harvengt, Clinical pharmacokinetic study of procetofene a new hypolipidemic drug in volunteers, Int J Clin Pharmacol Biopharm 16 (1978) 570 – 574.

[78] D. R. P. Guay, Update on fenofibrate, Cardiovascular Drug Reviews 20 (2002) 281 – 302.

[79] R. F. Henry, G. Z. Zhang, Y. Gao, I. S. Buckner, Fenofibrate, Acta Crystallographica Section E E59 (2003) o699 – o700.

[80] M. Vogt, K. Kunath, J. B. Dressman, Dissolution enhancement of fenofibrate by micronizationand cogrinding and spray-drying: Comparison with commercial preparations, European Journal of Pharmaceutics and Biopharmaceutics 68 (2008) 283 – 288.

[81] D. Wishart, C. Knox, A. Guo, D. Cheng, S. Shrivastava, D. Tzur, B. Gautam, M. Hassanali, Drugbank: a knowledgebase for drugsand drug actions and drug targets, Nucleic Acids Res. 36 (2008) D901–6.

[82] A. Polak, Mode of action studies. In: Chemotherapy of fungal diseases, Springer-Verlagand Berlin Heidelberg New York, 1990.

[83] C. Sohn, Evaluation of ketoconazole, Clin Pharm. 1 (1982) 217 – 224.

[84] R. Heel, R. Brogden, A. Carmine, P. Morley, T. Speight, G. Avery, Ketoconazole: a review of its therapeutic efficacy in superficial and systemic fungal infections, Drugs 23 (1982) 1 – 36.

[85] H. V. Bossche, Biochemical targets for antifungal azole derivatives: hypothesis on the mode of action, Curr Top Med Mycol. 1 (1985) 313 – 315.

[86] C. A. Hitchcock, K. Dickinson, S. B. Brown, E. G. V. Evans, D. J. Adams, Interaction of azole antifungal antibiotics with cytochrome p-450-dependent 14a-sterol demethylase purified from candida albicans, Biochem. J. 266 (1990) 475 – 480.

[87] Roquette, Betacyclodextrins kleptose - the new approach to molecular encapsulation for the chemical and fermentation, Tech. rep., Roquette frères.

[88] L. Pharmaceuticals, Technical data on Captisol - How to Solubilize a Drug with Captisol, Ligand Pharmaceuticals Inc., www.captisol.com (2012).

[89] D. Waitzberg, P. Lotierzo, A. Logullo, R. Torrinhas, C. Pereira, R. Meier, Parenteral lipid emulsions and phagocytic systems, British Journal of Nutrition 87 (2002) S49 – S57.

[90] K. Hilland, O. Rohde, Sugar-based surfactants for consumer products and technical applications, European Journal of Lipid Science and Technology 101 (1990) 25 – 33.

[91] E. Kostwicz, U. Brauns, R. Becker, J. Dressman, Forecasting the oral absorption behavior of poorly soluble weak bases using solubility and dissolution studies in biorelevant media, Pharmaceutical Research 19 (2002) 345 – 349.

[92] U. S. P. Commission, United States Pharmacopeia (USP), Stationery Office Books, 2007.

[93] I. Sunshine (Ed.), CRC Handbook of Analytical Toxicology, Cleveland: The Chemical Rubber Co, 1969.

[94] E. B. Souto, R. H. Müller, Sln and nlc for topical delivery of ketoconazole, Journal of Microencapsulation 22 (2005) 501 – 510.

[95] Sasol, MIGLYOL® 810, 812, 818, 829, 840 Neutral Oils for Pharmaceuticals and Cosmetics, Sasol Germany GmbH, Arthur-Imhausen-Str. 92, 58453 Witten, Germany, 09th Edition.

[96] H. S. Y. Singh, A practical guide to saxs, by Anton Paar GmbH (2006).

[97] D. Svergun, M. H. J. Koch, Small-angle scattering studies of biological macromolecules in solution, Rep. Prog. Phys. 66 (2003) 1735 – 1782.

[98] J. S. Pedersen, M. C. Gerstenberg, Scattering form factor of block copolymer micelles, Macromolecules 29 (1996) 1363 – 1365.

[99] J. Kohlbrecher, User guide for the SASfit software package A program for fitting elementary structural models to small angle scattering data, Paul Scherrer Instituteand Laboratory for Neutron Scattering (LNS) (January 2011).

[100] W. Oliver, G. Pharr, An improved technique for determining hardness and elastic modulus using load and displacement sensing indentation experiments, Journal of Material Research 7 (1992) 1564–1583.

[101] S. LINDNER, SiLibeads® Ceramic beads, SIGMUND LINDNER GmbH Germany (2008).

[102] T. Higuchi, A. Connors, Phase-solubility techniques, Advances in Chemical Instrumentation 4 (1965) 212–217.

[103] T. Loftsson, M. Masson, J. Sigurjonsdottir, Methods to enhance the complexation efficiency of cyclodextrins, STP Pharma Sciences 9 (1999) 237–242.

[104] W.-H. Wu, Parenteral nanoemulsions - compositionand preparation and cellular uptake, Ph.D. thesis, University of Freiburg (2007).

[105] Ryoto® sugar esters. produktinformation., Tech. rep., Mitsubishi-Kagaku Foods Corporation and Tokyo and Japan.

[106] B. V. Eerdenbrugh, J. Vermant, J. A. Martens, L. Froyen, J. V. Humbeeck, P. Augustijns, G. V. den Mooter, A screening study of surface stabilization during the production of drug nanocrystals, Journal of Pharmaceutical Sciences 98 (6) (2009) 2091–2103. doi:10.1002/jps.21563.
URL http://dx.doi.org/10.1002/jps.21563

[107] Willy A. Bachofen AG, Muttenz, Switzerland, DYNO®-MILL RESEARCH LAB Operating Instructions.

[108] R. Perez, H. Jiang, E. Lavernia, C. Dogan, Grain growth of nanocrystalline cryomilled fe-al powders, Metallurgical and Materials Transactions A 29 (1998) 2469–2475, 10.1007/s11661-998-0218-7.
URL http://dx.doi.org/10.1007/s11661-998-0218-7

[109] F. Zhou, D. Witkin, S. Nutt, E. Lavernia, Formation of nanostructure in al produced by a low-energy ball milling at cryogenic temperature, Materials Science and Engineering: A 375 (2004) 917–921, eleventh International Conference on Rapidly Quenched and Metastable Materials. doi:DOI:10.1016/j.msea.2003.10.235.
URL http://www.sciencedirect.com/science/article/pii/S092150930301270X

[110] M. Crisp, C. Tucker, T. Rogers, R. III, K. Johnston, Turbidimetric measurement and prediction of dissolution rates of poorly soluble drug nanocrystals, Journal of Controlled Release 117 (2007) 351–359.

[111] B. Rabinow, J. Kipp, P. Papadopoulos, J. Wong, J. Glosson, J. Gass, C. Sun, T. Wielgos, R. White, C. Cook, K. Barker, K. Wood, Iitraconazole iv nanosuspension enhances efficacy through altered pharmacokinetics in the rat, International Journal of Pharmaceutics 339 (2007) 251–260.

[112] J. Hildebrand, R. Scott, The solubility of non-electrolytes, Reinhold Pub. Corp., 1950.

[113] C. Hansen, The universality of the solubility parameter, Ind. Eng. Chem. Prod. Res. Dev. 8 (1969) 2 – 11.

[114] K. Adamska, A. Voelkel, K. Heberger, Selection of solubility parameters for characterization of pharmaceutical excipients, Journal of Chromatography A 1171 (2007) 90 – 97.

[115] A. Forster, J. Hempenstall, I. Tucker, T. Rades, Selection of excipients for melt extrusion with two poorly water-soluble drugs by solubility parameter calculation and thermal analysis, International Journal of Pharmaceutics 226 (2001) 147 – 161.

[116] P. Hoftyzer, D. V. Krevelen, Properties of polymers, Elsevier New York, 1976.

[117] K. L. Hoy, New values of the solubility parameters from vapor pressure data, Journal of paint technology 42 (1970) 76 – 118.

[118] R. Fedors, A method for estimating both the solubility parameters and molar volumes of liquids, JPL Quarterly Technical Review 3 (1973) 45 – 53.

[119] F. Mohamed, Y. Xun, Correlations between the minimum grain size produced by milling and material parameters, Materials Science and Engineering: A 354 (1-2) (2003) 133–139. doi:DOI:10.1016/S0921-5093(02)00936-X.
URL http://www.sciencedirect.com/science/article/pii/S092150930200936X

[120] L. Taylor, D. Papadopoulos, P. Dunn, A. Bentham, N. Dawson, J. Mitchell, M. Snowden, Predictive milling of pharmaceutical materials using nanoindentation of single crystals, Organic Process Research & Development 8 (4) (2004) 674–679. arXiv:http://pubs.acs.org/doi/pdf/10.1021/op0300241, doi:10.1021/op0300241.
URL http://pubs.acs.org/doi/abs/10.1021/op0300241

[121] R. Dukino, M. Swain, Comparative measurement of indentation fracture toughness with berkovich and vickers indenters, Journal of the American Ceramic Society 75 (12) (1992) 3299–3304. doi:10.1111/j.1151-2916.1992.tb04425.x.
URL http://dx.doi.org/10.1111/j.1151-2916.1992.tb04425.x

[122] F. Ingels, S. Deferme, E. Destexh, M. Oth, G. V. den Mooter, P. Augustijns, Simulated intestinal fluid as transport medium in the caco-2 cell culture model, International Journal of Pharmaceutics 32 (2002) 183 – 192.

[123] N. P. B. Forbes, Use of simulated intestinal fluids with caco-2 cells and rat ileum, Drug Development and Industrial Pharmacy 32 (2006) 151 –161.

[124] M. Kataoka, Y. Masaoka, S. Sakuma, S. Yamashita, Effect of food intake on the oral absorption of poorly water-soluble drugs: In vitro assessment of drug dissolution and permeation assay system, Journal of Pharmaceutical Sciences 95 (2006) 2051 – 2061.

[125] M. V. Rekharsky, M. P. Mayhew, R. N. Goldberg, P. D. Ross, Y. Yamashoji, Y. Inoue, Thermodynamic and nuclear magnetic resonance study of the reactions of alpha- and beta-cyclodextrin with acids, aliphatic amines and cyclic alcohols, J. Phys. Chem. B 101 (1997) 87 – 100.

[126] G. Yang, N. Jain, S. H. Yalkowsky, Combined effect of sls and (sbe)7m-beta-cd on the solubilization of nsc-639829, International Journal of Pharmaceutics 269 (2004) 141 – 148.

[127] R. D. Lisi, G. Lazzara, S. Milioto, N. Muratore, Characterization of the cyclodextrin-surfactant interactions by volume and enthalpy, J. Phys. Chem. B 107 (2003) 13150 – 13157.

[128] N. Funasaki, S. Ishikawa, S. Neya, 1:1 and 1:2 complexes between long-chain surfactant and alpha-cyclodextrin studied by nmr, J. Phys. Chem. B 108 (2004) 9593 – 9398.

[129] Y. Liu, L. Li, Y. Chen, L. Yu, Z. Fan, F. Ding, Molecular recognition thermodynamics of bile salts by beta-cyclodextrin dimers: Factors governing the cooperative binding of cyclodextrin dimers, The Journal of Physical Chemistry B 109 (9) (2005) 4129–4134, pMID: 16851473. arXiv:http://pubs.acs.org/doi/pdf/10.1021/jp045332v, doi:10.1021/jp045332v.
URL http://pubs.acs.org/doi/abs/10.1021/jp045332v

[130] F. Ollila, O. Pentikäinen, S. Forss, M. Johnson, J. Slotte, Characterization of bile salt/cyclodextrin interactions using isothermal titration calorimetry, Langmuir 17 (22) (2001) 7107–7111. arXiv:http://pubs.acs.org/doi/pdf/10.1021/la0109258, doi:10.1021/la0109258.
URL http://pubs.acs.org/doi/abs/10.1021/la0109258

[131] T. G. Anderson, A. Tan, P. Ganz, J. Seelig, Calorimetric measurement of phospholipid interaction with methyl-beta-cyclodextrin, Biochemistry 43 (2004) 2251 –2261.

[132] L. Hu, H. Wu, F. Niu, C. Yan, X. Yang, Y. Jia, Design of fenofibrate microemulsion for improved bioavailability, International Journal of Pharmaceutics 420 (2011) 251–255.

[133] M. Harshal, S. Tanvir, B. Dheeraj, W. Rajendra, Design and development of solid self-microemulsifying drug delivery system (smedds) of fenofibrate, International Journal of Pharmacy and Pharmaceutical Sciences 3and Suppl. 4 (2011) 163–166.

[134] A. Patel, P. Vavia, Preparation and in vivo evaluation of smedds (self-microemulsifying drug delivery system) containing fenofibrate, The AAPS Journal 9 (2007) E344–E352.

[135] T. D. Thi, M. V. Speybroeck, V. Barillaro, J. Martens, P. Annaert, P.Augustijns, J. V. Humbeeck, J. Vermantd, G. V. den Mooter, Formulate-ability of ten compounds with different physicochemical profiles in smedds, European Journal of Pharmaceutical Sciences 38 (2009) 479 – 488.

[136] K. Mohsin, M. Long, C. Pouton, Design of lipid-based formulations for oral administration of poorly water-soluble drugs: Precipitation of drug after dispersion of formulations in aqueous solution, Journal of Pharmaceutical Sciences 98 (2009) 3582–3595.

[137] G. Lancz, M. Avdeev, V. Petrenko, V. Garamus, M. Koneracká, P. Kopcanský, Sans study of poly(ethylene glycol) solutions in d2o, Acta physica polonica A 118 (2010) 980 – 982.

[138] J. Coon, W. Knudson, K. Clodfelter, B. Lu, R. S. Weinstein, Solutol hs 15and nontoxic polyoxyethylene esters of 12-hydroxystearic acidand reverses multidrug resistance, Cancer Research 51 (1991) 897 – 902.

[139] I. Buttle, O/w-emulsionen für die intravenöse applikation von arzneistoffen, Ph.D. thesis, Freie Universität Berlin (2004).

[140] D. Korner, S. Benita, G. Albrecht, A. Baszkin, Surface properties of mixed phospholipid - stearylamine monolayers and their interaction with a non-ionic surfactant (poloxamer), Colloids and Surfaces B: Biointerfaces 3 (1994) 101 – 109.

[141] P. Gupta, J. Cannon, Emulsions and microemulsions for drug solubilization and delivery, Denver: Interpharm Press, 2000.

[142] V. Torchilin, Recent advances with liposomes as pharmaceutical carriers, Nature Reviews Drug Discovery 4 (2005) 145 – 160.

[143] I. J. A. Baker, D. N. Furlong, F. Grieser, C. J. Drummond, Sugar fatty acid ester surfactants: Base-catalyzed hydrolysis, Journal of surfactants and detergents 3 (2000) 29 – 32.

[144] R. K. Gupta, K. James, F. J. Smith, Sucrose esters and sucrose ester/glyceride blends as emulsifiers, Journal of the American Oil Chemists' Society 60 (1983) 862 – 869.

[145] M. Ausborn, H. Schreier, G. Brezesinski, H. Fabian, H. Meyer, P. Nuhn, The protective effect of free and membrane-bound cryoprotectants during freezing and freeze-drying of liposomes, Journal of Controlled Release 30 (2) (1994) 105–116. doi:DOI:10.1016/0168-3659(94)90257-7.
URL http://www.sciencedirect.com/science/article/pii/0168365994902577

[146] Application of nanotechnology: A case study in the pharmaceutical arena, Tech. rep., Elan Drug Delivery Inc. (2008).

[147] E. Bilgilia, R. Hameyb, B. Scarlett, Nanomilling of pigment agglomerates using a wet stirred media mill: Elucidation of the kinetics and breakage mechanisms, Chemical Engineering Science 61 (2006) 149–157.

[148] A. Kwade, J. Schwedes, Autogenzerkleinerung in ruehrwerkmuehlen, Chemie Ingenieur Technik 68 (1996) 809 – 812.

[149] S. Breitung-Faes, A. Kwade, Einsatz unterschiedlicher rührwerkskugelmühlen für die erzeugung von nanopartikeln, Chemie Ingenieur Technik 79 (2007) 241–248.

[150] F. Stenger, W. Peukert, The role of particle interactions in suspension rheology - application to submicron grinding in stirred media mills, Chemical Engineering & Technology 26 (2003) 177–183.

[151] J. Konkel, A. Myerson, Empirical molecular modelling of suspension stabilisation with polysorbate 80, Molecular Simulation 34 (2008) 1353–1357.

[152] S. Verma, B. Huey, D. Burgess, Scanning probe microscopy method for nanosuspension stabilizer selection, Langmuir 25 (21) (2009) 12481–12487, pMID: 19791747. arXiv:http://pubs.acs.org/doi/pdf/10.1021/la9016432, doi:10.1021/la9016432.
URL http://pubs.acs.org/doi/abs/10.1021/la9016432

[153] P. Buch, P. Langguth, M. Kataoka, S.Yamashita, Ivivc in oral absorption for fenofibrate immediate release tablets using a dissolution/permeation system, Joun 98 (2008) 1520 – 6017.

[154] F. Ingels, B. Beck, M. Oth, P. Augustijns, Effect of simulated intestinal fluid on drug permeability estimation across caco-2 monolayers, International Journal of Pharmaceutics 274 (2004) 221 – 232.

[155] S. Clarysse, J. Brouwers, J. Tack, P. Annaert, P. Augustijns, Intestinal drug solubility estimation based on simulated intestinal fluids: comparison with solubility in human intestinal fluids, European Journal of Pharmaceutical Sciences 43 (2011) 260 – 269.

[156] A. Okazaki, T. Mano, K. Sugano, Theoretical dissolution model of poly-disperse drug particles in biorelevant media, Journal of Pharmaceutical Sciences 97 (2008) 1843 – 1852.

[157] L. Lindfors, P. Skantze, U. Skantze, J. Westergren, U. Olsson, Amorphous drug nanosuspensions. 3. particle dissolution and crystal growth, Langmuir 23 (2007) 9866 – 9874.

[158] H. Bergerhausen, Absorption base containing sucrose ester (1993).

[159] E. Csizmazia, G. Eros, O. Berkesi, S. Berk, P. Szab-Revesz, E. Csnyi, Ibuprofen penetration enhance by sucrose ester examined by atr-ftir in vivo, Pharmaceutical Development and Technology 17 (2012) 125 – 128.

[160] A. Ganem-Quintanar, D. Quintanar-Guerrero, F. Falson-Rieg, P. Buri, Ex vivo oral mucosal permeation of lidocaine hydrochloride with sucrose fatty acid esters as absorption enhancers, International Journal of Pharmaceutics 173 (1998) 203 – 210.

[161] F. Ahsan, J. J. Arnold, E. Meezan, D. J. Pillion, Sucrose cocoateand a component of cosmetic preparationsand enhances nasal and ocular peptide absorption, International Journal of Pharmaceutics 251 (2003) 195 – 203.

[162] K. Azuma, K. Ippoushi, H. Ito, H. Higashio, J. Terao, Combination of lipids and emulsifiers enhances the absorption of orally administered quercetin in rats, J. Agric. Food Chem. 50 (2002) 1706 – 1712.

[163] Y. Nakada, N. Awata, C. Nakamichi, I. Sugimoto, The effect of additives on the oral mucosal absorption of human calcitonin in rats, J. Pharmacobio-Dyn. 11 (1988) 395 – 401.

Publications and presentations

- Commentary on the European Pharmacopeia 6.1 "5.15 functionality related characteristics"
- Commentary on the European Pharmacopeia 6.0 "6.0/2396 macrogol 40 sorbitol heptaoleate"
- Oral presentation „Studies on the formation process of microemulsions" PBP world meeting 2008, Barcelona, Spain
- Poster presentation "Evaluation of nanomilling methods in preformulation development" CRS German Chapter Annual Meeting 2008, Braunschweig, Germany